

# **Modeling Study of Domain Wall Motion in Dual Magnetic Layers Driven by Spin Hall Effect**

Submitted in partial fulfillment of the requirements for

the degree of

Doctor of Philosophy

in

Electrical and Computer Engineering

Xi Liu

B.S., Materials Science and Engineering, Wuhan University of  
Technology  
M.S., Energy Science Technology and Policy, Carnegie Mellon  
University

Carnegie Mellon University  
Pittsburgh, PA

December, 2019

© Xi Liu, 2019

All Rights Reserved

## ABSTRACT

Future high density data storage also desires fast read/write and low power capability. One of the candidates for meeting the demand is current-driven domain wall motion memory. Domain walls can be moved by current via the Spin Hall effect in the presence of Dzyaloshinskii–Moriya interaction (DMI). In such a case, the domain wall motion is propelled by the polarized pure spin current injected into the magnetic layer from the electron flow in an adjacent heavy-metal layer. Much of existing work has been focusing on enhancing the domain wall motion by interlayer interaction, including exchanging coupling and dipolar interaction. Here, we focus on creating fast domain wall motion, required for high speed switching, with increased spin injection efficiency. In particular the magnetic layer are sandwiched by two heavy metal layers, enabling spin injection from both the top and bottom sides of the magnetic layer. In this thesis, we present a micromagnetic modeling investigation on symmetric dual magnetic layers with heavy metals on both sides. Specifically, the domain wall motion behavior of symmetric Pt/Co/Ir/Co/Pt multilayer has been investigated. The study focuses on the effect of interlayer interaction between the two magnetic layers during the current driven domain wall motion.

We first verified that we could adjust the spin current and chirality of the domain wall to control domain wall motion by manipulating the Pt/Co/Ir film stack order. Based on such understanding, the magnetic layer in the dual magnetic layers system with ferromagnetic/antiferromagnetic coupling is further investigated. We

discover that the velocities increase while the ferromagnetic exchanging coupling strength decreases.

The inner magnetization of domain walls in different layers will create a certain angle to facilitate the domain wall motion. The velocities saturate when they create a 180-degree angle. On the other hand, the domain wall motion is accelerated once the two magnetic layers are antiferromagnetic coupled together. The exchange coupling interaction creates an extra torque, which increases the velocities of the domain wall. The domain wall also transforms into an “S” shape instead of being linear to reduce the demagnetization field. Hence the domain wall motion is faster at low current density.

## **ACKNOWLEDGEMENTS**

There are many people that I need to thank for helping me with my time in graduate school. My graduation and thesis would not be possible without following people: my supervisors, my thesis committee members, my lab mates, my funding agencies, and my family.

First of all, I want to thank Prof. Zhaojun Liu and Prof. Elias Towe. From the first day of my graduate school, Prof.Liu and Prof.Towe gave me tremendous support. My first two years of my PhD, Prof.Liu, gave me the opportunities to study at the Hong Kong University of Science and Technology. The days in HKUST taught me how to conduct my research into semiconductors. Prof. Towe taught me how to define research problems and publish the results. They inspired me to be a motivated and hardworking student. Although the collaboration ended due to funding issues, my gratitude will not stop.

I am also indebted to my advisor, Prof. Jimmy Zhu. At the most challenging and struggling time of my PhD, he not only did not give up on me but has given me endless patience and support. I will always be grateful for that. Under his supervision, he has helped me expand my vision from experiment to simulation. Furthermore, I learned how to solve a research problem scientifically. On a personal level, he also taught me to be steadier and earnest. To summarize, I would give Prof.Zhu most of the credit for helping me become the kind of scientist I am today.

Furthermore, besides my supervisor, I would also like to thank Prof. David Laughlin, Prof. Jim Bain, and Prof. Vincent Sokalski for being my committee members. Their critique and insight have been significant input for guiding my project. They challenged me to push my project further and develop a more sophisticated understanding.

I also really appreciate the help of DSSC. The Data Storage Systems Center proved financial supports and the necessary tools for conducting my research. I am also very grateful for having my lab mates whom I have had the pleasure to work with and their continued support over the past few years. I would first like to thank Yang Liu for offering me guidance and advice with my research. His knowledge of magnetism, device fabrication, device testing, characterization certainly made my life more comfortable, and I am grateful for his willingness to help and teach. I would also thank Dr. Derek Lau, who help me develop a model and characterization method for domain wall motion. His previous work and help are crucial for my experiment and simulation. I would be also grateful for the support of Maxwell Li, Zhengkun Dai, and Bing Zhou, who has helped me with the tools and skills to complete my work. My thesis would not be possible without their help. I am also extremely grateful for the expertise and the dedication of the Nanofabrication staff at CMU, and I am thankful for all their support over the years.

During my time in Pittsburgh, I am grateful that I have made great friends who give me lots of support and joyful times. I want to thank Wenbo Zhao, Yandong Wen, Xu Yan, Qiaozhi Qian, Xu Lu, and Yang Gao. We all have been through the JIE issue, and we have all survived from it. Thanks for Jenny, Zoe, Yvnoe, Lewis,

during my CSSA time. Thanks to all my labmates for helping me. Special shout-out to Jingjing He, Baxi Chong, and Boyuan Yang for their friendship and all the whiskey we share. Thank you all for understanding in me and being there for me.

Finally, I would like to thank my family and friends for their support. I would not be the person I am today without them. Thanks to my mother, Shuqin Li, and my father, Huijian Liu. Without their help and patience, I would never graduate from CMU. Thanks to Uncle Meng He and Aunt Huajun Huang. They have treated me as their family since the first day I arrived in the US. Their suggestions and kindness help me overcome the challenges during my Ph.D. I will carry their hope and love to achieve and conquer in the future.

# TABLE OF CONTENTS

<b>ABSTRACT</b>	<b>i</b>
<b>ACKNOWLEDGEMENTS</b>	<b>iii</b>
<b>TABLE OF CONTENTS</b>	<b>vi</b>
<b>LIST OF FIGURES</b>	<b>ix</b>
<b>LIST OF SYMBOLS AND ABBREVIATIONS</b>	<b>xvii</b>
<b>CHAPTER 1. Motivation</b>	<b>1</b>
1.1 Domain wall device	1
1.2 Simulation for the domain wall motion	2
1.3 Motivation	4
1.4 Outline	6
<b>CHAPTER 2. Background</b>	<b>8</b>
2.1 Energies of ferromagnetic system	8
2.2 Zeeman energy	9
2.3 Exchange Energy	10
2.4 Magneto-static Energy	12
2.5 Magneto-crystalline anisotropy energy	13
2.5.1 Perpendicular magnetic materials	15
2.6 Magnetic Domain and domain wall formation	16
2.7 Bloch wall and Néel wall properties	18
2.8 Domain wall motion	20
2.9 Field Driven Domain Wall Motion	22
2.9.1 Field induced domain wall dynamics	23
2.9.2 Creep and flow regimes of the domain wall motion	25
2.10 Current induced domain wall motion	26
2.10.1 Spin transfer torques	26
2.10.2 Spin hall effect and spin-orbit torque	28
2.11 Dzyaloshinskii-moriya interaction	30
2.12 Chiral domain wall structure due to DMI	32
2.13 SOT driven domain wall motion in the present of DMI	33
2.14 Ruderman–Kittel–Kasuya–Yosida Intercation	34
2.15 RKKY interaction impact on multilayer system domain wall motion	35
<b>CHAPTER 3. Simulation Tool Verification</b>	<b>37</b>
3.1 Simulation package	37
3.2 Standard Problems	37

3.2.1	Standard Problem 1	38
3.2.2	Standard Problem 2	39
3.2.3	Standard Problem 4	40
3.2.4	Standard Problem 5	41
<b>3.3</b>	<b>External Problems</b>	<b>42</b>
3.3.1	Domain wall width and energy	42
3.3.2	Dzyaloshinskii–Moriya interaction field	45
3.3.3	Spin transfer torque domain wall motion	46
<b>CHAPTER 4. Simulation of Field and current induced single Co layer domain wall motion</b>		<b>48</b>
<b>4.1</b>	<b>Single Co layer domain wall motion induced by external field</b>	<b>49</b>
4.1.1	Perpendicular field-induced domain wall motion	50
4.1.2	In-plane field-induced domain wall motion	52
<b>4.2</b>	<b>Current induced single layer domain wall motion</b>	<b>53</b>
4.2.1	In-plane field and Spin Hall effect induced domain wall motion	54
4.2.2	Spin Hall induced chiral domain wall motion with DMI	56
4.2.3	Direction dependent of domain wall motion	59
<b>4.3</b>	<b>Comparison of Field and Current induced single layer domain wall motion</b>	<b>错误!未定义书签。</b>
<b>CHAPTER 5. Simulation of Current induced multi Co layer DWM with FM coupling</b>		<b>62</b>
<b>5.1</b>	<b>Effect of dipolar interaction on multilayer structure</b>	<b>64</b>
<b>5.2</b>	<b>Multilayer structure without interlayer exchanging coupling</b>	<b>66</b>
<b>5.3</b>	<b>Multilayer structure with ferromagnetic interlayer exchanging coupling</b>	<b>68</b>
5.3.1	Interlayer exchanging coupling effect on domain wall motion speed and inner magnetization angle	70
<b>CHAPTER 6. Simulation of Current induced multi Co layer domain wall motion with DW antiparallel</b>		<b>79</b>
<b>6.1</b>	<b>DWM in dual magnetic structure with FM interlayer exchanging coupling and DWs antiparallel coupled</b>	<b>82</b>
6.1.1	Exchanging coupling effect on domain wall motion speed and inner magnetization angle	84
6.1.2	Current effect on domain wall motion speed and inner magnetization angle	87
<b>6.2</b>	<b>DWM in dual magnetic structure with AFM interlayer exchanging coupling and DWs antiparallel coupled</b>	<b>90</b>
6.2.1	Interlayer exchanging coupling effect on domain wall motion speed and inner magnetization angle	93
6.2.2	Current effect on domain wall motion speed and inner magnetization angle	96
<b>6.3</b>	<b>Comparison between FM coupling and AFM coupling</b>	<b>98</b>
<b>CHAPTER 7. Conclusions and Outlook</b>		<b>101</b>

<b>7.1</b>	<b>Summary and comparison</b>	<b>101</b>
<b>7.2</b>	<b>Outlook on future developments</b>	<b>105</b>
<b>7.3</b>	<b>Skyrmion dynamics in synthetic antiferromagnetic structures</b>	<b>105</b>
<b>7.4</b>	<b>Interaction between the domain walls in synthetic antiferromagnetic wires</b>	<b>109</b>
<b>7.5</b>	<b>Synthetic antiferromagnets in magnetic tunnel junctions</b>	<b>110</b>
	<b>REFERENCES</b>	<b>113</b>

## LIST OF FIGURES

Figure 2-1 The transition from single domain state to multidomain configuration to lower the total energy in magnetic system. ....	17
Figure 2-2 (a) The schematic diagrams opposite magnetization domains with perpendicular anisotropy. b) The Néel DW. The magnetization inside the domain wall varies its direction along the DW length. c) The Bloch DW. The magnetization rotates out of plane to the DW length. Replotted from with permission from M. D. Dejong and K. L. Livesey, <i>Phys. Rev. B</i> , vol. 92, p. 214420, 2015. Ref.[29].....	20
Figure 2-3 The domain wall motion in nanowires in presence of a) an external field (Hz) and b) an electric current (I). The field induced domain wall motion results in expansion or contraction of the magnetic domains whereas the current induced domain wall motion results in the displacement of magnetic domains along the nanowire. ....	21
Figure 2-4 (a) The schematic diagram of the velocity versus the applied external field amplitude. The velocity shows two linear regimes, the steady state regime and the oscillatory or turbulent regime, separated by the Walker breakdown at field $H_W$ . b) Schematics of the different torques acting on a single magnetization at the center of the Bloch domain wall. The applied field ( $H_a$ , shown in blue) is associated with as torque $T_a$ that rotates the magnetization in the plane and creates an in-plane dipolar field ( $H_{D_{\text{Demag}}}$ shown in green). The damping torque $T_{D_{\text{Damp}}}$ associated to the motion induced by $H_{D_{\text{Demag}}}$ then compensates $T_a$ . Finally, $T_{D_{\text{Demag}}}$ pulling the magnetization out of plane results in the domain wall motion. ....	24
Figure 2-5 Three regimes of DW dynamics driven by a magnetic field and/or spin-polarized current. Replotted with the permission from S. Emori and G. S. D. Beach, <i>J. Phys. Condens. Matter</i> , vol. 24, no. 2, Jan. 2012. Ref. [30].....	26
Figure 2-6 Spin polarized current flows through the magnetic layer and change its magnetization.....	27

Figure 2-7 Spin hall effect in FM/HM/FM system. When the current goes through the heavy metal, spin current with different polarization is injected into the FM layers. ....	29
Figure 2-8 Spin canting and interfacial DMI induced by structural asymmetry and its coordinate system. Replotted with the permission from A. Fert, V. Cros, and J. Sampaio, <i>Nature Nanotechnology</i> , vol. 8, no. 3. Nature Publishing Group, pp. 152–156, 2013. Ref. [31].....	31
Figure 2-9 Top and side view for domain wall configuration of differnt DMI sign. (a) domain wall configuration when $DMI < 0$ (b) domain wall configuration when $DMI = 0$ (c) domain wall configuration when $DMI > 0$ .....	33
Figure 2-10 Possible DMI,chirality and SOT combination. The black arrow is the original spin orientation while the white arrow is the orientation under the effect of SOT.....	34
Figure 2-11 Exchange coupling constant as a function of Ru thickness in Co Ru Co tri-layers. Reprinted with permission from S. S. P. Parkin and D. Mauri, <i>Phys. Rev. B</i> , vol. 44, no. 13, pp. 7131–7134, Oct. 1991. Ref. [32].....	35
Figure 2-12 Schematic representing domains and DWs in antiferromagnetically coupled bilayer structures. Minimization of dipolar coupling between the DWs via flux closure in SAF structures. (Red arrows).....	36
Figure 3-1 Standard problem one: (a) initial vortex state of simulated permalloy rectangle, hysteresis loop of (b) Mumax3 simulation result and (c) reference solution from Mag website. ....	38
Figure 3-2 Standard problem two: remanence for standard problem 2 as a function of the magnet size $d$ expressed in ex- change lengths $l_{ex}$ .(a) Mumax3 (b) reported result from uMag .....	40
Figure 3-3 Standard problem four: simulation result for my (a) Mumax3 (b) reported result from uMag.....	41
Figure 3-4 Standard problem five: simulation result of Mumax3 (a) initial, (b) after current and reported result (c) initial, (d) after current from uMag .....	42

Figure 3-5 (a)Simulation (black dot) and calculation (red line) result of domain wall width changes with the uniaxial anisotropy.(b) Magnetization image for the simulated thin film with $K_{\text{eff}} = 10 \times 10^5 \text{J/m}^3$ and (c) $K_{\text{eff}} = 5 \times 10^5 \text{J/m}^3$ .....	44
Figure 3-6 (a)Simulation setup for domain wall for Bloch wall and Neel Wall. (b)simulation result of domain wall energy for both Bloch wall (black) and Neel wall(red). .....	44
Figure 3-7 Simulation result of domain wall configuration with external magnetic field in x axis (a) $H_x = 0$ , (b) $H_x = 15 \text{mT}$ .....	46
Figure 3-8 Simulation (red line) and experiment (black dot) result of spin transfer torque domain wall motion under electrical current.....	47
Figure 4-1 Top view of initial state of domain and domain walls for the simulation. Red region representing up domain while the blue region is the down domain. The white region is the domain wall and the arrows are representing the inner magnetization of the domain wall.....	50
Figure 4-2 Perpendicular field induced Bloch domain wall motion. (a)domain wall motion velocities and external z-axis field relation, (b)magnetization and velocities of domain wall in steady regime in (a).....	52
Figure 4-3 In plane field induced Bloch domain wall motion. a)domain wall motion velocities and external x-axis field relation, (b)magnetization and velocities of domain wall.....	53
Figure 4-4 In plane field and Spin Hall induced Bloch domain wall motion.(a) schematic diagram for the simulated in plane field and Spin Hall field (b)domain wall motion velocity map for different current and in plane field strength.....	56
Figure 4-5 Domain wall velocity under different strength of DMI effect, (a)negative DMI will rise a right-handed domain wall. (b)without DMI, Bloch domain wall in more energy favorable thin film. (c) under positive DMI, domain wall is left- handed.....	58
Figure 4-6 The velocities of domain wall motion under different sign and strength of DMI and Spin hall effect. ....	59
Figure 4-7 (a) Co/Pt (Pt on the top of Co) sample with negative DMI and negative Spin Hall effect. It moves the domain wall towards down domain expand direction	

(b) Pt/Co (Pt on the bottom of Co) sample gives the domain wall a positive DMI and spin Hall effect, .....	60
Figure 4-8 (a)Co/Pt domain wall motion velocity under different DMI strength (b) Pt/Co domain wall motion velocity under different DMI strength .....	61
Figure 5-1 Simulation set up for multilayer domain wall motion with ferromagnetic coupling. Light blue regions are the domains while the yellow area representing the domain walls. The black arrows are the magnetization direction. The color arrows are the coupling types. ....	63
Figure 5-2 (a) Top layer and bottom layer velocity difference under different current. (b) upper layer and bottom layer velocity, which is the white line in (a).	66
Figure 5-3 (a) Upper layer magnetization angle $\theta_t$ and bottom layer magnetization $\theta_b$ during motion. The color and size of the dot is representing the velocity of the domain wall (b) Bottom layer and top layer domain wall shape and magnetization angle during movement at $I = 1 \times 10^{11} \text{ A/m}^2$ and $I = 1 \times 10^{12} \text{ A/m}^2$ .....	68
Figure 5-4 Current and the velocity of domain wall relationship for different exchanging constant. Inserted image is the different exchanging constant cases' velocity comparing to $J = 0 \text{ mJ/m}^2$ case. The step is $0.1 \text{ mJ/m}^2$ .....	70
Figure 5-5 Upper layer magnetization angle $\theta_t$ and bottom layer magnetization $\theta_b$ during motion for different exchanging coupling constant and current. The color and size of the dot is representing the velocity of the domain wall.....	72
Figure 5-6 (a) Upper layer magnetization angle $\theta_t$ and bottom layer magnetization $\theta_b$ during motion at $I = 1 \times 10^{12} \text{ A/m}^2$ . The color and size of the dot is representing the velocity of the domain wall (b) Bottom layer and top layer domain wall shape and magnetization angle during movement at $1 \text{ mJ/m}^2$ to $0.4 \text{ mJ/m}^2$ .....	74
Figure 5-7 Fixed $I = 1 \times 10^{12} \text{ A/m}^2$ Upper layer magnetization angle $\theta_t$ and bottom layer magnetization $\theta_b$ at (a) $J_{\text{ex}} = 1 \text{ mJ/m}^2$ and (b) $J_{\text{ex}} = 0.4 \text{ mJ/m}^2$ .....	75
Figure 5-8 (a) Upper layer magnetization angle $\theta_t$ and bottom layer magnetization $\theta_b$ during motion at $J_{\text{ex}} = 0.4 \text{ mJ/m}^2$ . The color and size of the dot is representing the velocity of the domain wall (b) Bottom layer and top layer domain wall shape	

and magnetization angle during the movement at  $I = 1 \times 10^{11} \text{ A/m}^2$  and  $I = 1 \times 10^{12} \text{ A/m}^2$ ..... 76

Figure 5-9 Fixed  $J_{\text{ex}} = 0.4\text{mJ/m}^2$  upper layer magnetization angle  $\theta_t$  and bottom layer magnetization  $\theta_b$  at (a)  $I = 1 \times 10^{11} \text{ A/m}^2$  and (b)  $I = 1 \times 10^{12} \text{ A/m}^2$ ..... 78

Figure 6-1 Simulation set up for multilayer domain wall motion with (a) anti-ferromagnetic coupling (b) interlayer exchanging coupling is ferromagnetic coupling, but the strength is smaller than the DMI effect. The yellow area representing the domain area. .... 80

Figure 6-2 Current and the velocity of domain wall relationship for different exchanging constant. Inserted image is the different exchanging constant cases' velocity comparing to  $J_{\text{ex}} = 0\text{mJ/m}^2$  case. The step is  $0.05\text{mJ/m}^2$ . .... 83

Figure 6-3 Upper layer magnetization angle  $\theta_t$  and bottom layer magnetization  $\theta_b$  during motion for different exchanging coupling constant and current density. The size of the dot is representing the velocity of the domain wall. The color is representing different  $J_{\text{ex}}$  from  $J_{\text{ex}} = 0.3\text{mJ/m}^2$  to  $J_{\text{ex}} = 0\text{mJ/m}^2$  cases with current densities from  $I = 1 \times 10^{11} \text{ A/m}^2$  to  $I = 1 \times 10^{12} \text{ A/m}^2$ ..... 84

Figure 6-4 Upper layer magnetization angle  $t$  and bottom layer magnetization  $b$  during motion at of  $J_{\text{ex}} = 0.3\text{mJ/m}^2$  (Blue dots) and of  $J_{\text{ex}} = 0.05\text{mJ/m}^2$  (blue dots). The size of the dot is representing the velocity of the domain wall. .... 85

Figure 6-5 Fixed  $I = 5 \times 10^{11} \text{ A/m}^2$  upper layer magnetization angle  $\theta_t$  and bottom layer magnetization  $\theta_b$  at (a)  $J_{\text{ex}} = 0.05\text{mJ/m}^2$  and  $J_{\text{ex}} = 0.3\text{mJ/m}^2$ ..... 86

Figure 6-6 Bottom layer and top layer domain wall shape and magnetization angle during movement of  $J_{\text{ex}} = 0.05\text{mJ/m}^2$  and  $J_{\text{ex}} = 0.3\text{mJ/m}^2$  at  $I = 1 \times 10^{11} \text{ A/m}^2$  ..... 87

Figure 6-7 Upper layer magnetization angle  $\theta_t$  and bottom layer magnetization  $\theta_b$  during motion at  $I = 1 \times 10^{11} \text{ A/m}^2$  (blue circle) and  $I = 1 \times 10^{12} \text{ A/m}^2$  (red circle). The size of the dot is representing the velocity of the domain wall. The dots in the circle is reduced from  $J_{\text{ex}} = 0.3\text{mJ/m}^2$  to  $J_{\text{ex}} = 0\text{mJ/m}^2$ ..... 89

Figure 6-8 Fixed  $J_{\text{ex}} = 0.2\text{mJ/m}^2$  upper layer magnetization angle  $\theta_t$  and bottom layer magnetization  $\theta_b$  at (a)  $I = 1 \times 10^{11} \text{ A/m}^2$  and (b)  $I = 1 \times 10^{12} \text{ A/m}^2$ ..... 89

Figure 6-9 Bottom layer and top layer domain wall shape and magnetization angle during movement at $I = 1 \times 10^{11} \text{ A/m}^2$ and $I = 1 \times 10^{12} \text{ A/m}^2$ at $J_{ex} = 0.1 \text{ mJ/m}^2$ .....	90
Figure 6-10 Current and the velocity of domain wall relationship for different exchanging constant. The top line is the $J_{ex} = -0.2 \text{ mJ/m}^2$ case and bottom line is $J_{ex} = 0 \text{ mJ/m}^2$ . The step is $-0.05 \text{ mJ/m}^2$ .....	92
Figure 6-11 Upper layer magnetization angle $\theta_t$ and bottom layer magnetization $\theta_b$ during motion for different exchanging coupling constant and current. The size of the dot is representing the velocity of the domain wall. The color is representing different $J_{ex}$ from $J_{ex} = 0 \text{ mJ/m}^2$ to $J_{ex} = -0.2 \text{ mJ/m}^2$ cases with current densities from $I = 1 \times 10^{11} \text{ A/m}^2$ to $I = 1 \times 10^{12} \text{ A/m}^2$ .....	93
Figure 6-12 Upper layer magnetization angle $t$ and bottom layer magnetization $b$ during motion at $J_{ex} = 0.2 \text{ mJ/m}^2$ , $J_{ex} = 0 \text{ mJ/m}^2$ , $J_{ex} = -0.1 \text{ mJ/m}^2$ and $J_{ex} = -0.2 \text{ mJ/m}^2$ . The size of the dot is representing the velocity of the domain wall. The different dot is representing current from $I = 1 \times 10^{11} \text{ A/m}^2$ to $I = 1 \times 10^{12} \text{ A/m}^2$ .....	94
Figure 6-13 Bottom layer and top layer domain wall shape and magnetization angle during movement of $J_{ex} = -0.05 \text{ mJ/m}^2$ and $J_{ex} = -0.2 \text{ mJ/m}^2$ at $I = 1 \times 10^{12} \text{ A/m}^2$ .....	96
Figure 6-14 Upper layer magnetization angle $t$ and bottom layer magnetization $b$ during motion at $I = 1 \times 10^{11} \text{ A/m}^2$ , $I = 3 \times 10^{11} \text{ A/m}^2$ , $I = 6 \times 10^{11} \text{ A/m}^2$ , and $I = 10 \times 10^{11} \text{ A/m}^2$ . The size of the dot is representing the velocity of the domain wall. The exchanging stiffness is fixed at $J_{ex} = -0.2 \text{ mJ/m}^2$ .....	97
Figure 6-15 Bottom layer and top layer domain wall shape and magnetization angle during movement at $I = 1 \times 10^{11} \text{ A/m}^2$ and $I = 1 \times 10^{12} \text{ A/m}^2$ with fixed $J_{ex} = -0.2 \text{ mJ/m}^2$ .....	98
Figure 6-16 Comparison of from Upper layer magnetization angle $\theta_t$ and bottom layer magnetization $\theta_b$ for different $J_{ex}$ and current, (a) Fixed $I = 1 \times 10^{11} \text{ A/m}^2$ with $J_{ex}$ various from $0.2$ to $-0.2 \text{ mJ/m}^2$ (b) fix $J_{ex} = -0.2 \text{ mJ/m}^2$ and change the current from $I = 1 \times 10^{11} \text{ A/m}^2$ and $I = 1 \times 10^{12} \text{ A/m}^2$ .....	99

Figure 6-17 Comparing the domain wall configuration at (a) $J_{ex} = 0.1 \text{ mJ/m}^2$ and (b) $J_{ex} = -0.2 \text{ mJ/m}^2$ . The different color representing the same domain wall at different time under $I = 1 \times 10^{12} \text{ A/m}^2$ . .....	100
Figure 7-1 Simulation set up for different exchanging coupling cases. ....	103
Figure 7-2 (a) Current and velocity relation for different ex- changing coupling state films. Simulation set up for different cases (b) $J_{ex} = 0.6 \text{ mJ/m}^2$ (c) $J_{ex} = -0.6 \text{ mJ/m}^2$ (d) $J_{ex} = 0 \text{ mJ/m}^2$ and (e) $J_{ex} = -0.2 \text{ mJ/m}^2$ .....	105
Figure 7-3 (a) Sketch of the Pt/FM/Au/FM/Pt stack. The black arrows indicate magnetization orientation inside the two layers (b) Series of images showing skyrmion shift along the track between 3 ns, $j = 3.9 \times 10^{11} \text{ A/m}^2$ electric pulses. Scale bar, 500 nm. Reprinted with the permission from A. Hrabec <i>et al.</i> , <i>Nat. Commun.</i> , vol. 8, Jun. 2017. Ref.[33] .....	106
Figure 7-4 Schematic diagram for skyrmion memory. (a) The skyrmion are annihilated at the edge of PMA wires due to Magnus force. (b) The skyrmion moves in a straight line in SAF wire. Replotted with the permission from R. Tomasello <i>et al.</i> , <i>J. Phys. D: Appl. Phys.</i> , vol. 50, no. 32, Jul. 2017. Ref.[34] .	108
Figure 7-5 (a) Schematic illustrations of DWs in the upper (UM) and lower (LM) magnetic layers in perpendicularly magnetized with antiferromagnetic coupling (b) as a function of $t_{Ru}$ for 20 TaN 15 Pt 3 Co 7 Ni 1.5 Co  $t_{Ru}$ Ru 1.5 Co 7 Ni 1.5 Co 50 TaN. Orange and blue shaded regions correspond to SF ( $J_{ex} > 0$ ) and SAF ( $J_{ex} < 0$ ), respectively (c) Kerr microscope images of a single DW moving along a nanowire formed from 20 TaN 15 Pt 3 Co 7 Ni 1.5 Co  $t_{Ru}$ Ru 1.5 Co 7 Ni 1.5 Co 50 TaN with and $t_{Ru} = 8$ (SAF) . Reprinted with the permission from S.-H. Yang, K.-S. Ryu, and S. Parkin, <i>Nat. Nanotechnol.</i> , vol. 10, p. 221, Feb. 2015. Ref. [35] .....	110
Figure 7-6 Anomalous Hall voltage as a function of injected current density in the Ir layer with various external magnetic fields $H_x$ along the current direction. Bottom SAF is set as (a) $\rightleftharpoons$ , and (b) $\leftrightsquigarrow$ . Reprinted with the permission from Y. Liu, B. Zhou, and J.-G. (Jimmy) Zhu, <i>Sci. Rep.</i> , vol. 9, p. 325, 2019. Ref.[1] .....	112



## LIST OF SYMBOLS AND ABBREVIATIONS

1D, 2D, 3D: One-, two- and three-dimensional AHE: Anomalous Hall effect

AMR: Anisotropic magnetoresistance

ANE: Anomalous Nernst effect

CIDM: Current-induced domain wall motion DMI: Dzyaloshinskii-Moriya  
interaction DWM: Domain wall motion

FMR: Ferromagnetic resonance

iSGE: Inverse spin galvanic effect

LLG: Landau-Lifshitz-Gilbert (equation)

MRAM Magnetic random access memory

NM/FM: Nonmagnetic metal/ferromagnet

NM/AF: Nonmagnetic metal/antiferromagnet OOMMF:Object-Oriented

Micromagnetic Framework PMA:Perpendicular magnetic anisotropy

RF: Radio frequency

RKKY: Ruderman-Kittel-Kasuya-Yosida (interaction) SEM:Scanning electron  
microscope SGE: Spin galvanic effect SHE: Spin Hall effect

SOT: Spin-orbit torque

ST-FMR: Spin torque ferromagnetic resonance

STT: Spin transfer torque

TMR: Tunnelling magnetoresistance

## **CHAPTER 1. MOTIVATION**

In this chapter, the background and motivation of this thesis are discussed. The domain wall motion devices are first introduced along with discussions on various challenges and limitations in practical applications. Double-sided spin current injection could be a possible solution to some of the challenges. Understanding the interlayer interaction, especially exchanging coupling, in between the top and bottom magnetic layers hold key to practical implementation. The understanding of the physical outcome associated with the interaction is essential for extending the limit of the DWM based devices. It is this demand for insight understanding motivates our modeling study of the exchanging coupling effect in the symmetric dual magnetic layers system.

The outline of the thesis is also listed in the chapter.

### **1.1 Domain wall device**

Domain wall motion devices in confined geometrics are considered to play a significant role in next generation spintronics, including MRAM[1], racetrack memory[2], and mLogic[3]. All devices above need well defined domain wall configurations and fast and controllable domain wall motion[4]. Recently, researchers have come to realize that DMI in a magnetic thin film actually helps to achieve chiral domain wall and provide certain stability and controllability of domain wall motion [5]. This discovery along with the utilization of the Spin Hall effect

provides a new and efficient way for current driven domain wall motion which can be scaled along with the device physical dimensions [6]. In such a device, the domain walls store bits of information and are shifted by current. The shifted domain walls can be caught by the read head without the need to move physically any material. These memory and logic devices have spurred tremendous research, especially with a variety of materials selection and optimization for well-defined domain walls and fast domain wall motion. The critical parameters to be optimized are mainly domain wall lateral sizes, directly governing the possible information density, and domain wall movement and pinning/depinning processes that determine access time and energy consumption. One way to reduce access time and energy consumption is using the interlayer interaction in multilayer ferromagnetic/antiferromagnetic system, including exchanging coupling, dipolar interaction and stray field [7]. A better understanding of chiral magnetism, interlayer ferromagnetic structure interaction, spin-orbit phenomena, and the more complicated net effect will move the technologies advance and closer to industry. The ability to control and manipulate domain walls precisely opens up avenues to designing a range of novel and highly competitive devices.

## **1.2 Simulation for the domain wall motion**

Micromagnetic model has been widely used for research on magnetization phenomena between the quantum mechanical scale of individual atoms and the macroscopic scale. For the regime of this scale, there are many practical and

important applications, including spintronics, nanomagnetic logic devices and memory devices. In micromagnetics, the magnetization is treated as a continuous vector field with constant magnitude. The dynamics of magnetization is governed by the Landau–Lifshitz–Gilbert (LLG) equation. [8][9]

A free software of micromagnetic simulation first became available to public in 1998 when Object Oriented MicroMagnetic Framework was released . Since then, numerical simulation packages have been available for researchers, either commercially or freeware[10][11]. There are many motivations to perform micromagnetic research, including (1) to confirm or interpret experimental results, (2) to test or optimize a device design, (3) to predict new phenomena, and (4) to validate (approximate) analytical theories. For instances, micromagnetic simulations can be performed before conducting expensive or time-consuming experiments. It enable researchers to navigate the parameter space when we design the experiments. Micromagnetic simulations also gives us opportunities to explore physical phenomena that may not be easy to access experimentally. Micromagnetic modeling could also provide us in-depth understanding of the phenomena under study. In the investigation presented here, we use micromagnetic simulations to study domain wall formation and current/field-induced domain wall motion.

In order to have micromagnetic simulation study to provide us correct understanding of the principle behind various phenomena that we study, we need to first validate the model as well as obtain clear understanding as we can various

parameters over a relative broad region. This has been the guideline for the research presented throughout this thesis.

### 1.3 Motivation

The improvement of semiconductor fabrication and information technology creates a predicament between shrinking device size and increasing information needed for storage. The next generation of the information storage system, like racetrack memory and magnetic random-access memory, needs to be energy-efficient and high speed. Therefore, Current-induced domain wall motion in perpendicular magnetocrystalline anisotropy (PMA) multilayer has attracted extensive research interest. [12], [13] It usually consists of a thin ferromagnetic layer which is sandwiched by heavy metals (HM), including Pt[14], W[15], [16] and Ta[17]. This structure can induce a high effective field ( $\gg 10 \text{ Oe}/10^{11} \text{ A/m}^2$ ) while obtains high velocities ( $400 \text{ m/s}$ )[18]. It shows great potential as a candidate for replacing conventional hard disk devices[19][20].

In perpendicular magnetic systems without interfacial interaction or free of external field, Bloch walls, in which the magnetization rotates within the wall plane, are more energetic favorable[21]. In contrast, the Néel walls, in which magnetization rotates perpendicular to the plain, are energetically favored types for ultra-thin films[22][23]. However, the Néel wall can be formed by either applying external magnetic fields[24] or by the existence of an anisotropic interfacial Dzyaloshinskii-Moriya exchange interaction (DMI). [25][26]

Compared to spin-transfer torque, spin-orbit torques caused by the Spin Hall effect (SHE) need much lower current to drive the domain wall. [27]–[34] However, SHE cannot move Bloch type of domain walls in symmetric Pt/Co/Pt multilayer[35], because the inner magnetization is parallel to the polarization of SHE current from heavy metal[36]. To break the symmetry, some research have sandwiched the Co layer with different heavy metals, for instance, Pt and Ta. [37] Breaking the symmetric film stack introduces DMI at the Co interface, which stabilized the domain wall as a Néel wall with chirality. Chiral Néel wall has been widely proven that can be driven by the Spin Hall effect in different materials system, both theoretically and experimentally[38][39] In other words, both chirality and the Spin Hall effect are essential to domain wall motion.

Moreover, along with the chirality and Spin Hall effect, exchanging coupling can optimize the domain wall motion in the synthetic antiferromagnetic magnetic system (SAF)[2][40]. SAF usually consists of two layers of ferromagnetic layers and a non-magnetic spacer layer. It can be represented by Heavy metal/Ferromagnetic metal/Spacer/Ferromagnetic metal/(Heavy metal). In this system, the domain wall can be driven more efficiently and faster ( $750m/s$ ) compared to the single ferromagnetic layer system [39]. This is mainly due to the chiral Néel wall configuration and the exchanging coupling between FM layers[41] The interfacial and interlayer interactions are the critical parameters of the DW dynamic in the system.

All studies above are based on antisymmetric structure, while symmetric multilayers has not attracted any significant attention. Moreover, the SAF needs

specific materials as the insert layer to create AFM coupling between different layers, like Ru. However, it limits the selection of the material. On the other hand, a globally symmetrical situation of magnetic bilayer can also facilitate the domain wall velocity by controlling the domain wall chirality and energy. Due to the symmetric structure, the domain walls can be coupled by the strong stray field. The stray field further promotes the Néel walls with opposite chirality and reduce the domain wall energy. It will reduce the depinning field and accelerates the motion under low current. DMI and dipolar coupling are all favoring the different layer domain walls to move in the direction. Meanwhile, the dipolar coupling force them to act like one wall by coupling them together.[22][42]Hence, the symmetric structure might be a good candidate for a domain wall motion-related device, like racetrack memory and MRAM. For this reason, how the interfacial and interlayer interaction affects the domain wall statically (chirality) and dynamically (motion velocity and configuration) an intriguing topic to investigate. Here, we perform a serious of computational studies on magnetic layer domain wall motion, to understand the role of interfacial interaction, interlayer interaction and Spin Hall effect in this symmetric thin-film system.[1], [15]

## 1.4 Outline

**Chapter 1** raises the introduction and motivation of our work. At the end of the chapter, we give the hypothesis of this work. **Chapter 2** introduce the background of our study. **Chapter 3** demonstrate the verification of the simulation tool. After

that, the simulation and experiment result of our study is the following. **Chapter 4** is the single-layer magnetic domain wall motion under current or magnetic field simulation results. **Chapter 5** and **Chapter 6** is the simulation result double magnetic layer domain wall motion with FM and AFM RKKY effect, respectively. The relation between our experiment and reported result is demonstrated in **Chapter 7**. The last chapter, **Chapter 8**, is the comparison with reported work and summary, and the experimental result can direct further research.

## **CHAPTER 2. BACKGROUND**

In this chapter, we discuss the fundamentals of the ferromagnetic system, domain walls, chiral magnetism, and the dynamics of domain wall motion. All these concepts are important for understanding the behavior of magnetic domain walls formation and their movement. In addition, the fundamentals of micromagnetic theory are also included in the sections to follow.

### **2.1 Energies of ferromagnetic system**

In this section, the energy terms are discussed based on the classical theories of magnetism. The transformation of energy term to an effective field term is also demonstrated.

Micromagnetic simulation is a continuous description of ferromagnetic materials that exhibit spontaneous magnetization under the critical temperature. [43]–[49] In most of the cases, the magnetic materials consist of numbers of magnetic domains that have uniform magnetization. Between these domains, there are narrow regions that magnetization orientation rotates inside. These regions are called domain walls. In order to describe such entities, the static magnetic energy needs further discussion. In ferromagnetic materials, both internal and external interaction has influences on the total magnetic energy in the system. A magnetic state corresponds to a local minimum of the total energy of the system. For the magnetic thin film, this magnetic energy comes from Zeeman energy,

demagnetizing energy, magnetocrystalline anisotropy, and exchange energy, which will be described below.

### 2.1.1 Zeeman energy

External magnetic fields are often used to manipulate the magnetization of ferromagnets. In this thesis, all the external field are treated as spatially uniform, because the ferromagnets are small. The energy caused by the external magnetic field is known as Zeeman energy. The Zeeman Energy is due to the interaction between the external magnetic field and internal magnetic moment. The external magnetic field will align the magnetization to the field direction. It can be described as the following equation:

$$E_{Zeeman} = -\overrightarrow{H_{ext}}(i) \cdot \overrightarrow{M} \quad (.)$$

where  $\mu_0$  is the magnetic permeability of vacuum,  $\overrightarrow{H_{ext}}$  is the external magnetic field,  $\overrightarrow{M}$  is the magnetization. The magnetic field is the derivative of the energy by the magnetization, which is shown following:

$$\overrightarrow{H_{Zeeman}}(i) = \frac{\partial E_{Zeeman}(i)}{\partial \overrightarrow{M}_i} = \overrightarrow{H_{ext}}(i) \quad (.)$$

In the simulation tool we used, the external field is directly adding to the effective field.

### 2.1.2 Exchange Energy

The exchanging energy is caused by the magnetization coupling of two near atoms. There are two alignment configurations, anti-parallel and parallel, for anti-ferromagnetic coupling and ferromagnetic coupling, respectively. Exchanging energy can be written as follows:

$$E_{ex}(\vec{r}) = A \left( \left( \frac{\partial m_x}{\partial x} \right)^2 + \left( \frac{\partial m_y}{\partial y} \right)^2 + \left( \frac{\partial m_z}{\partial z} \right)^2 \right) \quad (.)$$

where  $A$  is the exchanging stiffness constant of the materials which is proportional to its Curie temperature. Positive  $A$  favors the ferromagnetic coupling while the negative one favors the anti-ferromagnetic coupling. By nature, the exchanging interaction is isotropic, which means there is no favorable orientation of the magnetization along the crystal axis. The exchange interaction is isotropic, resulting in no preferential orientation of the magnetization for the crystal axis.

In a discretized computational model, the partial derivatives in equation 3 have to be replaced by finite different quotients. The effective exchanging coupling energy can express as following:

$$E_{ex}(i) = -\frac{2A}{M_s^2 a^2} \vec{M}_i \cdot \sum_{n.n} \vec{M}_j \quad (.)$$

where  $A$  is the exchanging stiffness,  $M_s$  is the saturation magnetization,  $a$  is the center to center spacing of two neighboring domains and  $\vec{M}_i$  is the magnetization of  $i$ th cell. The effective field is

$$\vec{H}_{ex}(i) = -\frac{\partial E_{ex}(i)}{\vec{M}_i} = \frac{2A}{M_s a^2} \sum_{n.n} \vec{m}_j \quad (.)$$

where A is the exchanging stiffness,  $M_s$  is the saturation magnetization, a is the center to center spacing of two neighboring domains and  $\vec{m}_j$  is the unit magnetization of j<sup>th</sup> cell. In the case that there is interlayer exchanging coupling between two different materials, the energy term can be re-modeled as:

$$E_{ex}(i) = -\frac{\sigma S}{V_i} (\vec{m}_i \cdot \vec{m}_j) \quad (.)$$

where  $\sigma$  is the interfacial exchange stiffness, S is the area of the interface and V is the volume of the grain. The effective field is calculated as

$$\vec{H}_{ex}(i) = -\frac{\partial E_{ex}(i)}{\vec{M}_i} = \frac{\sigma}{M_s(i)t_i} \vec{m}_j \quad (.)$$

where  $M_s(i)$  and  $t_i$  are the saturation magnetization and thickness of the layer to which the i-th grain belong, respectively.

In mumax3, the effective field of exchanging energy between the n region is expressed as following:

$$\vec{H}_{ex} = 2 \frac{\frac{A_{ex1}}{M_{sat1}} \frac{A_{ex2}}{M_{sat2}}}{\frac{A_{ex1}}{M_{sat1}} + \frac{A_{ex2}}{M_{sat2}}} \sum_i \frac{(\vec{m}_i - \vec{m})}{\delta_i^2}$$

where  $A_{ex1}$  and  $A_{ex2}$  is the exchanging stiffness of two neighboring cells,  $M_{sat1}$  and  $M_{sat2}$  is the saturation magnetization of neighboring cells, and  $\delta_i$  is the cell size.

### 2.1.3 Magneto-static Energy

There are different names for the magnetostatic interaction. Here we call it stray field outside the ferromagnet and demagnetizing field inside. Magnetostatic interaction energy expresses the magnetic interaction between two magnetic dipoles. In a ferromagnetic system, each magnetic moment act as a dipole that produces a field experienced by other magnetic moments. Therefore, the nearest dipoles try to minimize its energy by antiparallel to each other. It is worth to mention that the exchange and magnetostatic energy are competing. In a ferromagnet, exchanging interaction usually tries to align the near moments in the same direction, while the magnetostatic interaction forms oppositely aligned moments. Hence, the size of the domains is a result of the strength ratio of these two interactions. Moreover, comparing to local exchange interaction, the magnetostatic field is global, which means it is the sum over the contribution of all the magnetic moments in the ferromagnetic system. The computation is much more time consuming than other terms. Mathematically, demagnetizing field can be expressed as

$$\vec{H}_{dem}(i) = \int \int \int \nabla \cdot \vec{M}_j \frac{\vec{r}_{ij}}{r_{ij}^3} - \int \int \vec{n} \cdot \vec{M}_j \frac{\vec{r}_{ij}}{r_{ij}^3} d^3\vec{r}_j \quad (.)$$

where  $\vec{M}_j$  is the magnetic moment of the j-th grains and  $\vec{r}_{ij}$  is the vector pointing from the mesh points of i-th grain to those of the j-th grains. In the model, the magnetic moment is uniform within so the first term on the right-hand side is literally zero. The expression can also be expressed as:

$$\vec{H}_{dem}(i) = - \int \int \vec{n} \cdot \vec{M}_j \frac{\vec{r}_{ij}}{r_{ij}^3} dS_j = - \sum_j \vec{D}_{ij} \cdot \vec{M}_j \quad (.)$$

where  $\vec{D}_{ij}$  is the magnetostatics interaction matrix where it only depends on the geometry of the mesh array and the mesh shape. The demagnetizing field does require heavy computation for uniform magnetization, contrary to the general case of nonuniform magnetization. The tensor  $\vec{D}_{ij}$  is diagonal if expressed on the basis of the principal axes:

$$D = \begin{pmatrix} D_{xx} & 0 & 0 \\ 0 & D_{yy} & 0 \\ 0 & 0 & D_{zz} \end{pmatrix} \quad (.)$$

The demagnetizing coefficients are all positive and the trace of them is equal to 1. The calculation of demagnetizing coefficient is well known. For instance, due to symmetry, for sphere magnet,  $D_{xx} = D_{yy} = D_{zz} = 1/3$ . In our simulation, we only study the continuous thin film. In this case,  $D_{xx} = D_{yy} = 0$  and  $D_{zz} = 1$ .

#### 2.1.4 Magneto-crystalline anisotropy energy

In some certain crystals, the magnetic energy is lower if the magnetization is aligned to some specific crystal axes. The energy related to the phenomenon is called magneto-crystalline energy, or magneto-crystalline anisotropy. These specific axes are called easy axes, while the hard axes represent the crystal axes with the highest energy. The energy and preferential axes are both dependent on the system. It can be defined by the bulk of the material or the interfaces of layers. In a system with uniaxial crystalline anisotropy, the magneto-crystalline anisotropy energy can be written as:

$$E_{ans}(i) = K_U(i) \sin^2 \theta_i = K_U(i) \left(1 - (\vec{k}_i \cdot \vec{m}_i)^2\right) \quad (.)$$

where  $K_U(i)$  is the anisotropy energy constant in the  $i$ -th grain and  $\theta_i$  is the angle between the anisotropy easy axis and the magnetization direction. And  $\vec{k}_i$  and  $\vec{m}_i$  are the unit vectors of the easy axis orientation and magnetization. The effective field can be obtained by simple taking the derivative of the energy density with respect to the magnetization vector and then adding a negative sign. However, the expression of the effective field of the crystalline anisotropy is

$$\vec{H}_{ans}(i) = -\frac{\partial E_{ani}(i)}{\partial \vec{M}_i} = \frac{2K_U}{M_S} H_K(i) (\vec{k}_i \cdot \vec{m}_i) \vec{k}_i \quad (.)$$

where  $K_U$  is the uniaxial magnetocrystalline energy constant and the  $\theta$  is the angle between the magnetization and easy axis. For instant, hexagonal cobalt the values are:  $K_{U1} = 4.1 \times 10^5 \text{ J/m}^3$  ( $4.1 \times 10^6 \text{ ergs/cc}$ ) and  $K_{U2} = 1.0 \times 10^5 \text{ J/m}^3$  ( $1.0 \times 10^6 \text{ ergs/cc}$ ).

In the Mumax3, the anisotropy field is expressed as following:

$$\vec{H}_{ans} = \frac{2K_{u1}}{M_s} (\vec{u} \cdot \vec{m}) \vec{u} + \frac{4K_{u2}}{M_s} (\vec{u} \cdot \vec{m})^3 \vec{u} \quad (.)$$

where  $K_{u1}$  is the first order anisotropy constant,  $K_{u2}$  is the second order anisotropy,  $\vec{u}$  is the unit vector indicating the anisotropy direction.

#### 2.1.4.1 Perpendicular magnetic materials

The magneto-crystalline anisotropy can be both originate from bulk and the interface. In our magnetic thin film system, the interface anisotropy is critical. The interfacial anisotropy may exceed the in-plane shape anisotropy and shift the easy axis from in-plane to out-of-the plane.

In the experiment, we only use thin films with perpendicular magnetic anisotropy. There are two main kinds of magnetic thin films we used. Pt/Co/Pt and Pt/Co/Ir. The perpendicular magnetic anisotropy mainly comes from the Pt/Co interface. The value of the anisotropy field is around 800mT. We can describe  $K_u$  for the system by the following equation:

$$K_u = K_v + \frac{2K_s}{t} = 2\pi M_s^2 + \frac{2K_s}{t} \quad (.)$$

where  $K_v$  corresponds to the volume anisotropy,  $K_s$  is the interfacial anisotropy, and  $t$  is the thin film thickness. If the interfacial anisotropy overcomes volume anisotropy, the easy magnetization axis is perpendicular to the magnetic thin film

surface. Furthermore, we can also reduce the magnetic layer thickness to increase the effective anisotropy. When the thickness reduces to the critical point, the easy axis will be perpendicular. It is well studied in many Co systems.

Furthermore, to simplifying the calculation, we usually use  $K_{eff}$  to describe the whole anisotropy, which includes magnetocrystalline, shape, and interfacial anisotropy. The relation of effective anisotropy ( $K_{eff}$ ) and saturation magnetization  $M_s$  can be used to calculate the anisotropy field ( $H_k$ ), using following equation:

$$\mu_0 H_k = \frac{2K_{eff}}{M_s} \quad (.)$$

Both of these relationships have been applied extensively in this thesis for the experimental characterization of magnetic properties and the modeling of chiral domain wall behavior.

## 2.2 Magnetic Domain and domain wall formation

The cross-section of a single ferromagnetic crystal with uniaxial anisotropy along its long axis is shown in Figure 2.1. If the spontaneous magnetization in the domains is parallel aligned with the easy axis, the anisotropy energy is minimum. Besides, the domains are formed to reduce the demagnetizing fields too. Figure 2.1 (a) is a saturated single domain with free magnetic poles on the surface. The magnetostatic energy is in the order of  $M_s^2$ , where  $M_s$  is the spontaneous magnetization. When the crystal subdivides into two domains with magnetization

in opposite directions, the total magnetostatic energy can reduce about a factor of two, shown in Figure 2.1 (b). The magnetostatic energy can further reduce by dividing the crystal into more parallel stripes. Comparing to the configuration in (a), the energy is reduced by about a factor of  $1/N$  ( $N$  is the number of stripes).

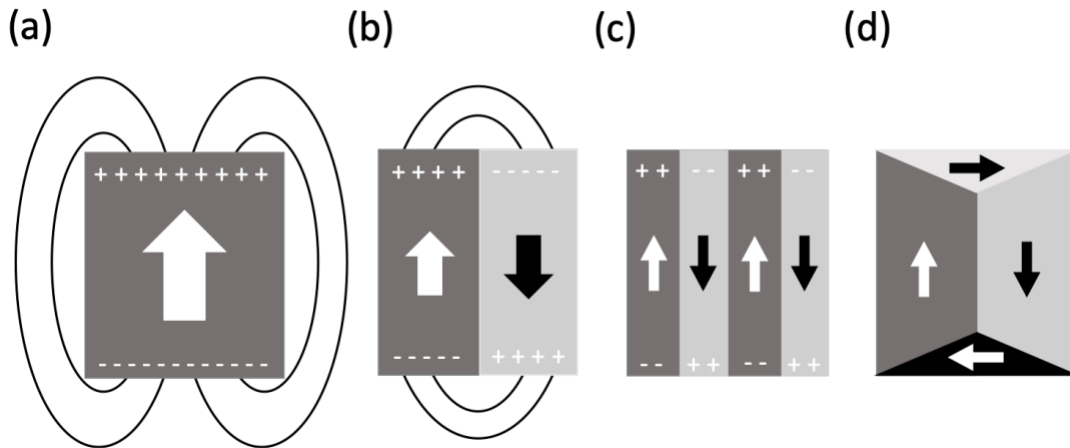


**Figure 2-1 The transition from single domain state to multidomain configuration to lower the total energy in magnetic system.**

To minimize energy, the final structure creates a small region between two domains where the magnetic spins transition from one orientation to the other. Domain wall introduces an extra energy term due to the contradiction to exchange interaction and anisotropy energy. However, it sharply reduces the demagnetizing energy making the configuration energy favorable. In the domain wall, the magnetization rotates gradually from one domain to the other. The domain wall width of  $\Delta$  is related to exchange energy and anisotropy, as shown:

$$\Delta \sim \sqrt{\frac{A}{K}} \quad (.)$$

where  $A$  is the exchanging stiffness and the  $K$  is the anisotropy. Exchange energy attempts to keep the nearest magnetic moment separated by small angles, which contribute to a large domain wall width. While large anisotropy energy will reduce the number of the magnetic moment which not aligns with the easy axis, hence reduces the width. The energy associated with the domain walls is in the order  $10^{-3} \text{ J/m}^2$  ( $1 \text{ erg/cm}^2$ ).

In the end, the reduction in magnetostatic cannot be further reduced because of the establishment of an additional domain wall. The subdivision process comes to an end at a certain point. The formation of closure domains on the surface reduces the free poles on the surface of the crystal. In this case, the component of the magnetization normal to the domain wall is continuous across the boundary by forming a 45 degree angle between domains and domain walls. However, the closure domains would increase the total energy because they align along the hard axes. It can be seen from this simple discussion that a number of factors are involved in any consideration of domains and the final configuration would be determined by minimizing the total energy, taking all the competing contributions into consideration.

### **2.3 Bloch wall and Néel wall properties**

Domain walls can be different of types depending on the way the magnetization rotates inside the domain wall. In my experiments, I only studied out-of-plane magnetic systems. Hence, the discussion on the DW presented in the coming section will be focused only on magnetic systems with out-of-plane magnetic anisotropy. In this case, the magnetization of the domains is directed either up or down. The magnetization inside the domain wall rotates from up to down or vice versa.

There are two main types of domain wall: Bloch walls and Néel wall, shown in Figure 2.2 For Néel wall, the magnetization rotates in the plane, while out to the plane for Bloch wall. Usually, the width of the domain wall is smaller than the width of nanowires in a perpendicular magnetic thin film. Besides, magnetization rotates along the domain wall width will cost more energy than perpendicular to the domain wall. Hence, in magnetic thin films, the domain wall favors the Bloch structure.

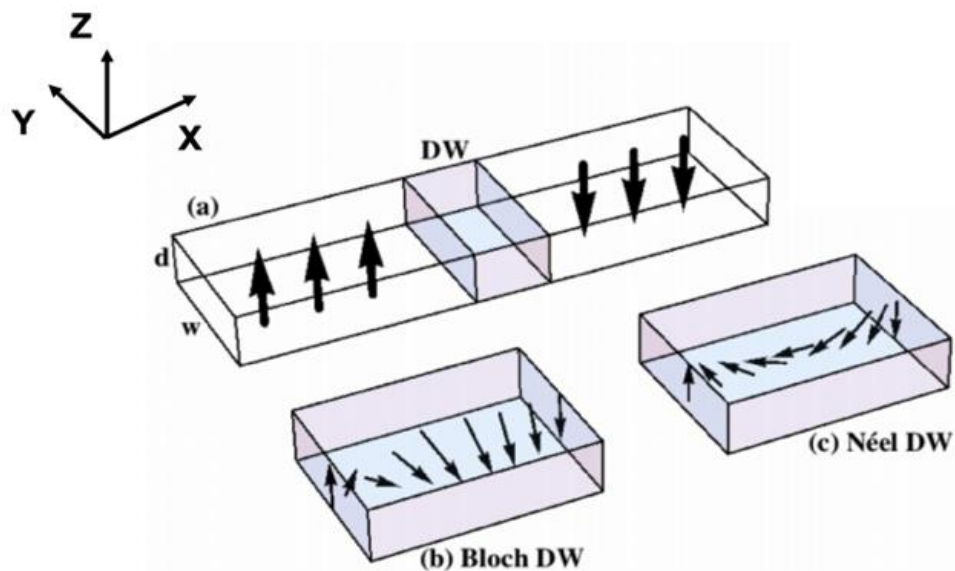


**Figure 2-2 (a) The schematic diagrams opposite magnetization domains with perpendicular anisotropy. b) The Néel DW. The magnetization inside the domain wall varies its direction along the DW length. c) The Bloch DW. The magnetization rotates out of plane to the DW length. Replotted from with permission from M. D. Dejong and K. L. Livesey, *Phys. Rev. B*, vol. 92, p. 214420, 2015. Ref.[50]**

The energy density can be described as the following equation:

$$\Delta_{Bloch} = 4 \sqrt{AK_{eff}} \quad (.)$$

where A is the exchanging stiffness and  $K_{eff}$  is the effective anisotropy. The domain wall width, or the length of the transition region is given by the equation:

$$\lambda_{Bloch} = \sqrt{\frac{A}{K_{eff}}} \quad (.)$$

## 2.4 Domain wall motion

Figure 2.3 presents the difference between two different kinds of domain wall motion, current-driven or field-driven. The field-driven domain wall motion mechanism is the reduce of Zeeman energy. The magnetization tends to point along with the direction of the field to minimize its energy. As a consequence, the domain expands or shrinks according to the external field.

On the other hand, the current-driven domain wall motion is due to the spin torque effects. The spins of the conducting electrons interact with the local magnetization and transfer their angular momentum. The magnetic field produces bidirectional

domain wall motion. The magnetic domain parallel to the external field is more energetically favorable and expand, while the antiparallel domains shrink. In this case, the two adjacent domain walls moves simultaneously and opposite to each other. For the case of current-driven motion, the domain wall motion is unidirectional. When current applied, the torque is acting on the domain wall and moves all the walls in the same direction. Eventually, the whole magnetic configuration shifted, and no domain expands or shrinks. Hence, there is no information loss in the current-driven domain motion case, which is essential for data storage. All the data can be retained and retreated during the motion in contrast with the field-driven domain wall motion

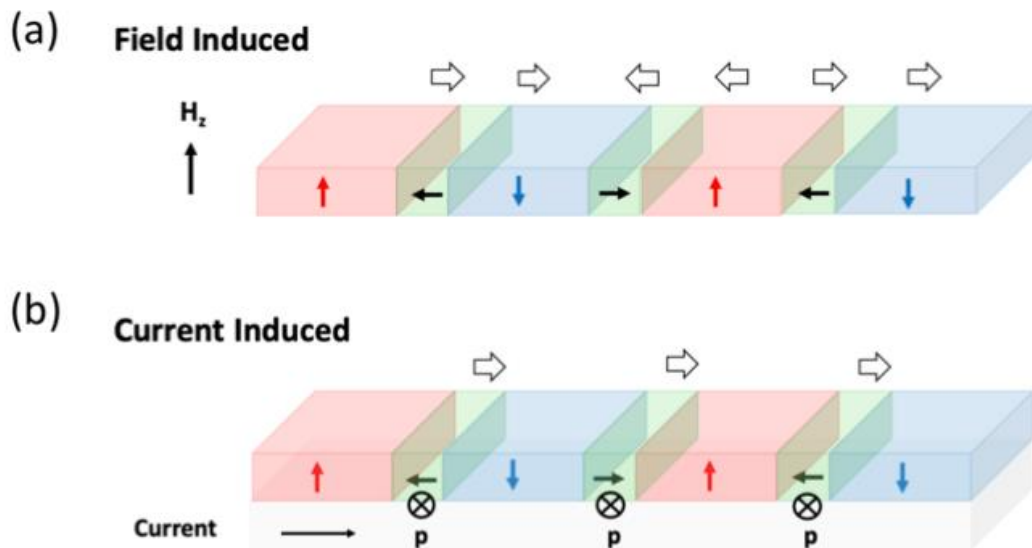


**Figure 2-3 The domain wall motion in nanowires in presence of a) an external field ( $H_z$ ) and b) an electric current ( $I$ ). The field induced domain wall motion results in expansion or contraction of the magnetic domains whereas the current induced domain wall motion results in the displacement of magnetic domains along the nanowire.**

## 2.5 Field Driven Domain Wall Motion

According to the discussion above, we can predict the energy and configuration of the static magnetic system. However, the energy terms cannot anticipate the dynamics of domain wall motion. The Landau-Lifshitz-Gilbert Equation (LLG) is used in micro-magnetic simulation models to predict the magnetic spin behaviors, and the Gilbert equation is described as following:

$$\frac{d\vec{M}}{dt} = -\gamma\vec{M} \times \vec{H} + \frac{\alpha}{M_s} \times \frac{d\vec{M}}{dt} \quad (.)$$

where  $\gamma$  is the gyromagnetic ratio,  $\alpha$  is the damping constant,  $\vec{M}$  is the magnetization vector,  $M_s$  is the saturation magnetization.

If we apply  $\vec{M} \times$  to both side of the Gilbert equation, we will get the LLG equation:

$$\frac{d\vec{M}}{dt} = -\frac{\gamma}{1 + \alpha^2} \vec{M} \times \vec{H} - \frac{\alpha\gamma}{(1 + \alpha^2)M_s} \times (\vec{M} \times \vec{H}) \quad (.)$$

The terms that make up the equation reflect the processes that occur when a magnetic moment switches, causing a change in orientation. The first term in the LLG equation describes the precession of magnetic moment around the effective field. If there is no energy dissipation, the magnetic moment precesses the field permanently. However, there is always a loss of energy during the switching process. It is described by the second term, which is the damping term of the LLG equation. This term makes sure the magnetic moment eventually aligns with the effective field. The LLG relationship shows that when an external field is applied,

a torque is produced to facilitate magnetization switching. Besides, in domain wall dynamics, the LLG equation is important to understand the propagation of domain walls.

### *2.5.1 Field induced domain wall dynamics*

The DW dynamics are relatively simple models even through the complexity of DW static magnetic texture. The static magnetization of the domain wall is fixed by all the energies discussed above, including anisotropy, exchange, and Zeeman energy. It is considered as constant when all the configuration and external field is set. The domain wall dynamic behavior was described by Walker. According to his model, the domain wall motion can primarily be classified into two categories: a steady-state regime and an oscillatory regime. Under low magnetic fields, the domain wall motion corresponds to steady state while the higher magnetic field corresponds to the oscillatory regime. The model can be seen in Figure 2.4. In the steady regime, the velocity of the domain wall increases linearly along with the magnetic field. However, when it reaches a critical field called Walker field, the inner magnetization of domain wall starts to oscillate, which sharply decrease the velocity. After the Walker breakdown, the domain wall motion becomes disturbed: the domain wall inner magnetization is no longer stable but continuously rotates from Bloch to Néel back and forward. The DW motion also changes back and forth in the oscillatory regime.

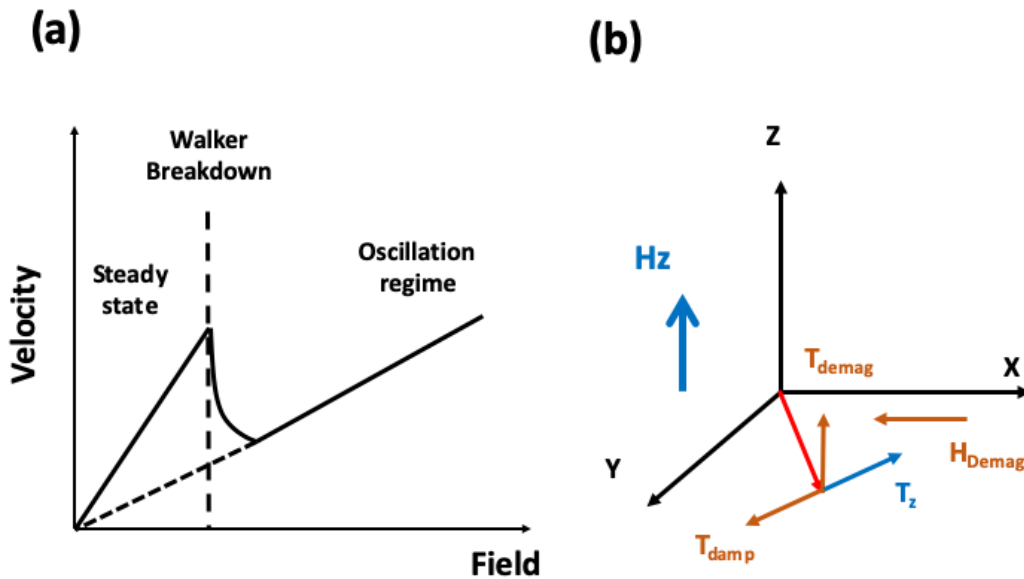


**Figure 2-4 (a)** The schematic diagram of the velocity versus the applied external field amplitude. The velocity shows two linear regimes, the steady state regime and the oscillatory or turbulent regime, separated by the Walker breakdown at field  $H_w$ . **(b)** Schematics of the different torques acting on a single magnetization at the center of the Bloch domain wall. The applied field ( $H_a$ , shown in blue) is associated with a torque  $T_a$  that rotates the magnetization in the plane and creates an in-plane dipolar field ( $H_{Demag}$  shown in green). The damping torque  $T_{Damp}$  associated to the motion induced by  $H_{Demag}$  then compensates  $T_a$ . Finally,  $T_{Demag}$  pulling the magnetization out of plane results in the domain wall motion.

There are two different main torques that determine the DW motion behaviors: the damping torque and the demagnetization torque. When an external field is applied ( $H_a$ ), the Bloch wall inner magnetization rotates in the XY planes according to  $H_a$  and its related torque  $T_a$ . It also produces a dipolar field  $H_{Demag}$  at the edges of the domain wall because of the magnetization changes. The  $H_{Demag}$  produces a torque at the Z-axis ( $T_{Demag}$ ) and changes the magnetization towards out of plane. However, the in-plane torque ( $T_{Damp}$  created by  $T_a$  damping) is also acting on the magnetization.

At equilibrium, they compensate, providing a steady in-plane angle for the magnetization. The DW velocity is given by  $T_{Demag}$  at this regime.

However, when the magnetic field continuously increases, the in-plane magnetization remains to rotate and increases  $T_{Demag}$ . The torque reaches the maximum when the in-plane angle of magnetization  $\theta = 45$ . After that, the  $T_a$  is no longer compensated by the  $T_{Damp}$ , and the magnetization starts to precess. The precession causes the turbulent of DW motion and the back and forth of the displacement. The domain wall motion is also smaller compared to the steady regime.

### *2.5.2 Creep and flow regimes of the domain wall motion*

The domain wall motion can be classified into three regimes: the creep regime, the depinning regime, and the flow regime. At the low magnetic field, the domain wall motion is negligible. The behaviors can be described as the elastic interface driven by force in the presence of weak disorder. This is the creep motion regime. When increasing the field with the thermal fluctuations, the depinning field drives the domain walls from the defects. The velocities increase sharply at this regime. This is the depinning regime. In the flow regime, the magnetic field frees the domain wall motion, and the domain wall becomes independent of the pinning defects. The domain wall motion velocity becomes linear.

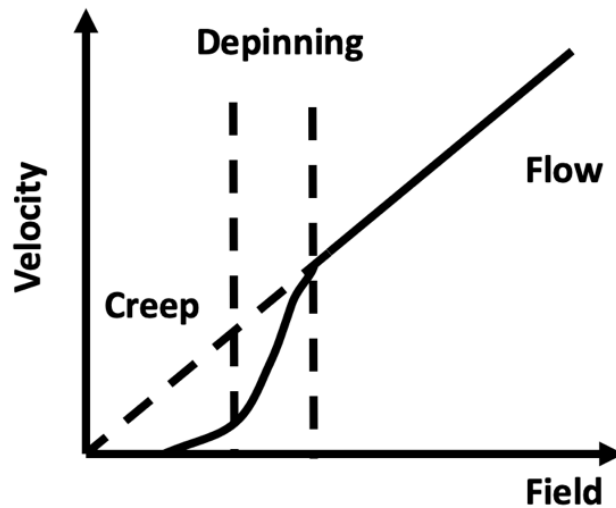


**Figure 2-5 Three regimes of DW dynamics driven by a magnetic field and/or spin-polarized current. Replotted with the permission from S. Emori and G. S. D. Beach, *J. Phys. Condens. Matter*, vol. 24, no. 2, Jan. 2012. Ref. [51]**

## 2.6 Current induced domain wall motion

Domain wall can be moved by both the magnetic field ( $H_{ext}$ ) and electrical current ( $I$ ). The domain wall can be moved towards either along or against the current. There two main types of torque involved: Spin-transfer torque (STT) and Spin-orbit torque (SOT).

### 2.6.1 Spin transfer torques

When a spin-polarized current flows through a magnetic material sample, the magnetization of the materials will tend to align with the spin direction. The main

mechanism behind this phenomenon is the conservation of angular momentum and the exchange between electrons and magnetic moments. The current will apply a torque on the magnetization which called STT. Fig 2.6 shows the process of how STT changes the magnetization of the ferromagnetic layer.

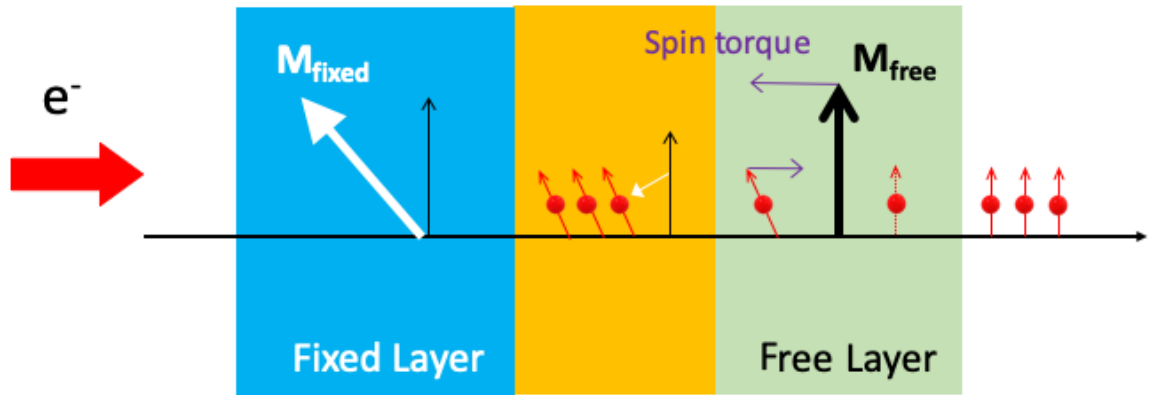


**Figure 2-6 Spin polarized current flows through the magnetic layer and change its magnetization.**

If the current flows through a magnetic nanowire containing a domain wall parallel to the wire cross section, the spin of the conduction electrons interacts with the magnetization of magnetic domain wall. Two torque terms model this interaction: an adiabatic term and a non-adiabatic term,

$$\left(\frac{\partial \vec{M}}{\partial t}\right)_{STT} = -(\vec{u} \cdot \nabla) \vec{m} - \beta \vec{m} \times [(\vec{u} \cdot \nabla) \vec{m}] \quad (.)$$

$\vec{u}$  is the unit velocity representing the spin polarized current density  $J_{app}$

$$\vec{u} = -\frac{g\mu_B P}{2eM_s V_s} J_{app} \quad (.)$$

where  $g = 2$  is the Landé factor of the free electron,  $\mu_B$  is the Bohr magneton,  $P$  is the current polarization fraction ( $0 < P < 1$ ). and  $e$  is the electron charge. The first term of the equation is adiabatic term and the second term is non-adiabatic term. It representing the current induced torque acting on the non-uniform or spatially varying magnetization. Naturally, this two torque are mutually orthogonal. In an adiabatic process, the electron angular momentum transfer to local magnetization of the wall. The non-adiabatic term may arise from linear momentum transfer, spin-flip scatter and spin relaxation. In general, the adiabatic STT is to distort the shape of the domain wall, while the non-adiabatic STT is express a pressure on the wall and induces its motion.

There are two main properties for domain wall motion that are important for applications: DW speed and current threshold required for the depinning of the DW. Usually, STT based DW motion need a large current to overcome the pinning potential usually caused by materials imperfections. However, increasing the current will generate joules effect which can damage the sample. Hence, an alternative mechanism to increase the DW speed rise more attention.

### 2.6.2 Spin hall effect and spin-orbit torque

Spin Hall effect (SHE) is one way of generating spin-polarization current which analogous to Hall effect. It is a transport phenomenon of current passing through

heavy metal or other materials like topology insulator due to spin-orbit coupling. When the current goes through, the lateral surfaces of the sample will accumulate spin with the opposite sign at different surface boundaries. Figure 2.7 shows the Spin Hall effect for a FM/HM/FM system.

Comparing to STT, the spin-orbit torque (SOT) does not require electron get polarized by passing any media. The angular momentum can be transferred from electron to the magnetization through spin-orbit interaction. Hence, SOT does not limit by the magnetic textures and maximum spin polarization.

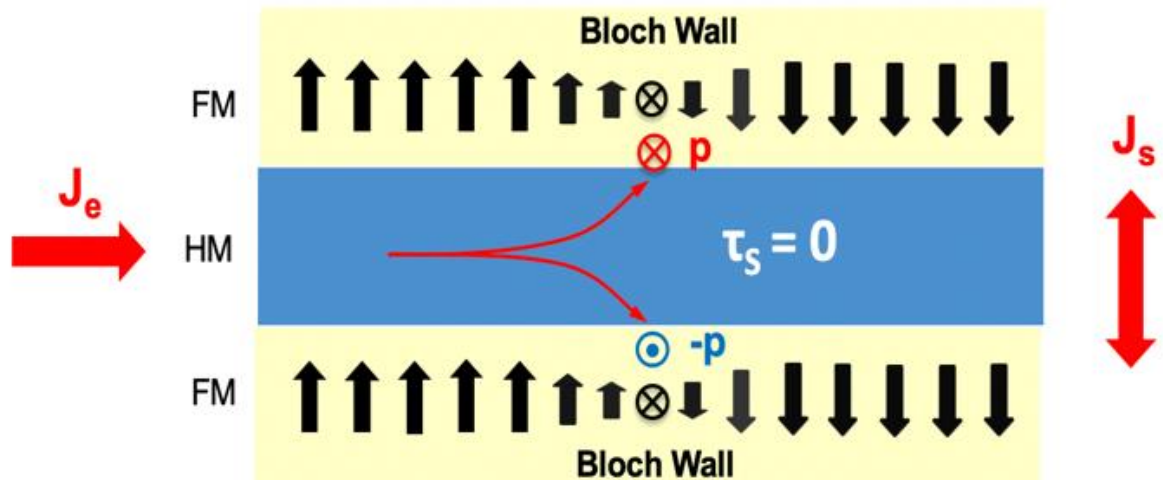


**Figure 2-7 Spin hall effect in FM/HM/FM system. When the current goes through the heavy metal, spin current with different polarization is injected into the FM layers.**

Spin current density can be written in the form as following:

$$J_s = \theta_{SH}(\sigma \times J_c) \quad (.)$$

where  $\theta_{SH}$  is the spin Hall angle,  $\sigma$  is the spin moment and  $J_c$  is the current density.  $\theta_{SH}$  is a material's property which is unique for different materials. For example,  $\theta_{Pt} = 0.2$  in our study.

Similar to STT, the SHE induced SOT can be mathematically expressed by followed equation.

$$\tau_{SHE} = -\frac{\hbar J_{HM} \theta_{SH}}{2eM_s t_{FM}} (\vec{m} \times (\vec{m} \times \vec{\sigma})) \quad (.)$$

where  $J_{HM}$  is the current density,  $\theta_{SH}$  is the spin Hall angle,  $t_{FM}$  is the ferromagnetic materials thickness,  $\vec{m}$  and  $\vec{\sigma}$  is the magnetization and current polarization direction respectively, and  $\hbar$  and  $e$  are reduced Plank constant and elementary constant.

## 2.7 Dzyaloshinskii-moriya interaction

The exchange interaction discussed above determines the magnetic configuration of bulk materials. The energy is minimized when the individual magnetic spins align parallelly or anti-parallelly. More recently, there is another exchange interaction called Dzyaloshinskii-Moriya interaction, or the antisymmetric exchange, arising a lot of research attention. The effective field of DMI can be described in the Mumax3 simulation tool as following:

$$H_{DMI} = \frac{2D}{M_{sat}} \left( \frac{\partial m_z}{\partial x}, \frac{\partial m_z}{\partial y}, -\frac{\partial m_x}{\partial x} - \frac{\partial m_x}{\partial y} \right) \quad (.)$$

where  $D$  is the DMI constant,  $M_{\text{sat}}$  is the saturation magnetization. By engineering the magnetic film stacks, the asymmetric film stack removes the inversion center of the bulk materials and introduce antisymmetric exchange at the interface. However, due to the short-range nature of exchange interaction, the magnetic film layers need to be extremely thin.

When interfacial DMI is introduced in a system, the Dzyaloshinskii-Moriya vector is adjusted to account for the new geometry:

$$\vec{D}_{ij} = -D_{\text{int}}(\vec{r} \times \vec{z}) \quad (.)$$

where  $D_{\text{int}}$  is a material dependent constant,  $r$  corresponds to the vector separating two neighboring spins and  $z$  corresponds to the vector perpendicular to the film surface. This interaction gives rise to unique spin textures and chiral domain walls, an important part of this thesis work to be discussed later in the document

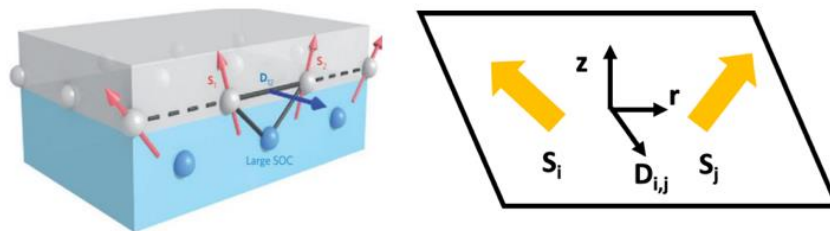


**Figure 2-8 Spin canting and interfacial DMI induced by structural asymmetry and its coordinate system. Replotted with the permission from A. Fert, V. Cros, and J. Sampaio, *Nature Nanotechnology*, vol. 8, no. 3. Nature Publishing Group, pp. 152–156, 2013. Ref. [52]**

### 2.7.1 Chiral domain wall structure due to DMI

In a magnetic thin film with perpendicular anisotropy, the magnetocrystalline anisotropy energy is more favorable for Bloch domain wall structure. It is due to the thickness of the domain wall is small. The demagnetization energy of domain wall is much lower when the magnetization of domain wall oriented out of the plain (Bloch wall), comparing to in the plain (Néel wall). As discussed above, we need an external in-plane field to move the Bloch wall besides current. However, for the application aspect, the external magnetic field is difficult to implement in the CMOS devices.

DMI effect can generate an effective in-plane field. The DMI can tilt two adjacent spins creating chirality, which is similar as an external magnetic field. Furthermore, the DMI effect is not strong enough to change the ferromagnetic order, and it mainly changes the configuration of the domain wall. Figure 2.9 represents three different scenarios. Figure 2.9(b) shows the domain wall structure of magnetic thin film without DMI. The domain wall is a Bloch wall. For negative DMI constant, it stabilizes the domain wall as right-handed Néel wall, while positive DMI constant rises a left-handed domain wall, which is shown in Figure 2.9(a) and Figure 2.9(c). With DMI, the chiral domain wall can be driven by the Spin Hall effect.

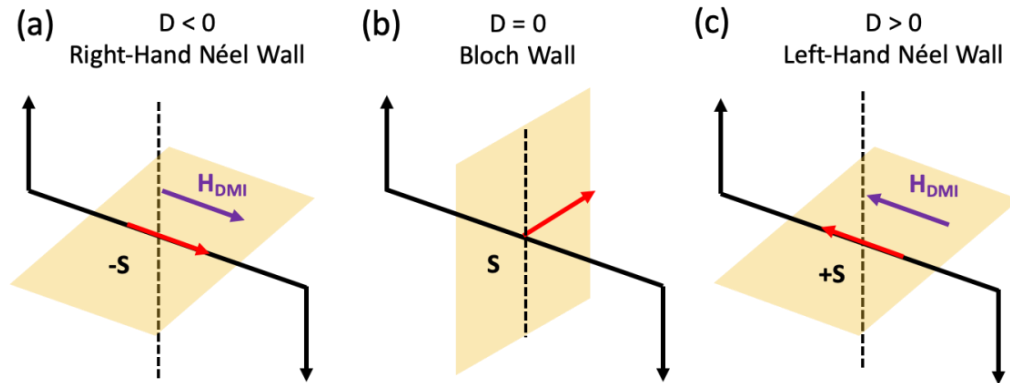


**Figure 2-9 Top and side view for domain wall configuration of different DMI sign. (a) domain wall configuration when  $DMI < 0$  (b) domain wall configuration when  $DMI = 0$  (c) domain wall configuration when  $DMI > 0$**

### 2.7.2 SOT driven domain wall motion in the presence of DMI

Spin Hall effect and DMI are both unique material properties. By combining the two effects together, we can control the domain wall motion under sets of conditions. Unlike STT devices, which the domain wall can only move against the current direction, SOT driven domain wall motion can either move along or against the current because of the different spin Hall angle. Figure 2.10 shows the possible combination of DMI and SOT and their outcome of domain wall motion direction after spin transfer.

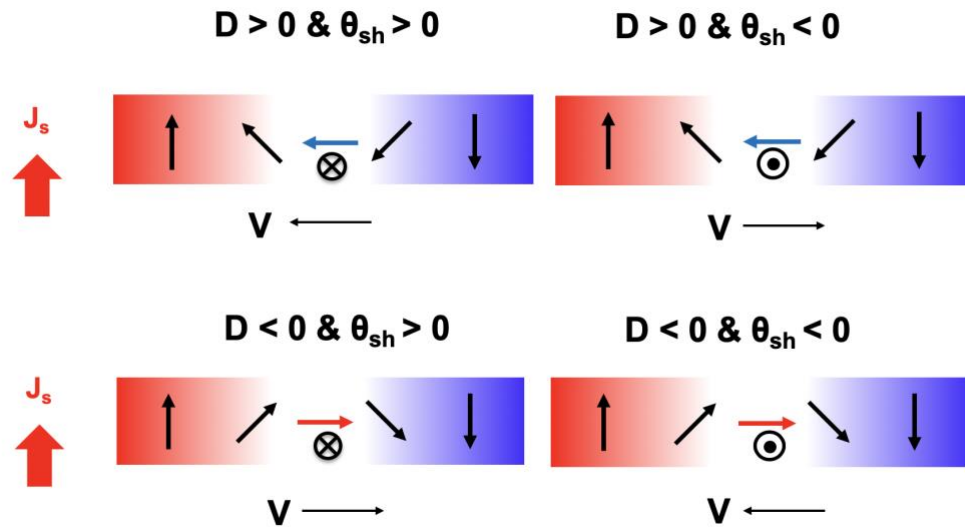


**Figure 2-10 Possible DMI, chirality and SOT combination. The black arrow is the original spin orientation while the white arrow is the orientation under the effect of SOT**

## 2.8 Ruderman–Kittel–Kasuya–Yosida Intercation

Ruderman–Kittel–Kasuya–Yosida (RKKY) refers to a coupling mechanism of the magnetic moment. It's an indirection exchange interaction between localized magnetic moments in metals. It's first to rise to explain the unusually broad unclear spin resonances in metallic silver. It uses a second-order perturbation theory to describe an indirect exchange coupling. It is also found in many ferromagnetic multilayer systems with nonmagnetic space layers like Ir, Ru, and Cu. Figure 2.11 shows the exchange coupling strength oscillates with the thickness of spacer layer Ru.

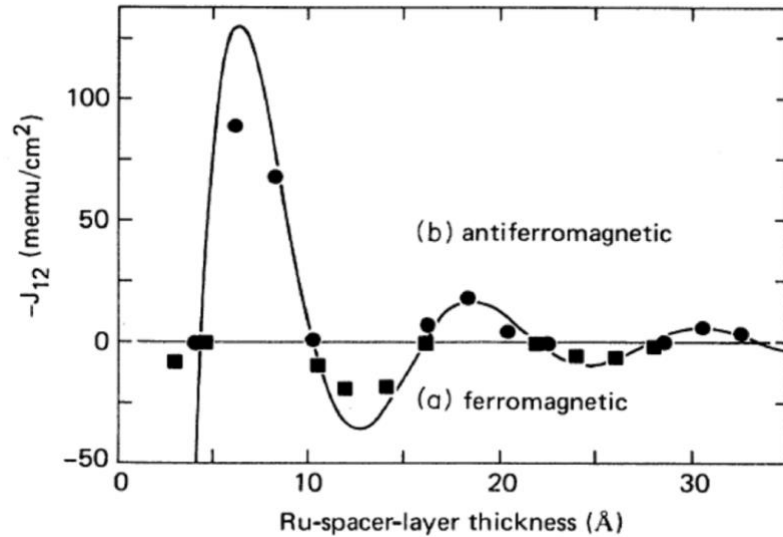


**Figure 2-11 Exchange coupling constant as a function of Ru thickness in Co|Ru|Co tri-layers. Reprinted with permission from S. S. P. Parkin and D. Mauri, *Phys. Rev. B*, vol. 44, no. 13, pp. 7131–7134, Oct. 1991. Ref. [53]**

## 2.9 RKKY interaction impact on multilayer system domain wall motion

For the application view of point, the storage density is limited by the dipolar coupling between the DWs. Using synthetic antiferromagnetic (SAF) structure can avoid dipolar coupling causing by DW stray magnetic fields. By RKKY interaction, an FM layer is coupled with another FM layer through ultrathin heavy metal like Ir or Ru. By tuning the thickness of breaking layer, the exchange coupling strength and sign can be altered. Figure 2.12 shows the two layers of FM with opposites magnetization which is stabilized by minimizing the exchange coupling energy. Besides, it will add an exchange coupling torque and increase the DWM velocities. The torque magnitude is proportional to the exchange coupling strength.

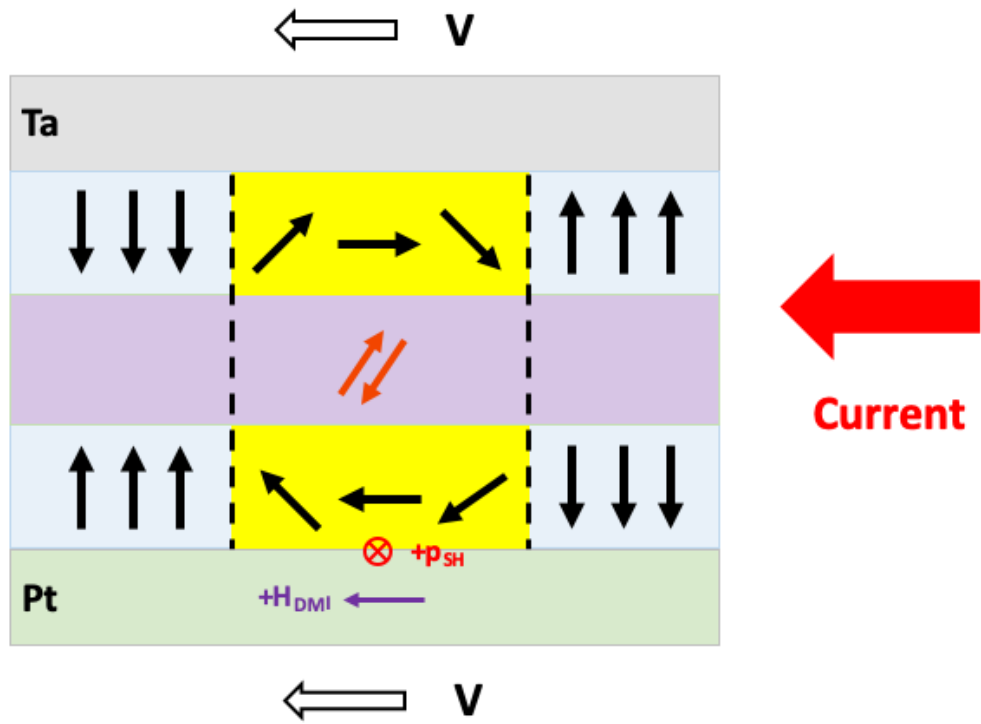


Figure 2-12 Schematic representing domains and DWs in antiferromagnetically coupled bilayer structures. Minimization of dipolar coupling between the DWs via flux closure in SAF structures. (Red arrows).

## **CHAPTER 3. SIMULATION TOOL VERIFICATION**

In this chapter, we are going to present some micromagnetic simulation for standard problems Mag modeling group by and external problems to verify the authentic of the simulation tool Mumax3. The reference solution is taken from uMag reported result and fundamentals of magnetism.

### **3.1 Simulation package**

Mumax3 [22] is a free software package developed by DyNaMat group of Prof. Van Waeyenberge at Ghent University. The model uses a graphical process unit (GPU) to utilize the finite difference method. It is generally faster and more efficient than computing processor unit (CPU)- based packages, like OOMMF. Mumax3 can solve time and space dependent magnetization evolution problems in nano to microscale. In our experiment, we use CUDA based NVIDIA Tesla K40c for our experiment. By using Mumax3, we conduct static and dynamics study in dual magnetic layer, including domain wall formation under DMI effect, single nanowires domain wall motion and multilayer domain wall configuration under RKKY and DMI effect.

### **3.2 Standard Problems**

### 3.2.1 Standard Problem 1

The first uMag standard problem is calculating the hysteresis loops of a 1x2 micrometer permalloy rectangle with 20 nm thickness. To simulate the permalloy, the materials parameter is set as following, exchanging stiffness  $A_{ex} = 1.3 \times 10^{-11} \text{ J/m}$ , saturation magnetization  $M_{sat} = 8 \times 10^5 \text{ A/m}$ , and uniaxial anisotropy  $K_{u1} = 5 \times 10^2 \text{ J/m}^3$ . The uniaxial easy axis parallel to the long edges of the rectangles. The external magnetic field applies along the easy axis from 50mT to -50mT. The initial magnetization state is shown in Figure 3.1(a), the same as the standard problem set up. The simulation result is shown in Figure 3.1 (b) and it is in good agreement with the reference result from mo96a shown in Figure 3.1 (c).

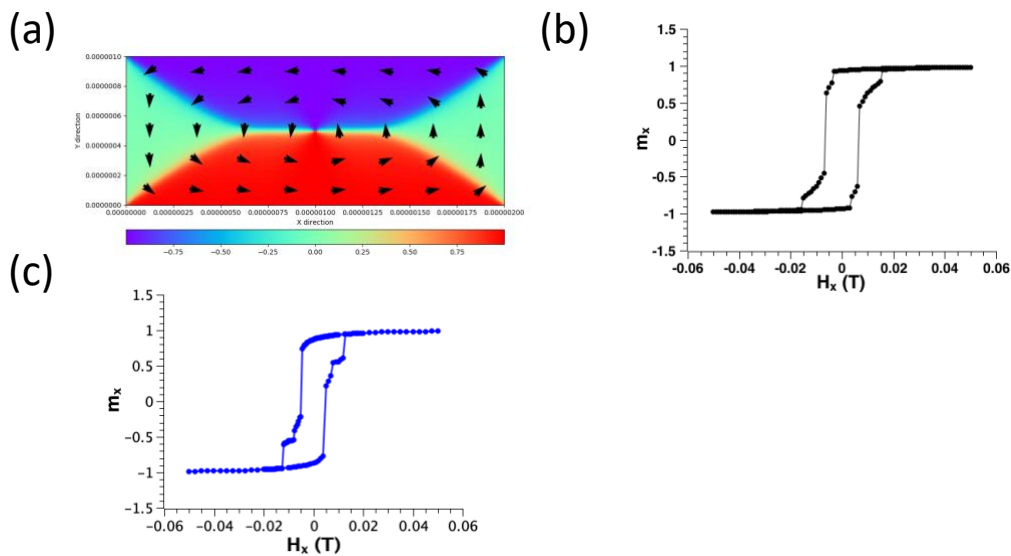


**Figure 3-1 Standard problem one: (a) initial vortex state of simulated permalloy rectangle, hysteresis loop of (b) Mumax3 simulation result and (c) reference solution from Mag website.**

### 3.2.2 Standard Problem 2

The second problem simulates the magnetization changes under magnetic field in [111] direction. The thin film has a width of  $d$ , length of 5 times and thickness  $0.1d$ . The simulation includes both magnetostatic and exchange energies but has the advantage of only one scaled parameter. If crystalline anisotropy is neglected and the geometry is fixed, scaling of the static micromagnetic equations (Brown's equations) yield a hysteresis loop which depends only on the scaled geometry to the exchange length when expressed as  $M/M_s$  versus  $H/H_m$ , where  $H_m = M_s$  (SI) or  $4\pi M_s$  (cgs/emu). The exchanging length  $l_{ex} = \sqrt{2A_{ex}/K_m}$  and magnetostatic energy density is  $K_m = 1/2\mu_0 M_s^2$ .  $A_{ex}$  is the exchange stiffness and  $K_m$  is the magnetostatic energy. The field is fixed at [1,1,1] direction. The simulation result of Mumax3 is shown in Figure 3.2. The result is consistent with the reported results. This problem is also a good test for the numerical integration of the Mumax3 demagnetizing kernel.

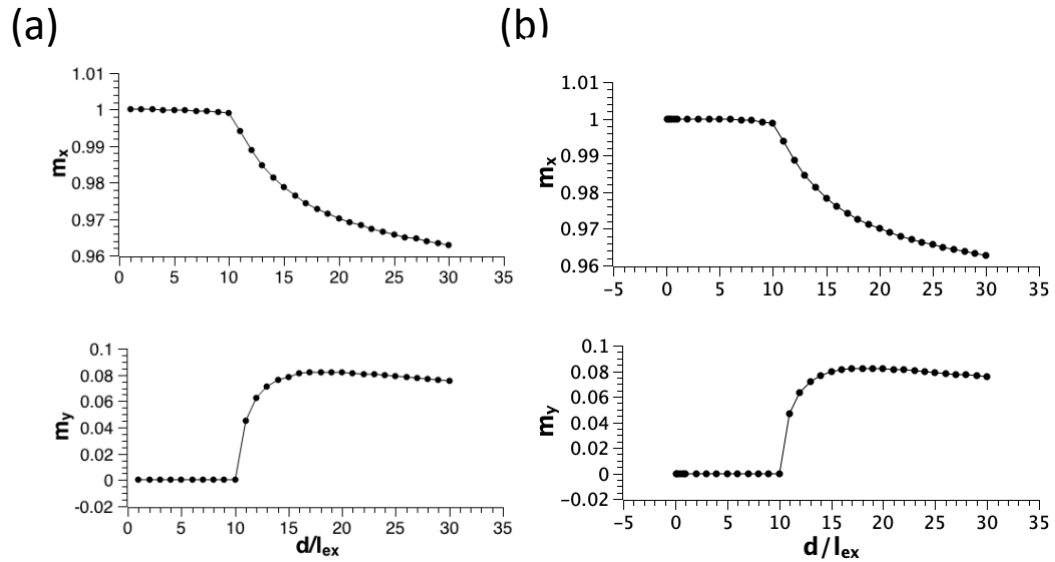


**Figure 3-2 Standard problem two: remanence for standard problem 2 as a function of the magnet size  $d$  expressed in exchange lengths  $l_{ex}$ .(a) Mumax3 (b) reported result from uMag**

### 3.2.3 Standard Problem 4

Standard problem four is a dynamic test of magnetization for a  $500 \text{ nm} \times 125 \text{ nm} \times 3 \text{ nm}$  Permalloy magnet. The materials parameter is following,  $A_{ex} = 1.3 \times 10^{-11} \text{ J/m}$ ,  $M_{sat} = 8 \times 10^5 \text{ A/m}$ ,  $K_{U1} = 0$ . The initial state is saturated along (1,1,1) direction and then reversed by field (-24.6, 4.3, 0) mT. The  $M_y$  data is compared with the reported result in Figure 3.3.

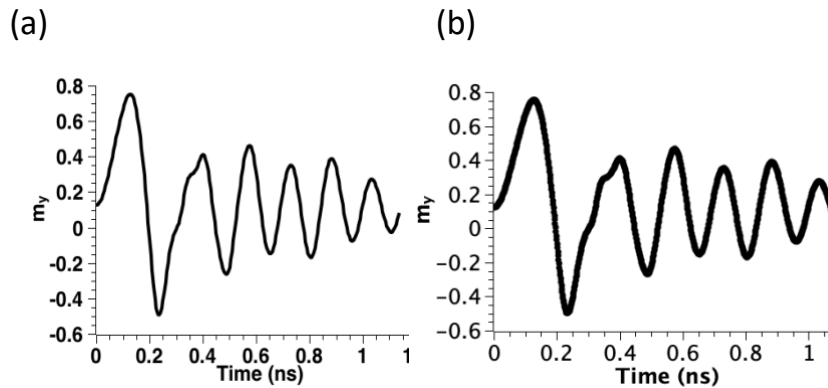


**Figure 3-3 Standard problem four: simulation result for  $m_y$  (a) Mumax3 (b) reported result from uMag**

#### 3.2.4 Standard Problem 5

This problem serves as a test of proper basic functioning of those micromagnetic solvers that include the effects of spin momentum transfer between in-plane polarized spin current and spatial patterns of magnetism. A  $100 \text{ nm} \times 100 \text{ nm} \times 10 \text{ nm}$  permalloy square with an initial vortex texture is used in the simulation. The materials parameter includes,  $A_{\text{ex}} = 1.3 \times 10^{-11} \text{ J/m}$ ,  $M_{\text{sat}} = 8 \times 10^5 \text{ A/m}$ ,  $K_U = 0$ ,  $\alpha = 0.1$ ,  $\xi = 0.05$ . An x-axis spin current  $j = 10^{12} \text{ A/m}^2$  is applied and drive the vortex to move and then relaxed. The obtained final state of magnetization is shown in Figure 3.4. It agrees well with the reported result.

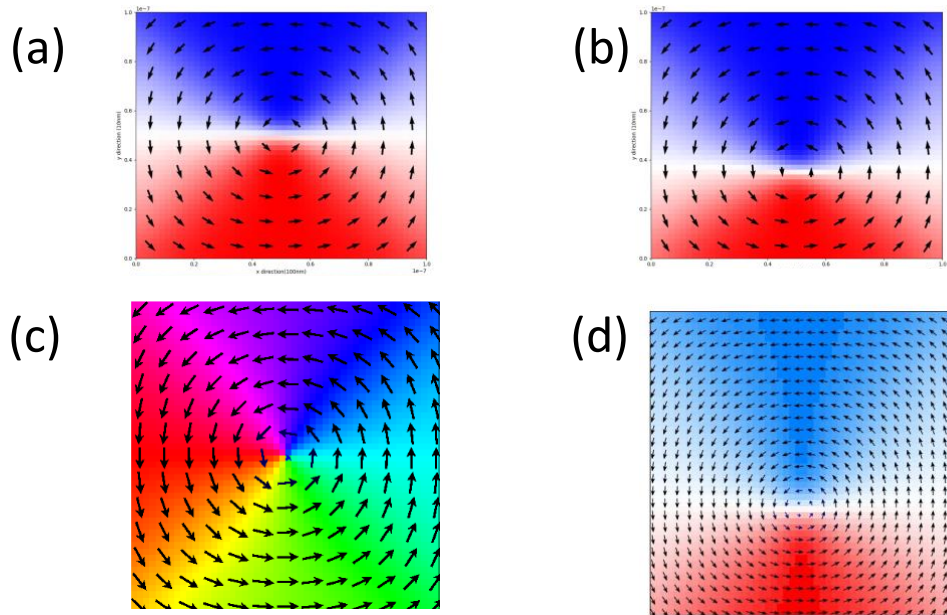


**Figure 3-4 Standard problem five: simulation result of Mumax3 (a) initial, (b) after current and reported result (c) initial, (d) after current from uMag**

### 3.3 External Problems

#### 3.3.1 Domain wall width and energy

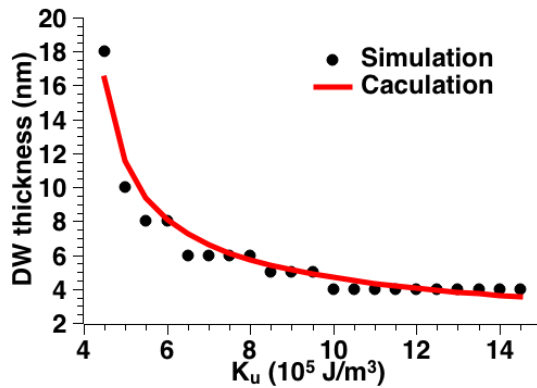
In this test, we take into account the demagnetization field and anisotropy. A thin film of  $128 \text{ nm} \times 68 \text{ nm} \times 1 \text{ nm}$  is used in the simulation. ( $M_{\text{sat}} = 8 \times 10^5 \text{ A/m}$ ,  $A_{\text{ex}} = 1.3 \times 10^{-11} \text{ J/m}$  and  $K_u$  range from  $4 \times 10^5 \text{ J/m}^3$  to  $14 \times 10^5 \text{ J/m}^3$ ). The easy axis is along the z-axis. The initial state of domain wall is Bloch wall, and the thickness of the wall can be calculated as following:

$$\lambda = \sqrt{A_{ex}/K_{eff}}$$

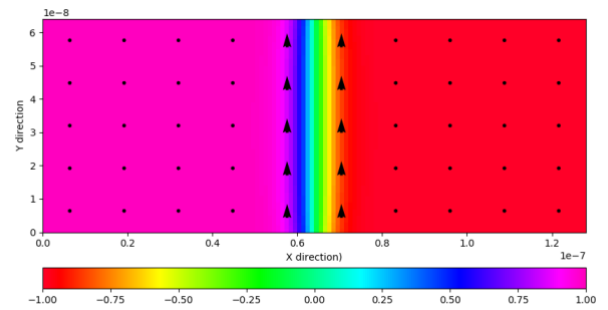
$$K_{eff} = K_u - \frac{\mu_0 M_{sat}}{2}$$

where  $\lambda$  is the domain wall width and  $K_{eff}$  is the anisotropy energy without demagnetization energy. The demagnetization energy is calculated according to thin film configuration. The simulation result and the calculated result is shown in Figure 3.5. The calculated result is represented in the red line and the simulation result is in black dots. The two results are a great match with each other.

(a)



(b)



(c)

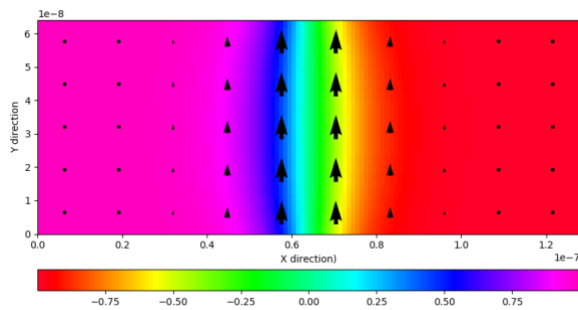


**Figure 3-5 (a)Simulation (black dot) and calculation (red line) result of domain wall width changes with the uniaxial anisotropy.(b) Magnetization image for the simulated thin film with  $K_{\text{eff}} = 10 \times 10^5 \text{J/m}^3$  and (c)  $K_{\text{eff}} = 5 \times 10^5 \text{J/m}^3$**

The next simulation is the comparison of domain wall energy for Bloch wall and Néel wall. The result is shown in Figure 3.6. We change the thin film thickness of  $t$  and  $K_{\text{eff}}$  to control the ratio between thin film thickness/domain wall width. For the Bloch wall, the domain wall energy decreases with the  $t/t_w$  ratio increase, while the Néel wall energy increase with the ratio. The energy crossover between these two configurations happens around  $t/t_w = 1$ . This simulation result is consistent with the theoretical prediction.

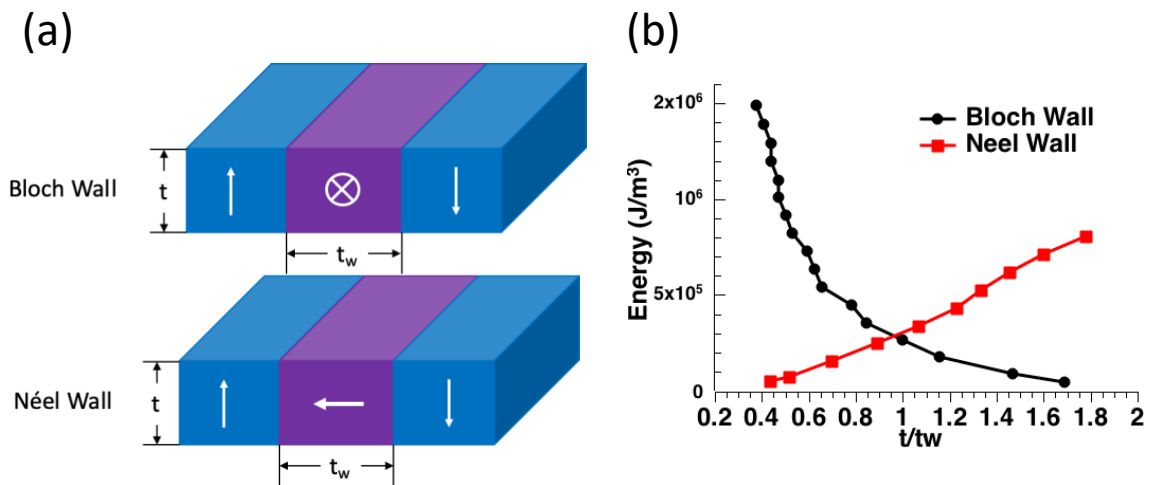


**Figure 3-6 (a)Simulation setup for domain wall for Bloch wall and Néel Wall. (b)simulation result of domain wall energy for both Bloch wall (black) and Néel wall(red).**

### 3.3.2 Dzyaloshinskii–Moriya interaction field

This problem is used to test the DMI field influence on domain wall configuration. The simulation is using a long nanowire thin film of  $1024 \text{ nm} \times 512 \text{ nm} \times 2 \text{ nm}$  with perpendicular uniaxial anisotropy. ( $M_{\text{sat}} = 8 \times 10^5 \text{ A/m}$ ,  $A_{\text{ex}} = 1.3 \times 10^{11} \text{ J/m}$  and  $K_u = 6 \times 10^5 \text{ J/m}^3$ ). In the first case, the DMI field in the x-direction is calculated as follows:

$$\mu_0 H_{DMI} = \frac{D_{ind}}{M_{\text{sat}} \lambda}$$

where is the DMI constant and  $\lambda$  is the width of the domain wall. In the first case, the DMI constant is set as  $D_{ind} = 0.1 \text{ mJ/m}^2$ . According to the calculation, the  $H_{DMI}$  should be around 16mT. In the simulation, we use an x-axis external magnetic field to compensate the  $H_{DMI}$ . The simulation result is shown in Figure 3.7. The initial domain wall is set as a Bloch wall. The Figure 3.7 (a) is the relaxed domain wall configuration. It is a canted domain wall with inner magnetization around 45 degrees. After applying the external magnetic field  $H_x = 15 \text{ mT}$ , the domain inner magnetization angle is shifted to align with the y-axis, which is close to the initial point. The  $H_{DMI}$  is equal to the external  $H_x$  at this point. It is matching with the calculation.

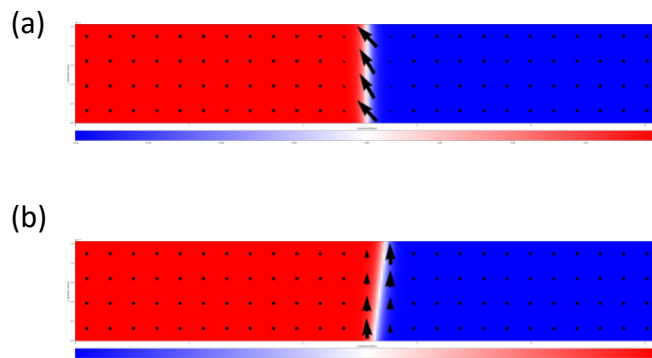


**Figure 3-7 Simulation result of domain wall configuration with external magnetic field in x axis (a)  $H_x = 0$ , (b)  $H_x = 15\text{mT}$**

### 3.3.3 Spin transfer torque domain wall motion

The last problem is used to test the simulation tool for using real experimental data. It simulates a domain wall driven by spin transfer torque in nanostrip. The STT driven domain wall motion data is taken from reported paper Jpn. J. Appl. Phys. 55, 093002 (2016) and the materials parameter is taken from PHYSICAL REVIEW B 70, 024417 (2004). In the experiment, the thin film stack is 50 Å Ta/15Å Au/3 Å Co/[7 Å Ni/1.5 Å Co]3/50 Å TaN. Hence, in the simulation, the grid is set as 4000nm 1000nm 2nm. The saturation magnetization and current polarization is linear superposition from reference. ( $M_{sat} = 8 \times 10^5 \text{ A/m}$ ,  $A_{ex} = 1.3 \times 10^{11} \text{ J/m}$  and  $K_u = 6 \times 10^5 \text{ J/m}^3$ ,  $P = 0.28$ ,  $\alpha = 0.1$ ,  $\xi = 0.05$ ). The simulation and reference data are shown in Figure 3.8. The red line is the simulation data while the experimental data taken from reference is representing as dots. The result is a great match with each other.

It proved that Mumax3 is a solid simulation tool for a real experiment.

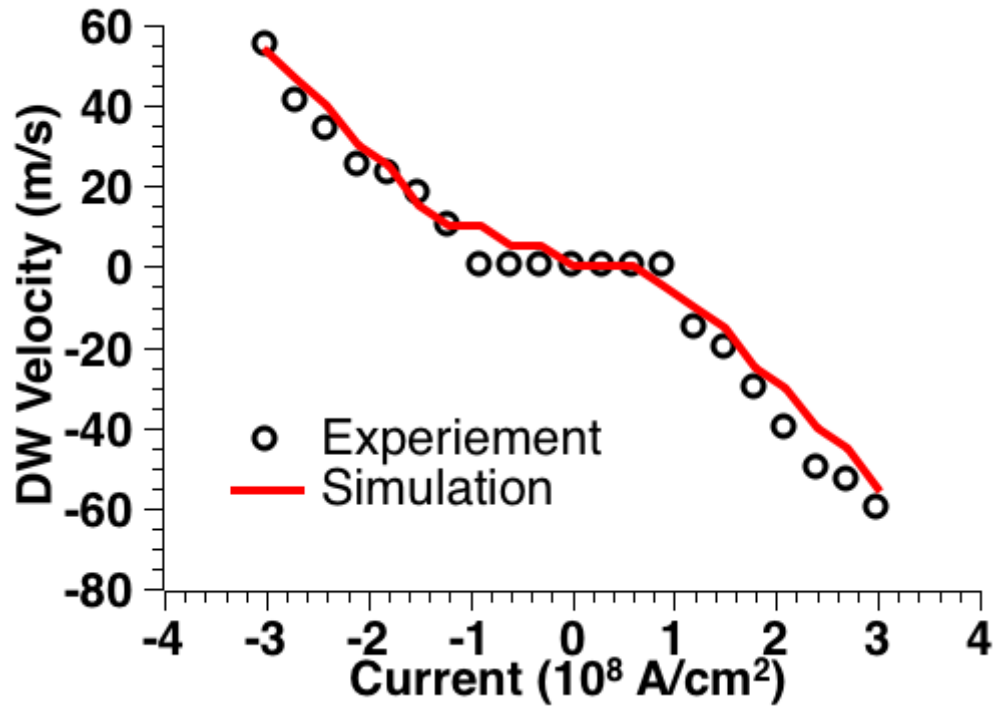


Figure 3-8 Simulation (red line) and experiment (black dot) result of spin transfer torque domain wall motion under electrical current.

## **CHAPTER 4. SIMULATION OF FIELD AND CURRENT**

### **INDUCED SINGLE CO LAYER DOMAIN WALL MOTION**

In this chapter, the single magnetic layer domain wall motion behavior is discussed. DW can be driven by either an external magnetic field or electrical current. These two different external sources of force cause DWM behaviors. The magnetic field driven domain wall motion is causing the domain to expand or shrink and then press the DW to move. On the other hand, the current induced domain wall motion is due to the angular momentous transfer from the polarized electrons to the spin. The polarized current creates a torque on the DW and drives the DW to move.

There are two main kinds of mechanism for inducing polarized spin current torque, spin transfer torque or spin orbit torque. Spin transfer torque is usually generated by passing a current through a thick magnetic layer and direct the current into a second, thinner magnetic layer. The polarized electrons from the first layer transfer angular momentous to the second layer spins and generate torque to change the orientation of the spins. This phenomenon is widely used in MRAMs. Another mechanism is spin orbit torque. In an HM/FM stack, when a current goes through the HM layer, polarized spins accumulates at the interface of HM/FM due to spin orbit coupling. The accumulation of spins creates a polarized spin current injecting into the FM and produces torque to change the FM layer magnetization. There are

two kinds of spin orbit torque, Spin Hall effect and Rashba effect. Here only spin hall effect induced torque is discussed in this thesis due to the narrative.

In this chapter, we first simulate magnetic field induce DWM of single magnetic layer with PMA. And then we demonstrate that Spin Hall effect induced domain wall motion need external field in x-axis to create torque and move the DW. We further simulate the Pt/Co and Co/Pt film stack with both DMI and PMA Spin Hall effect induced domain wall motion. In this system, Pt layer is both the spin current and DMI source, and the domains are in the Co layer. We hope in this chapter, the influence of DMI and spin hall on single magnetic layer DWM can be well addressed.

#### **4.1 Single Co layer domain wall motion induced by external field**

In the first section, we first simulate the DWM in a single Co layer induced by external perpendicular or in-plane field. With PMA, the DWs in the thin film tends to form a Bloch wall to minimize the system energy. As we discussed in Chapter 2, the domains tend to align with the external magnetic field to reduce the Zeeman energy. The external magnetic field will expand or shrink the domains and pushes the DWs to move. Here we first simulate the domain wall motion velocity and inner magnetization with either perpendicular or in-plane magnetic field. The initial state of the simulation a shown in the Figure 4.1. We also define up positive direction as shown in the Figure 4.1.

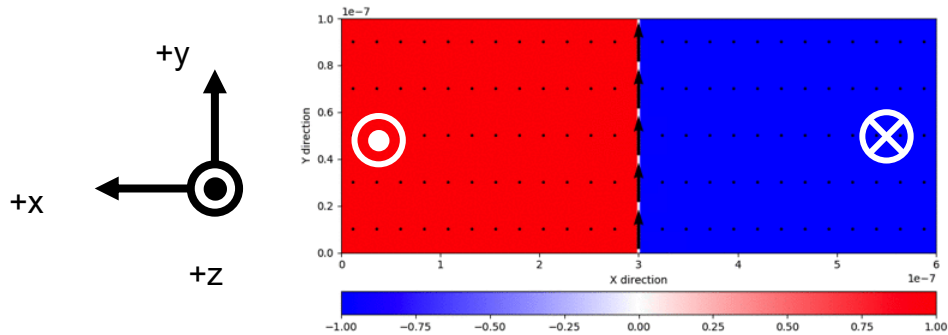


**Figure 4-1 Top view of initial state of domain and domain walls for the simulation. Red region representing up domain while the blue region is the down domain. The white region is the domain wall and the arrows are representing the inner magnetization of the domain wall.**

#### *4.1.1 Perpendicular field-induced domain wall motion*

As discussed above, domain walls can be moved by the external magnetic field because it expand or shrink the domains favoring the magnetic field direction before the walker breakdown. In the steady regime, the DW velocities increase linearly with the magnetic field. The inner magnetization angle rotates from 0 degree (Bloch wall) to 45 degree before oscillating clockwise or anticlockwise with negative or positive perpendicular magnetic field respectively.

Figure 4.2(a) provides the experimental data on Bloch wall motion induced by the perpendicular external magnetic field. We use the set up and the materials

parameters in Figure 4.1. The DW starts to move in negative direction when positive magnetic field applies. However, when the magnitude increase, DW motion starts to oscillate instead of moving toward the same direction. We have known that the domain wall inner magnetization is no longer stable but continuously rotates from Bloch to Néel back and forward after the Walker breakdown point. The DW motion also changes back and forth in the oscillatory regime. The simulation result is consistent to what we observed in experiment and reference. The same phenomena happen when we apply a negative perpendicular magnetic field, but only the domain wall moves in the opposite direction.

Another significant result of the DWM simulation is the relationship between domain wall velocity and domain wall inner magnetization angle, especially at the steady regime. The result is shown in Figure 4.2(b). When  $H_z$  increases, the domain wall inner magnetization angle shift from 90 degrees to nearly -145 or 45 degrees. If we continuously increase the magnetic field, the inner magnetization is no longer stable. Furthermore, the negative  $H_z$  drives the Bloch wall rotates clockwise, while positive  $H_z$  drives the wall rotates anticlockwise. The final angle is close to 45 degrees before Walker breakdown. The simulation result is pretty consistent with theoretical analysis.

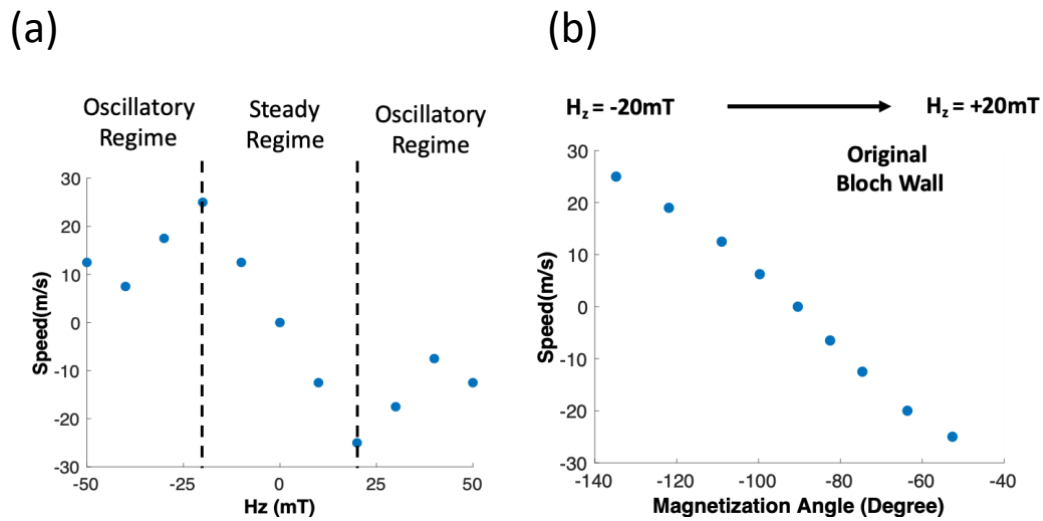


**Figure 4-2 Perpendicular field induced Bloch domain wall motion. (a) domain wall motion velocities and external z-axis field relation, (b) magnetization and velocities of domain wall in steady regime in (a)**

#### 4.1.2 In-plane field-induced domain wall motion

In this section, we find out, besides perpendicular field, DW can also be driven by in-plane magnetic field. The domain wall can stand higher external magnetic field compared to perpendicular magnetic field case without oscillation. The DWM velocities saturated at high magnitude magnetic field due to the inner magnetization align with the in-plane field.

We use the same initial state and materials parameter as the Figure 4.1 and apply external magnetic field in x direction. The simulation result is shown in Figure 4.3(a). Compared to perpendicular field, the domain wall can stand higher magnitude field. Hence, the domain wall velocity can be higher too. We apply a

magnetic field from -50mT to 50mT to study the velocities, and we did not observe oscillation in the simulation result. However, we observe the saturation of velocities at higher magnetic field in both directions. The inner magnetization is also stable compared to above case with perpendicular magnetic field shown in Figure 4.3(b). It is also obvious that the domain wall inner spins tend to align with the external in-plane field. In other words, negative  $H_x$  rotates the magnetization clockwise while the positive  $H_x$  rotates the magnetization anticlockwise. The saturation is due to the alignment of the spins at large magnetic field. Interestingly, when the magnetic field is small, the increase of domain wall motion velocity is linear.

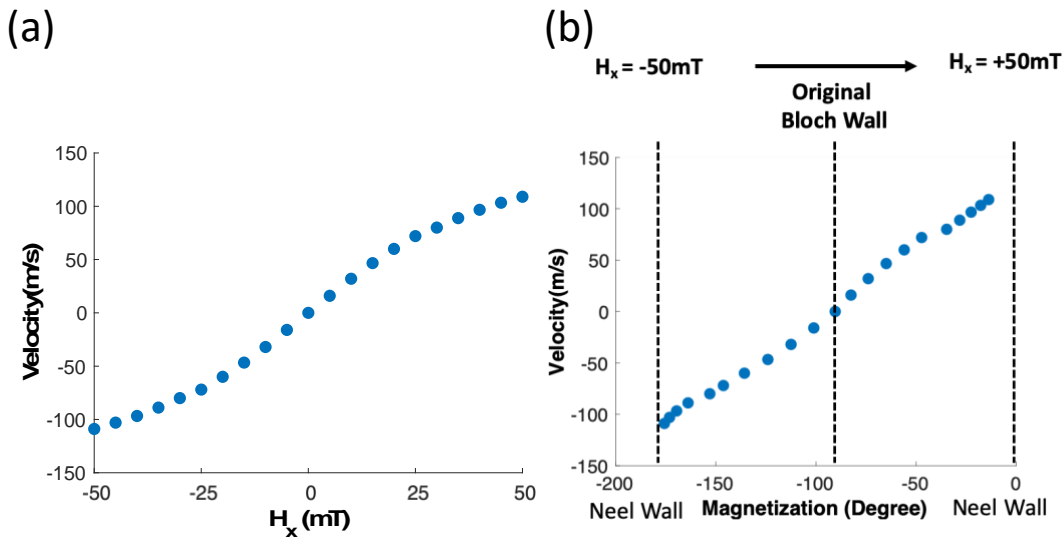


**Figure 4-3 In plane field induced Bloch domain wall motion. a)domain wall motion velocities and external x-axis field relation, (b)magnetization and velocities of domain wall**

## 4.2 Current induced single layer domain wall motion

As we discussed above, here we only investigated the Spin Hall effect, which creates spin current at the interface of NM/FM by the spin-orbit effect. Compared to spin-transfer torque, the spin-orbit torque needs much lower current to drive the domain wall. Besides, spin-orbit torque is not sensitive to the quality of the FM layer. Hence, the Spin Hall effect induced domain wall motion cause lot of research recently.

However, pure Spin Hall effect cannot drive the domain wall to move because the spin polarization direction align with the Bloch wall. However, combing with DMI effect, the domain wall can be moved. Furthermore, both DMI effect and Spin Hall effect is direction dependent. Hence, the simulation result of Pt/Co/Ta and Ta/Co/Pt is identical.

#### *4.2.1 In-plane field and Spin Hall effect induced domain wall motion*

By simulation, we find out that pure Spin Hall effect cannot driven the DMW motion on matter high large is the current. However, if we apply a magnetic field in x-axis and rotates the Bloch wall, the Spin Hall effect accelerate the DWM comparing to the case with only in-plane magnetic field.

In the HM/FM stack devices, the spin current accumulates at the interface due to the Spin Hall effect. The spin current injects into the upper magnetic layer along the z-axis from the heavy metal. It creates a field in the y-axis by transferring angular momenta. Since the field is parallel to the spins in Bloch wall, there is no

torque to drive the domain wall. Hence, without an external field to tilt the magnetization, the Bloch domain wall cannot be moved. As we discussed above, the in-plane magnetic field can shift the inner magnetization of the domain wall. Hence, we apply an in-plane external magnetic field with different amount and direction of current and study the domain wall behavior.

Figure 4.4 (a) is the model used in the simulation. The result of domain wall velocity with the different current and in-plane field is represented in Figure 4.4 (b). The map below illustrates the higher current and magnetic field both produce faster domain wall motion. More interesting, without a magnetic field, there is no domain wall motion at all which is represented the green area in the middle Figure 4.4 (b). For a certain strength of magnetic field, higher current increases the velocity. The same amount of current with different sign produces identical velocity. Further simulation results reveal the relative magnetization angle to the Bloch wall plays more important roles in the domain wall motion.

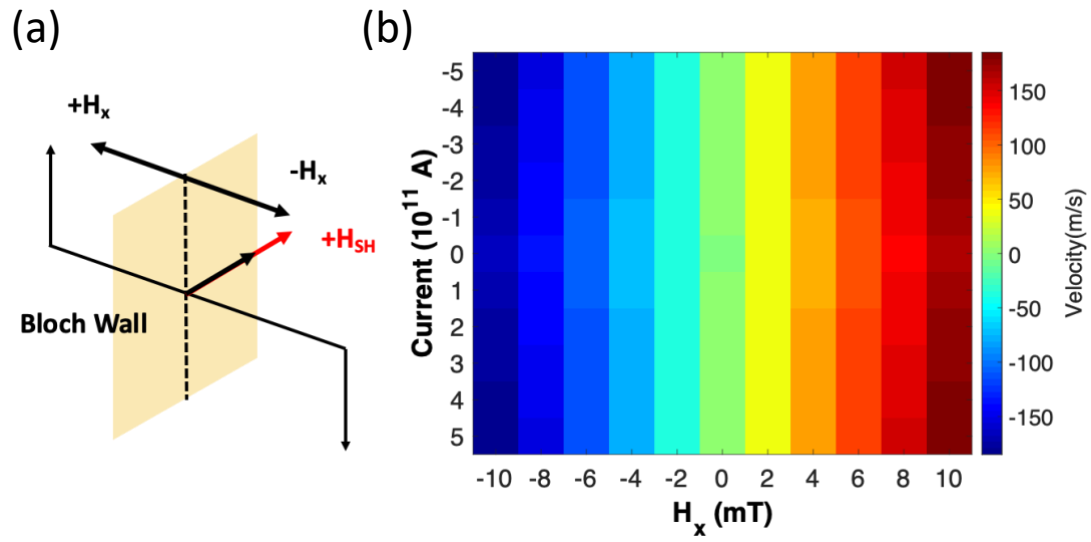


**Figure 4-4 In plane field and Spin Hall induced Bloch domain wall motion.(a) schematic diagram for the simulated in plane field and Spin Hall field (b)domain wall motion velocity map for different current and in plane field strength**

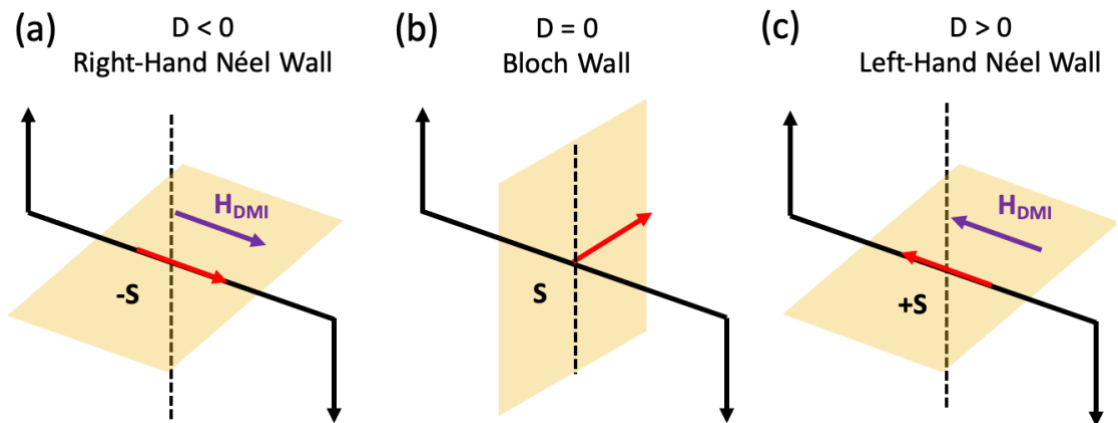
#### 4.2.2 Spin Hall induced chiral domain wall motion with DMI

DMI effect can induce an effective field in x-axis, which is similar to the influence of in-plane magnetic field. It will induce chirality for the domain walls and the chiral domain walls can be driven by Spin Hall effect. Here we demonstrate that positive DMI effect form left-handed Néel wall while negative DMI effect form right-handed Néel wall. Furthermore, the DMW velocities increase with DMI effect strength.

In a magnetic thin film with perpendicular anisotropy, it is more energy favorable to form Bloch domain wall structure. It is due to the small thickness of the thin film. The demagnetization energy of domain wall is much lower when the magnetization

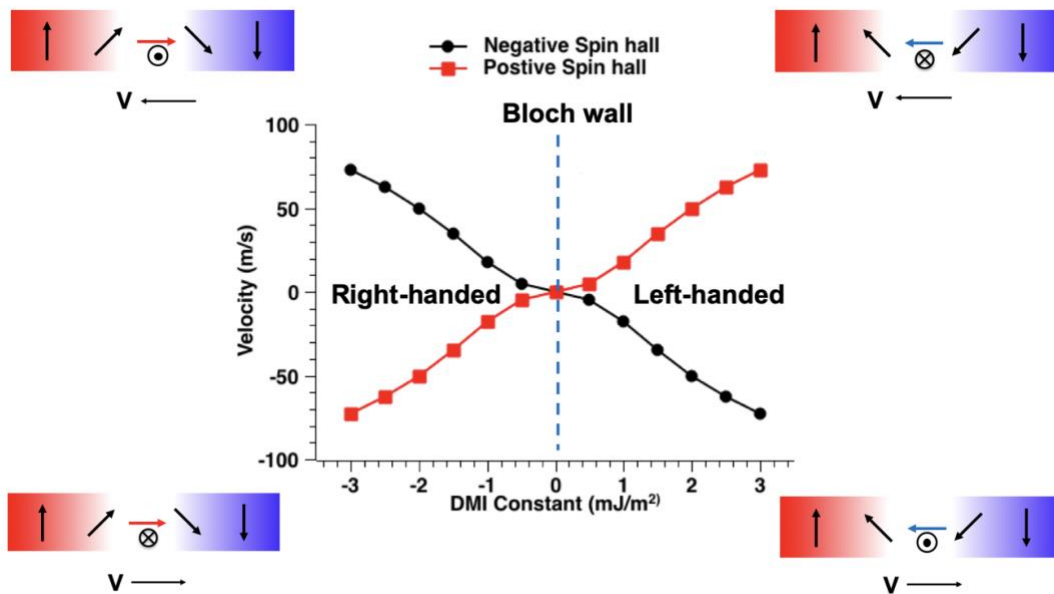
oriented out of the plane (Bloch wall), comparing to in the plane (Néel wall). As discussed above, we need an external field to move the Bloch wall besides current. However, for the application aspect, the external magnetic field is difficult to implement in the CMOS devices. The Dzyaloshinskii-Moriya interaction (DMI) can tilt two adjacent spins. Furthermore, the DMI effect is not strong enough to change the ferromagnetic order, and it mainly changes the configuration of the domain wall. DMI can introduce chiral Néel DW structure.

Figure 4.5 shows three different scenarios. Figure 4.5(b) shows the domain wall structure of magnetic thin film without DMI which usually is a Bloch wall. For negative DMI constant, right-handed Néel wall is the energetically preferred configuration, whereas a positive DMI constant would give rise to a left-handed domain wall. All three configurations are shown schematically in Figure 4.5(a) and Figure 4.5(c).



**Figure 4-5 Domain wall velocity under different strength of DMI effect, (a)negative DMI will rise a right-handed domain wall. (b)without DMI, Bloch domain wall in more energy favorable thin film. (c) under positive DMI, domain wall is left- handed**

With DMI, the chiral domain wall can be driven by the Spin Hall effect. The simulation result is shown in Figure 4.6. Firstly, the simulation result is the same as the theoretical prediction. With negative DMI constant, the domain wall is right-handed while positive DMI constant creates a left-handed domain wall. Figure 4.6 below also illustrates the domain wall motion direction is related to the current direction. Different chiral domain wall motion direction is opposite under the same current. More importantly, higher DMI constant will increase the domain wall motion. It is because of the spin tilt angle is large with stronger DMI. It is obvious, the movement of domain wall is highly dependent on both DMI and Spin Hall effect. If the two effects have the same sign, the domain wall tends to expand in the favor of down domain, while the opposite sign favors the up domain. The result indicates we can engineer the domain wall motion by manipulating DMI and Spin Hall effect.



**Figure 4-6** The velocities of domain wall motion under different sign and strength of DMI and Spin hall effect.

#### 4.2.3 Direction dependent of domain wall motion

Therefore, as the discussion above, by controlling the DMI and Spin Hall effect, we can control the DWM direction and speed. By controlling the DMI and spin current direction, we can also control the DWM behaviors. Here we show that Pt/Co and Co/Pt film stacks have very similar DWM behavior under the same DMI strength and current density.

DMI and Spin Hall effect are materials specified parameters. For instants, Pt [2] and Ta [5] have different DMI sign and different sign of Spin Hall angle. Additionally, the DMI and Spin Hall effect is also a direction-dependent parameter for the same material. Figure 4.7 shows the schematic diagram of Pt/Co and Co/Pt

film stack. If the Pt is on the top of Co, both DMI and Spin Hall have a negative sign. The domain wall moves to favor down domain direction. On the other hand, if the Pt is at the bottom of Co, both DMI and Spin Hall effect is positive. The domain wall still moves to favor the down domain expand direction.

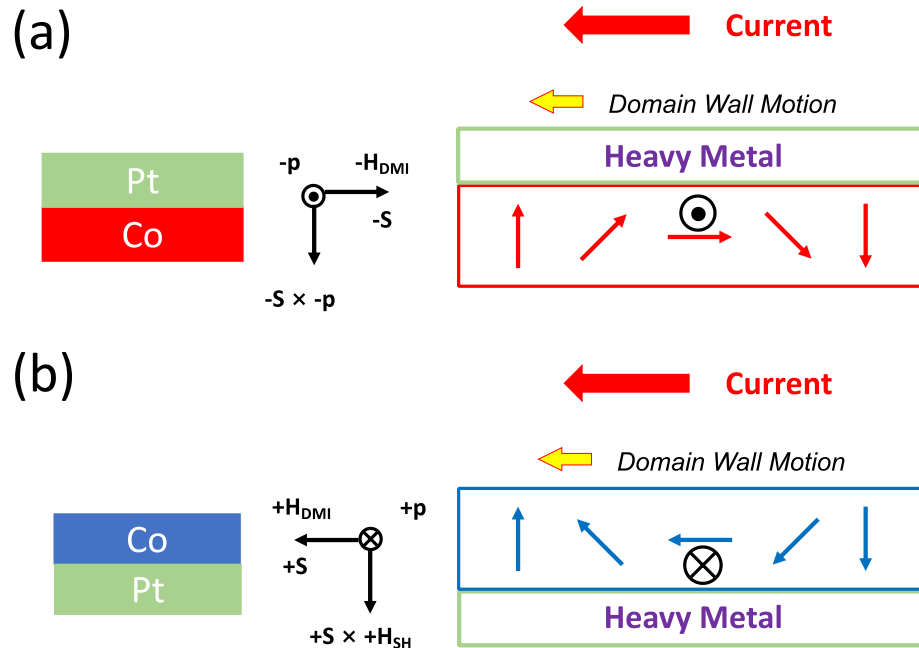


**Figure 4-7 (a) Co/Pt (Pt on the top of Co) sample with negative DMI and negative Spin Hall effect. It moves the domain wall towards down domain expand direction (b) Pt/Co (Pt on the bottom of Co) sample gives the domain wall a positive DMI and spin Hall effect,**

Figure 4.8 shows the simulation result for these two cases. Same as theoretical prediction, the domain wall in Figure 4.8 (a) and (b) are both left-handed. With a positive current, the domain wall moves towards the positive direction. Both higher current and larger DMI constant drive domain wall movement faster. The two plots

are identical, showing that by manipulating the film stacks, we can control the domain wall motion.

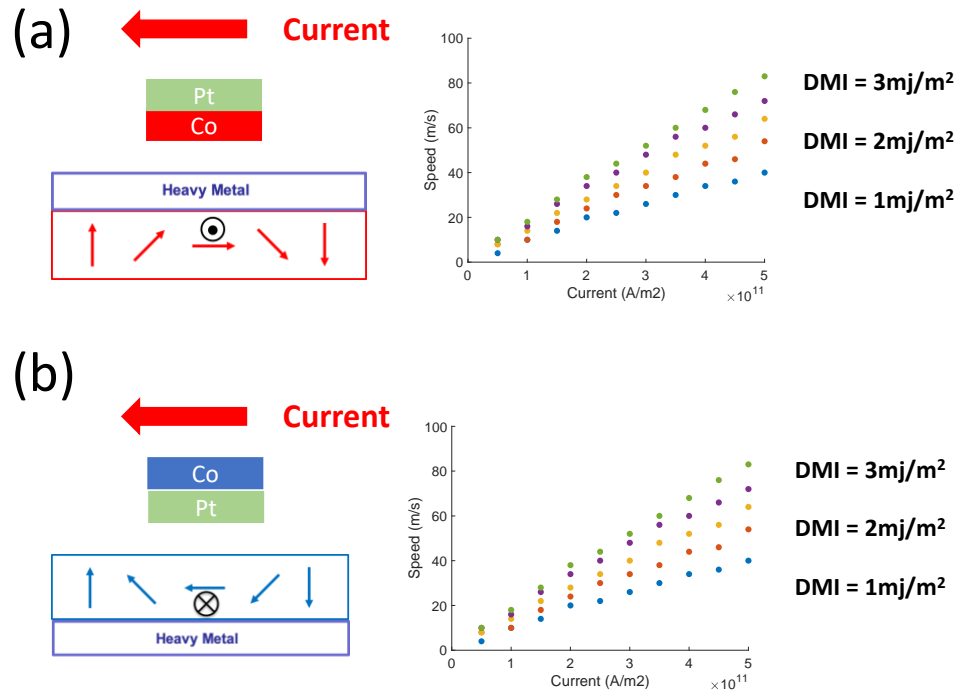


**Figure 4-8 (a)Co/Pt domain wall motion velocity under different DMI strength (b) Pt/Co domain wall motion velocity under different DMI strength**

## **CHAPTER 5. SIMULATION OF CURRENT INDUCED MULTI CO LAYER DWM WITH FM COUPLING**

Based on the simulation result above, both the DMI effect and the Spin Hall effect influences the single magnetic layer DWM behaviors. DMI effect can change the chirality of the domain wall. The Spin Hall effect can inject opposites sign of spin current when the electron current changes direction. We can engineer the film stacks to control the DMI and Spin hall effect to modify the DWM.

However, all the simulations shown so far are all single magnetic layer DWM. In this chapter, we will demonstrate how the interlayer exchanging coupling affect the DWM behaviors in dual magnetic layers. When there are multi magnetic layers in the film stack, interlayer magnetic interactions can alter the DWM behaviors. These interactions include both exchanging coupling and dipolar magnetostatic interaction. Here we will focus on how the exchanging coupling effect changes the domain wall behavior as the coupling facilitates itself as additional exchanging torque on local magnetization.

Figure 5. 1 shows the simulation set up for in chapter's experiments. The film stack we use in our experiment is Pt/Co/Ir/Co/Pt. Pt is both the DMI and spin current source. In this system, the upper and bottom layer of Co DWs couple together by dipolar interaction. Due to the coupling, the DWs travel together under electrical current. Due to strong interlayer exchanging coupling, the two domain walls are

parallel coupled together. Both layers have left-handed DWs. However, the upper layer and bottom layer DWs travel in the opposite direction due to the opposite sign of spin hall angle. Hence, we need to make sure the DWs are still coupled together in large current density.

In this chapter, we first ensure the two DWs in different layers are coupled together by applying different current in the top and bottom layers. The simulation result of a dual magnetic thin film that has no interlayer exchanging coupling is used as the reference case. With reference, we investigate DWM in the dual magnetic layer with FM exchanging coupling. We find out that both exchanging coupling strength and current density have a significant impact on the DWM behaviors.

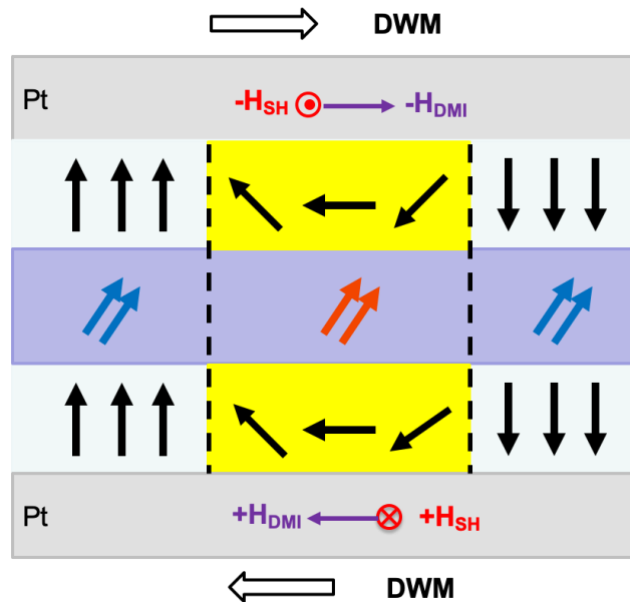


**Figure 5-1 Simulation set up for multilayer domain wall motion with ferromagnetic coupling. Light blue regions are the domains while the**

yellow area representing the domain walls. The black arrows are the magnetization direction. The color arrows are the coupling types.

The simulation materials parameter used in this chapter is included in the Table 5.1.

Parameter	Materials	Intensity	Unit	Explanation
Thickness	Co	0.8	nm	Two layer of Co
$M_{sat}$	Co	800000	A/m	Saturation magnetization
$K_u$	Co	300000	J/m <sup>3</sup>	Anisotropy constant
$A_{ex}$	Co	$1.5 * 10^{-11}$	J/m	Exchange stiffness
alpha	Co	0.1		Damping constant
$D_{ind}$	Pt	2	mJ/m <sup>2</sup>	Bottom Interfacial DMI strength
		2	mJ/m <sup>2</sup>	Top Interfacial DMI strength
Pol	Pt	0.2		Bottom layer Spin hall angel
		-0.2		Top layer Spin hall angel
anisU	Co	(0,0,1)		Uniaxial anisotropy direction
Lambda	Co	1		Damping like torque parameter
$J_{ex}$	Ir	0.4 ~ 1	mJ/m <sup>2</sup>	$H_{ex} > H_{DMI}$ FM coupling

**Table 5-1 Materials parameter that used in the simulation.**

### 5.1 Effect of dipolar interaction on multilayer structure

In the simulation, we are assuming the DWs in the top and bottom layers are coupled together. Hence, during the motion, they move together. However, the

DWs can be separated under large current, which induces different directions DWM. In order to rule out the possibility, we first simulate the DWM with a different current for the top and bottom layers of DWs. We find out that there is not sufficient current to separate the coupled DWs in our simulation space.

We use the configuration in Figure 5.1 and apply a different amount of current on the top and bottom layer of the magnetic layer. Driven by the Spin Hall effect, the domain wall moves in different velocity and even in the contrary direction. The spin current creates forces to separate the coupling of domain walls. Hence, it can tell us the strength of the dipolar interaction, and we can find out what is the current density to separate the coupled DWs.

We can see the simulation for this simulation result in Figure 5.2. It can be seen from the figure that there is no motion of DM for the most part of the simulation. It is because the sign of the Spin Hall angle is opposite for the top and bottom layers. Hence, the spin current counterbalances. However, when the spin current is the same sign, the different Spin Hall field breaks the dipolar interaction and creating a force to move the domain wall in a different direction. Figure 5.2(b) shows the domain wall speed for the diagonal line in Figure 5.2 (a). When the current is large enough, domain walls in both layers receive larger force to separate the coupling. The domain wall moves towards a different direction, and finally, it breaks the dipolar interaction. It can be seen from the data in Figure 5.2(b), the dipolar interaction breaks at around  $I = 5 \times 10^{12} A/m_2$ . The field creates by the Spin Hall effect is around  $H_{sp} = 103.03 mT$ . We did not apply such a large spin current density

in all the simulations, which means the domain wall is coupled and moves together in all our simulations.

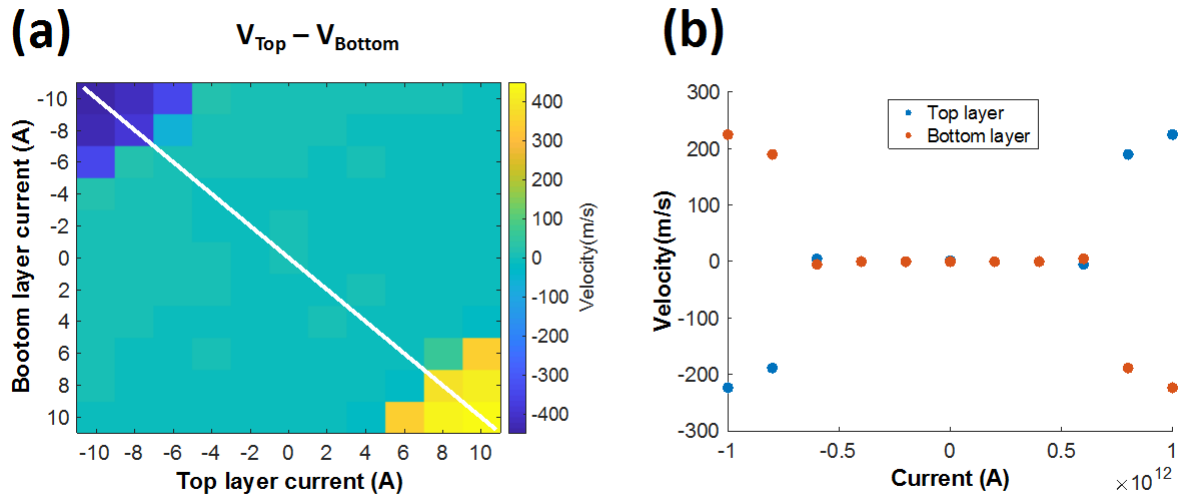


**Figure 5-2 (a) Top layer and bottom layer velocity difference under different current. (b) upper layer and bottom layer velocity, which is the white line in (a)**

## 5.2 Multilayer structure without interlayer exchanging coupling

To study the influence, we use the case without the exchanging coupling as the reference case. Here we first discuss the case without any interlayer exchanging coupling.

In this case, the result is very similar to stacking Pt/Co/Ir and Ir/Co/Pt together. The top layer is right-handed, while the bottom layer is left-handed. However, the upper

layer and bottom layer domain wall couples together by dipolar interaction. Furthermore, because of dipolar interaction, the two domain walls travel together under current.

Figure 5.3 shows the simulation result when we set the top Co layer and bottom Co layer interlayer exchanging constant as  $J_{ex} = 0 \text{ mJ/m}^2$ . It means there is no RKKY interaction in the simulation. Figure 5.3 (a) shows the magnetization angle and velocities of the top layer and bottom layer for different current. The spot's color and size is representing the velocity of the domain wall. The x-axis is the top layer domain wall magnetization, while the y-axis represents the bottom layer. Similar to the single magnetic sample, the velocity of the domain wall increases with the current. The domain wall magnetization starts to rotate during the motion. The upper and bottom layer starts as a Néel wall due to the DMI effect at the Pt/Co interface. The upper layer is right-handed, while the bottom layer is left-handed. The DMI effect of Ir is negligible in our experiment. When current applies, the upper domain wall rotates from 90 degrees (Néel wall) towards 180 degrees (Bloch wall). The bottom layer has a similar outcome.

Figure 5.3 (b) shows a closer look at the domain wall configuration. White  $\otimes$  represent perpendicular down and  $\bullet$  for down. The red area is the up domain, and the blue area represents the down domain. The white area where between red and blue is the domain wall. The black arrow is representing the magnetization angle. Both the bottom layer and top layer shows a clockwise movement from Néel wall to the Bloch wall when we increase the current. The tilted angle of the domain wall

also increases. It indicates the Bloch wall is energetically favorable during motion without any exchanging coupling between different layers.

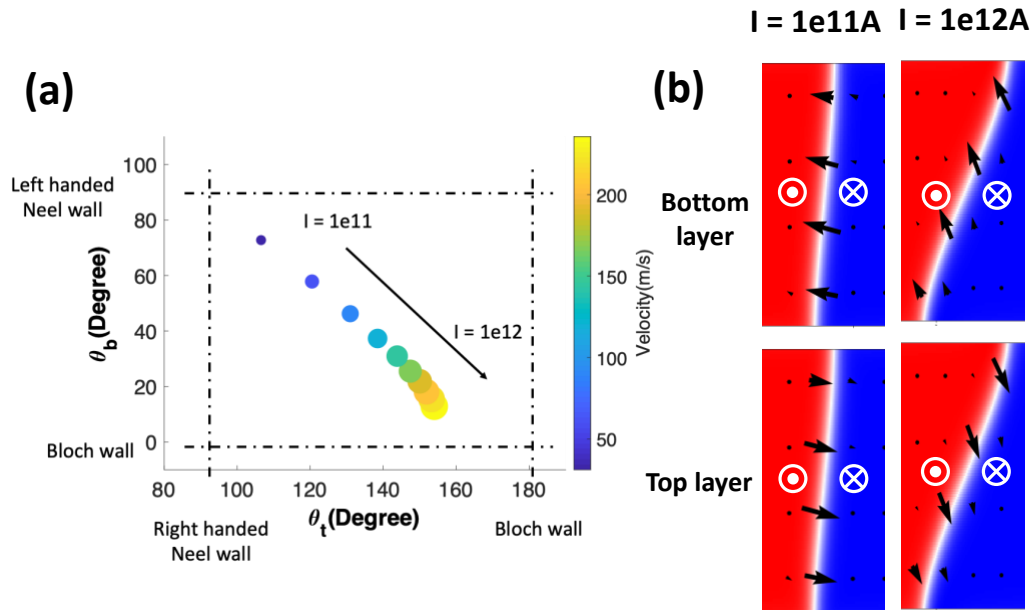


**Figure 5-3 (a) Upper layer magnetization angle  $\theta_t$  and bottom layer magnetization  $\theta_b$  during motion. The color and size of the dot is representing the velocity of the domain wall (b) Bottom layer and top layer domain wall shape and magnetization angle during movement at  $I = 1 \times 10^{11}$  A/m<sup>2</sup> and  $I = 1 \times 10^{12}$  A/m<sup>2</sup>**

### 5.3 Multilayer structure with ferromagnetic interlayer exchanging coupling

With the reference case, we can now discuss how the interlayer exchanging coupling influence on the DWM behavior. We compare the velocities of different exchanging coupling strengths under the same external electrical current. We find

out that the ferromagnetic exchanging coupling is a hindrance to the dual layer DWM.

Again, we use Pt/Co/Ir/Co/Pt film stack to simulate our experiment. The Pt/Co interface has the DMI effect, which forces the magnetization within the domain walls in upper and bottom layers to create a modified chiral configuration under the constrain of the additional interlayer interactions.

However, the magnetization of the two Co layers couple together by the RKKY effect. The RKKY effect can compete with the DMI effect and change the chirality of the domain walls. Here we discuss the simulation that the RKKY effect is predominate, and two domain walls are ferromagnetically coupling. In this case, the bottom layer is still left-handed Néel wall. However, due to the sizeable RKKY effect, the top layer ferromagnetically couples with the bottom layer. It overcomes the DMI effect and stabilizes the upper layer domain wall as a left-handed Néel wall. We simulate different scenarios Pt/Co/Ir/Co/Pt samples with a different exchanging coupling constant  $J_{ex}$ . The value of  $J_{ex}$  varies from  $1\text{mJ}/\text{m}^2$  to  $0.4\text{mJ}/\text{m}^2$ .

Figure 5.4 shows the domain wall velocity and current relationship for different  $J_{ex}$ . The data in Figure 5.4 indicate that the velocity increases with increasing the current. Moreover, the velocity increases while the  $J_{ex}$  is decreased. We can see from Figure 5.4, the velocity increases approximately three times when the  $J_{ex}$  decreases from  $1\text{mJ}/\text{m}^2$  to  $0.4\text{mJ}/\text{m}^2$  although, one should note that the velocity is still much smaller than that of the case with  $J_{ex} = 0$ . The inset in Figure 5.4 shows

the ratio of different  $J_{ex}$  samples and  $J_{ex} = 0$  sample. The fast case of FM coupling is only around 0.6 of the case without the RKKY effect. The result suggests that the RKKY effect ferromagnetic coupling is a hindrance for domain wall motion.

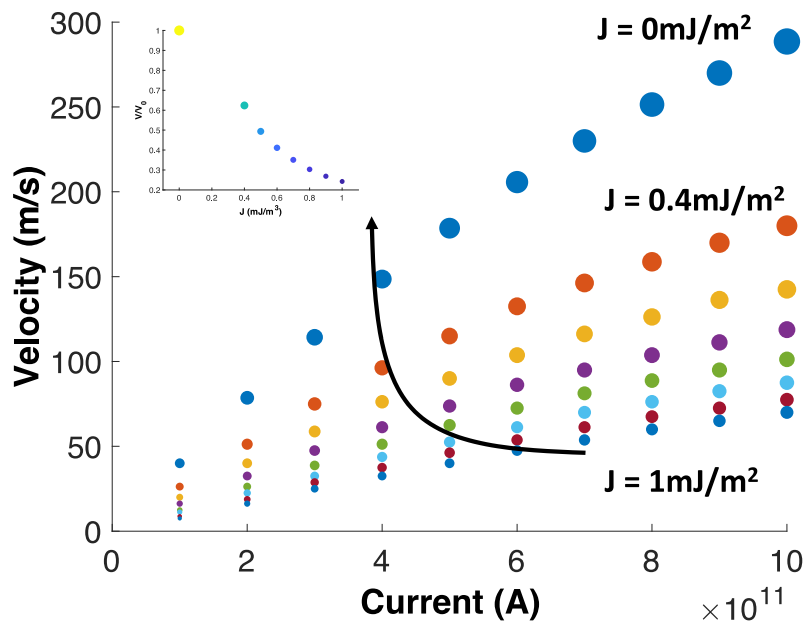


**Figure 5-4** Current and the velocity of domain wall relationship for different exchanging constant. Inserted image is the different exchanging constant cases' velocity comparing to  $J = 0 \text{ mJ/m}^2$  case. The step is  $0.1 \text{ mJ/m}^2$ .

### 5.3.1 Interlayer exchanging coupling effect on domain wall motion speed and inner magnetization angle

As we discussed above, the FM coupling is slowing down the DWM. By analysis of the inner magnetization angle and velocities relationship, we can see why the FM coupling RKKY effect is negatively influencing the domain wall motion.

There are two main parameters that we need to discuss in detail, exchanging coupling strength and current density. We find out that lowering the exchanging coupling strength increases the angle between the upper and bottom layer, which increase the velocities. The result also indicates that increasing the current not only increases the velocities but also aligns the spins with the y-axis, which causes the speed to saturate.

Figure 5.5 shows the top and bottom layer inner magnetization angle for different exchanging coupling constant  $J_{ex}$  and current density  $I$ . The velocities are representing in color and size of the spots. The domain walls are both left-handed Néel wall initially during to FM coupling. Figure 5.5 indicates both decreasing  $J_{ex}$  and increasing current increase domain wall velocities. More importantly, we can see a clear rotation of domain wall magnetization from Figure 5.5. Both the exchange coupling coefficient and the Spin Hall effect shows a strong influence on the domain wall inner magnetization for both layers. The different influences will be breaking down to explain in the following section.

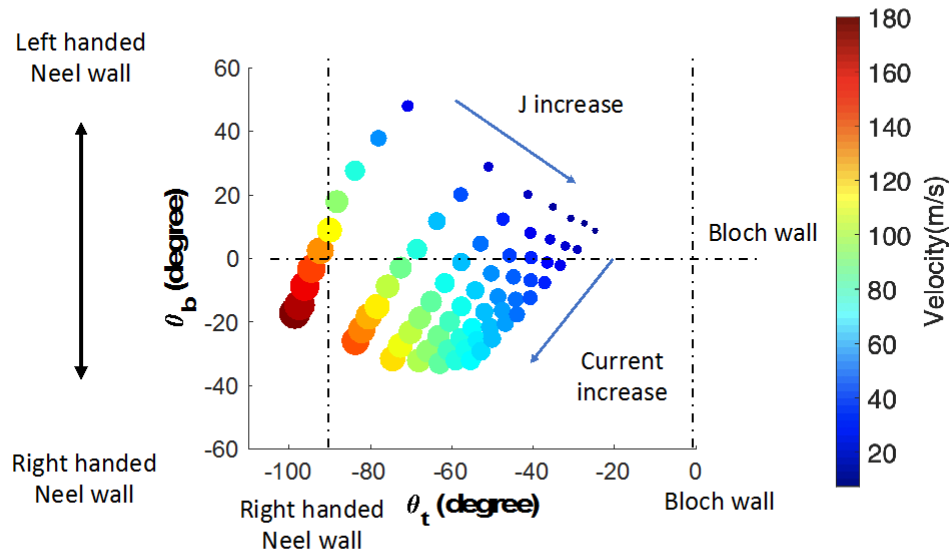


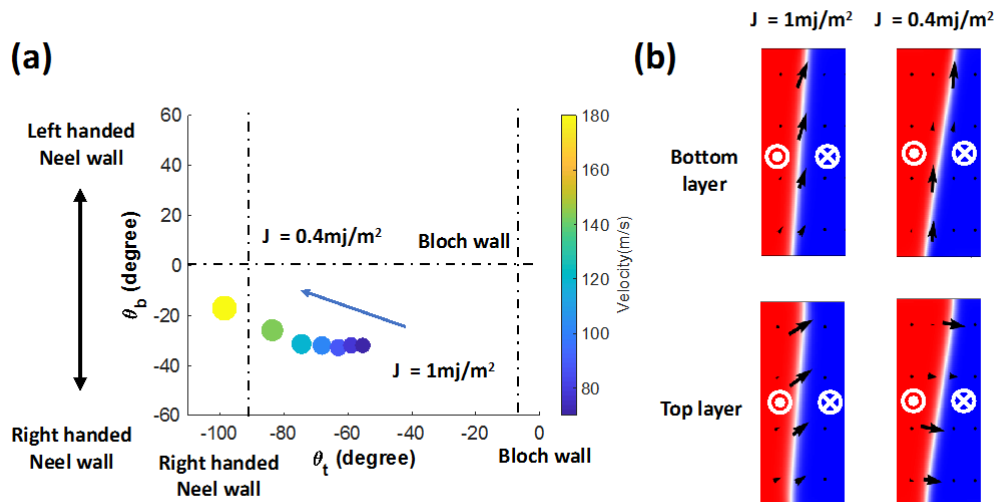
**Figure 5-5 Upper layer magnetization angle  $\theta_t$  and bottom layer magnetization  $\theta_b$  during motion for different exchanging coupling constant and current. The color and size of the dot is representing the velocity of the domain wall.**

### 5.3.1.1 Exchanging coupling effect on domain wall motion speed and inner magnetization angle

Exchanging coupling strength determines the strength of the force that couple the two DWs together. It is found that decreasing the exchanging coupling strength increases the relative angles between the top and bottom layer DW magnetization. Furthermore, when the angle is around 90 degrees, the velocity is largest.

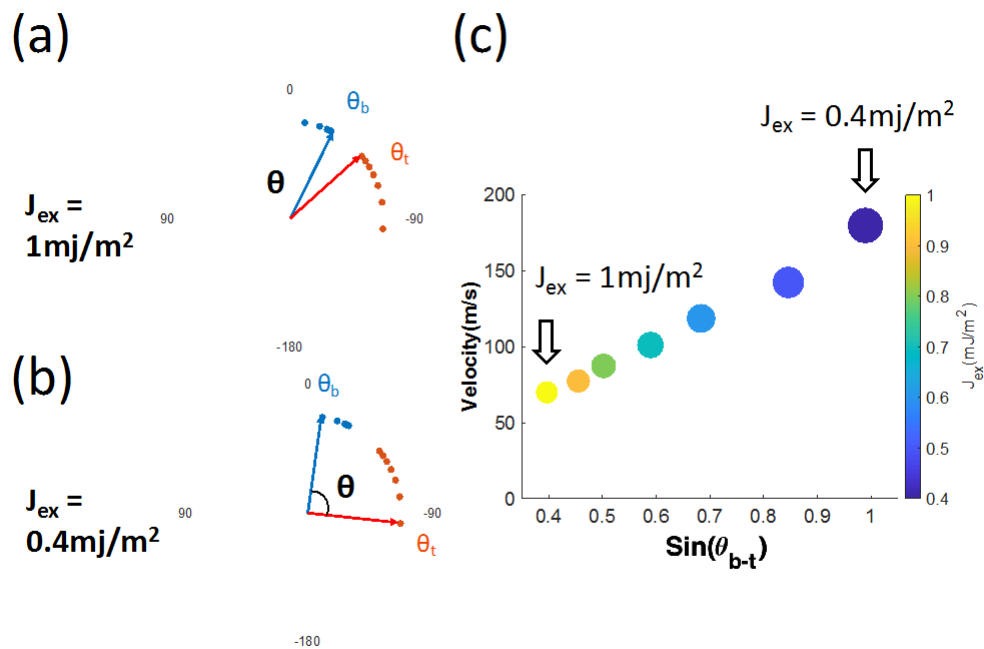
Let us see the results when we fix the current density,  $I = 1 \times 10^{12} \text{ A/m}^2$ , while vary the interlayer exchange coupling. Figure 5.6 (a) shows the velocities and inner magnetization angle for the top and bottom layers of different  $J_{\text{ex}}$ . Both the top layer and bottom layer domain wall magnetization rotates towards right-handed Néel wall when we reduce the  $J_{\text{ex}}$ . The speed also increases when  $J_{\text{ex}}$  reduces.

Figure 5.6 (b) provides a closer look at the actual domain wall magnetization. We can see that the bottom layer domain wall starts as a left-handed Néel wall under a small current and rotates towards direction parallel to the wall to form a Bloch wall with large currents. The upper layer domain wall rotates towards a right-handed Néel wall, even at a small current. At the larger current, the top layer domain wall magnetization increases closer to 180 degrees. All the results shown here are transient dynamic states.



**Figure 5-6 (a) Upper layer magnetization angle  $\theta_t$  and bottom layer magnetization  $\theta_b$  during motion at  $I = 1 \times 10^{12} \text{ A/m}^2$ . The color and size of the dot is representing the velocity of the domain wall (b) Bottom layer and top layer domain wall shape and magnetization angle during movement at  $1 \text{ mJ/m}^2$  to  $0.4 \text{ mJ/m}^2$ .**

Figure 5.7 shows how the domain wall inner magnetization angle changes. Due to the same chirality, there is no domain wall motion when we apply current to the film. The top and bottom layer Spin Hall effect cancel out with each other. However, due to the reduction of exchanging coupling constant, the force for the two-layer domain wall to align parallel reduces. The inner magnetization of the domain wall starts to rotate. When current applies, both the top and bottom layer domain walls magnetization changes towards the Bloch wall like the case  $J_{ex} = 0$ . However, due to the exchanging coupling force, the upper layer and bottom layer still FM couple together, and it competes with the Spin Hall effect and DMI effect. Therefore, the magnetization between two layers creates a certain angle. The angle increases towards 90 degrees to reduce the negative impact on the domain wall.



**Figure 5-7 Fixed  $I = 1 \times 10^{12} \text{ A/m}^2$  Upper layer magnetization angle  $\theta_t$  and bottom layer magnetization  $\theta_b$  at (a)  $J_{ex} = 1 \text{ mJ/m}^2$  and (b)  $J_{ex} = 0.4 \text{ mJ/m}^2$**

### 5.3.1.2 Current effect on domain wall motion speed and inner magnetization angle

The other important parameter is the current density. Increase the current density directly increase the velocities. Moreover, the current rotates the DW magnetization towards the y-axis in both layers.

When we fixed  $J = 0.4 \text{ mJ/m}^2$ , Figure 5.8(a) shows the speed and inner magnetization angle for both layers. The top layer and bottom layer domain wall

are changing towards right-handed Néel wall too when we increase the current. The speed also increases while  $I$  increase.

Figure 5.8(b) shows the closer look of the actual domain wall magnetization. We can see both the bottom and top layer domain wall starts as a left-handed Néel wall. However, the bottom layer domain wall changes to a Bloch wall when we apply current. The top layer domain wall changes to right-handed domain wall. In both cases, the domain wall changes even under small current. Again, all the simulation results shown here are transient dynamic states while current is applying. It is important to point out that the spin orbital torque generated by the Spin Hall effect is largely responsible for resulting in these magnetization configurations

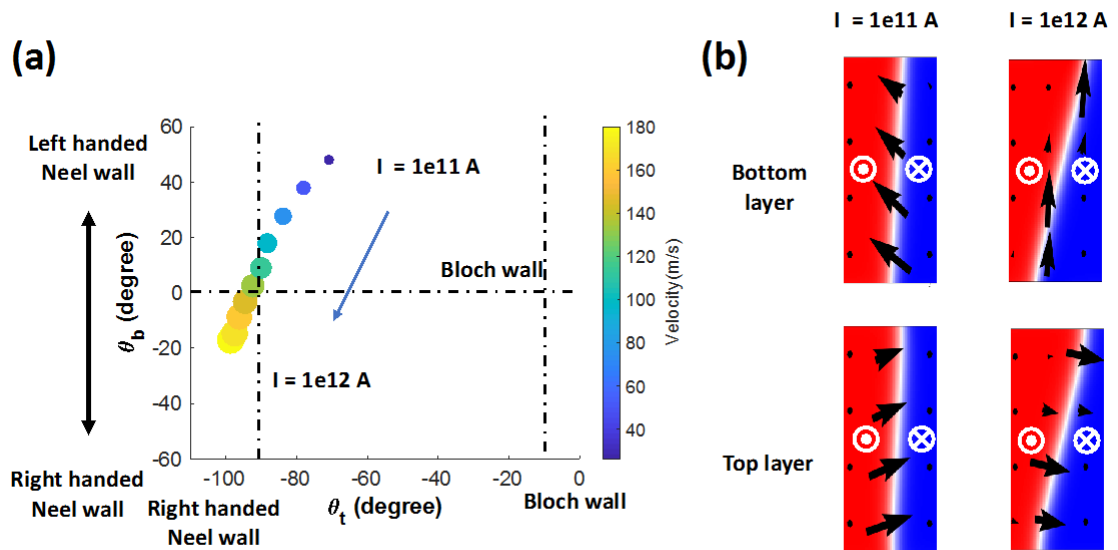
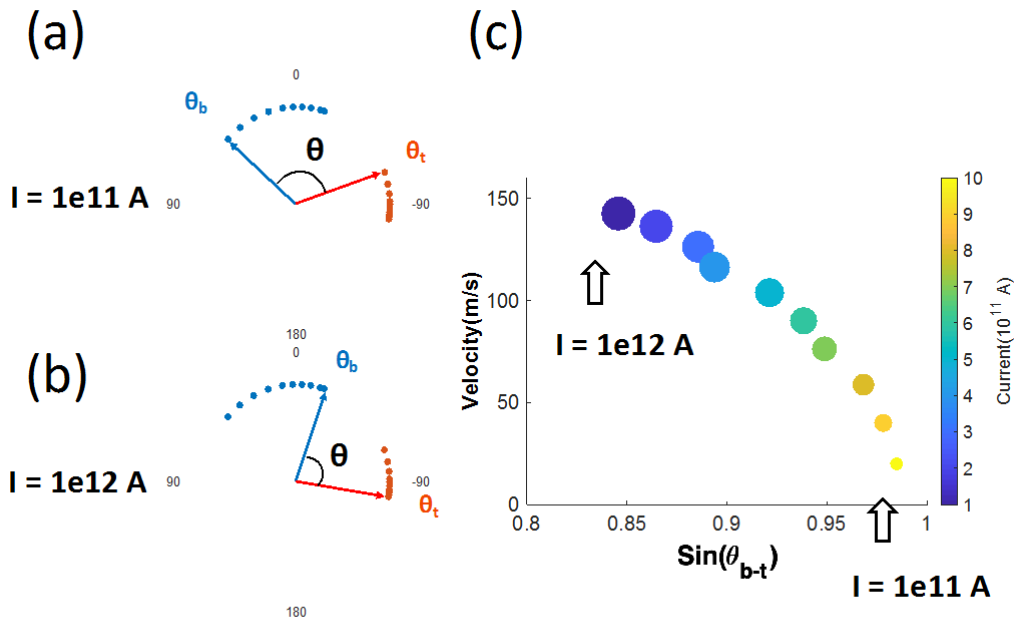


Figure 5-8 (a) Upper layer magnetization angle  $\theta_t$  and bottom layer magnetization  $\theta_b$  during motion at  $J_{ex} = 0.4\text{mJ/m}^2$ . The color and size of the

dot is representing the velocity of the domain wall (b) Bottom layer and top layer domain wall shape and magnetization angle during the movement at  $I = 1 \times 10^{11} \text{ A/m}^2$  and  $I = 1 \times 10^{12} \text{ A/m}^2$

Figure 5.9 shows a closer look at how the domain walls angle in the top and bottom layers changes. Due to the increase of current, the Spin Hall induced field increases. The Spin Hall effect is trying to align the domain wall inner magnetization with the y-axis. However, due to the exchanging coupling, the two domain walls are still forced to the couple. They cannot form tail to tail configuration, like  $J_{ex} = 0$  case, in Figure 5.3(b). Hence, the bottom layer and top layer magnetization angle are rotating clockwise together. It creates a balance, and further velocities saturate at a specified current.



**Figure 5-9 Fixed  $J_{ex} = 0.4\text{mJ/m}^2$  upper layer magnetization angle  $\theta_t$  and bottom layer magnetization  $\theta_b$  at (a)  $I = 1 \times 10^{11} \text{ A/m}^2$  and (b)  $I = 1 \times 10^{12} \text{ A/m}^2$**

## **CHAPTER 6. SIMULATION OF CURRENT INDUCED MULTI CO LAYER DOMAIN WALL MOTION WITH DW ANTIPARALLEL**

As we discussed in last chapter, the exchanging coupling can change from FM to AFM by varying the thickness of Ir interlayer. The type of interlayer exchanging coupling effect can also alter the DWM behaviors. In this chapter, we discuss the dual layer magnetic system that DWs are antiparallel coupled together. As shown in Figure 6.1, there are two scenarios that allow the DWs antiparallel coupled together.

In the first scenarios, shown in Figure 6.1 (a), the interlayer exchanging coupling is anti-ferromagnetic. Usually, the RKKY effect is much smaller comparing to anisotropy energy. Therefore, the RKKY effect does not change the magnetization of domains. However, the RKKY effect alters the domain wall magnetization since domain wall energy is much lower. Hence, the it satisfies both dipolar interaction and DMI effect.

In other words, the AFM coupling promote the DWs with walls with opposite chirality in both layers.

Figure 6.1 (b) indicates the other scenarios that the interlayer exchanging coupling is ferromagnetic. However, the effective field of exchanging coupling is smaller than the effective DMI field. Although the coupling field tends to align the DWs

parallel, the DMI effect overcomes it and promote different chirality in the top and bottom layer.

By controlling the RKKY effect, Spin Hall effect, and DMI effect, we can manipulate the DWM. If the upper layer Spin Hall effect sign is negative and bottom layer positive, both domain walls move towards the down domain expand direction.

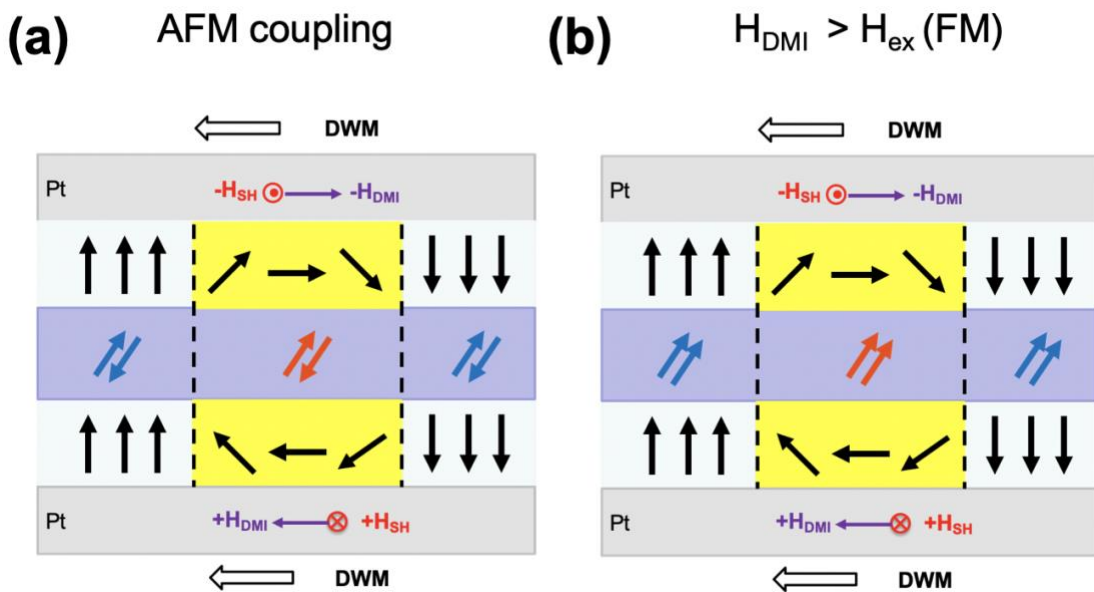


**Figure 6-1 Simulation set up for multilayer domain wall motion with (a) anti-ferromagnetic coupling (b) interlayer exchanging coupling is ferromagnetic coupling, but the strength is smaller than the DMI effect. The yellow area representing the domain area.**

As discussed above, in both scenarios, the upper layer and bottom layer domain walls are left-handed Néel wall, while the top layer has right-handed Néel wall. Both domain walls are moving in the same direction. In these scenarios, the

exchanging coupling constant various from  $J_{ex} = -0.2 \text{ mJ/m}^2$  to  $J_{ex} = 0 \text{ mJ/m}^2$  (AFM) and  $J_{ex} = 0 \text{ mJ/m}^2$  to  $J_{ex} = 0.3 \text{ mJ/m}^2$  (FM).

The simulation materials parameter used in this chapter is included in the Table 6.2.

Parameter	Materials	Intensity	Unit	Explanation
Thickness	Co	0.8	nm	Two layer of Co
$M_{sat}$	Co	800000	A/m	Saturation magnetization
$K_u$	Co	300000	J/m <sup>3</sup>	Anisotropy constant
$A_{ex}$	Co	$1.5 * 10^{-11}$	J/m	Exchange stiffness
alpha	Co	0.1		Damping constant
$D_{ind}$	Pt	2	mJ/m <sup>2</sup>	Bottom Interfacial DMI strength
		2	mJ/m <sup>2</sup>	Top Interfacial DMI strength
Pol	Pt	0.2		Bottom layer Spin hall angel
		-0.2		Top layer Spin hall angel
anisU	Co	(0,0,1)		Uniaxial anisotropy direction
Lambda	Co	1		Damping like torque parameter
$J_{ex}$	Ir	0 ~ 0.2	mJ/m <sup>2</sup>	$H_{ex} < H_{DMI}$ FM coupling
		-0.2 ~ 0	mJ/m <sup>2</sup>	Weak AFM coupling

**Table 6-1 Materials parameter that used in the simulation.**

For the simulation results of the DWM to be discussed in the following sections, we first compare the velocities of different exchanging coupling cases, and then the inner magnetization of DWs and DW shape changes is further discussed in detail.

## 6.1 DWM in dual magnetic structure with FM interlayer exchanging coupling and DWs antiparallel coupled

Figure 6.2 shows the domain wall velocity and current relationship for different  $J_{ex}$ . We find out that FM type of exchanging coupling is a hinderance for the dual magnetic layer DWM.

The data in Figure 6.2 indicates the velocities increase with the current. More importantly, the domain wall motion velocities still increase when the  $J_{ex}$  decreases. We can see from Figure 6.2 the velocities increase just a little when the  $J_{ex}$  decrease from  $0.2 \text{ mJ/m}^2$  to  $0 \text{ mJ/m}^2$ . However, the velocities are still much smaller than the scenario with  $J_{ex} = 0 \text{ mJ/m}^2$ . Nevertheless, it is still faster than all the FM coupling case. The velocities increase is not obvious.

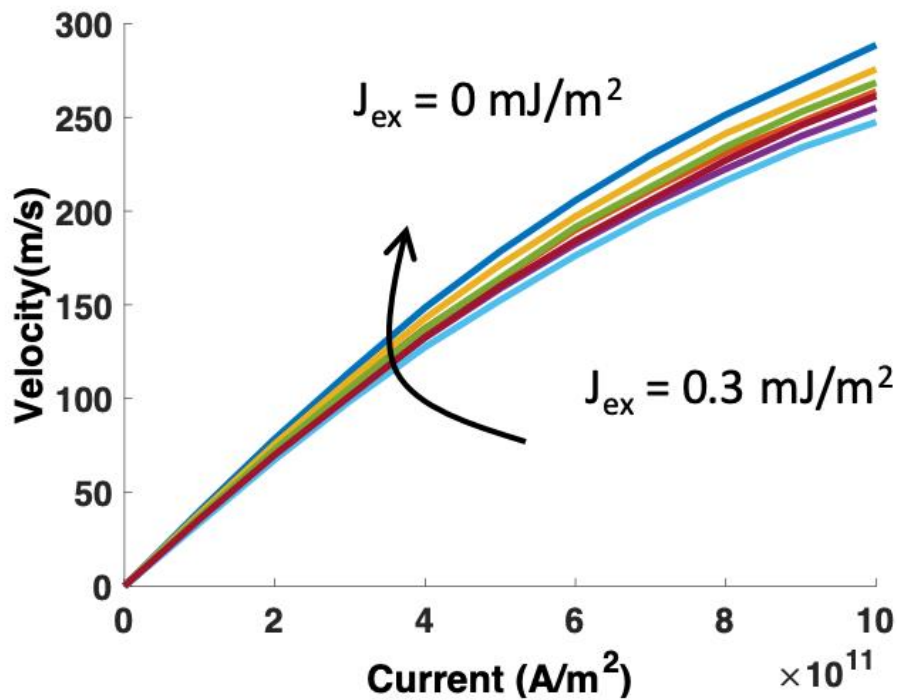


**Figure 6-2 Current and the velocity of domain wall relationship for different exchanging constant. Inserted image is the different exchanging constant cases' velocity comparing to  $J_{ex} = 0mJ/m^2$  case. The step is  $0.05mJ/m^2$ .**

The study of the inner magnetization angle gives us a better understand of the FM exchanging coupling influence. Figure 6.3 is the magnetization of top and bottom layer with different current and exchanging coupling strength. We find out that, in all cases, the magnetization rotates clockwise towards y-axis when the current increases.

Different  $J_{ex}$  result is in different color and the velocities are representing as the size of the spots in Figure 6.3. When decreasing the  $J_{ex}$  from  $J_{ex} = 0.3mJ/m^2$  to  $J_{ex} = 0mJ/m^2$ , the domain wall motion velocities only increase a little. With the increase of current, the dots became larger which means the velocities increase. More importantly, we can see all the dots fall into the same line when the increase. Comparing the parallel coupling cases in last chapter, the change of magnetization is much smaller. The bottom domain wall starts as a left-handed Néel wall while the top layer is right-handed Néel wall. When the current increases, the bottom layer domain wall starts to rotate and tend to form a Bloch wall. The top layer also rotates from the right-handed Néel wall to a Bloch wall. Again, we will discuss the impact of exchanging coupling strength and current in the following section.

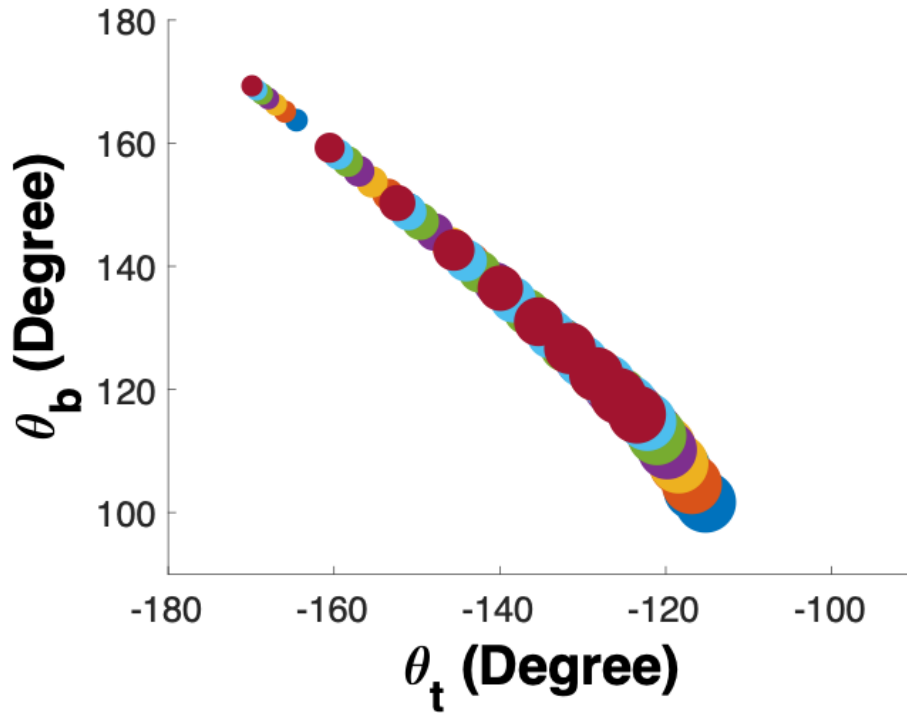


**Figure 6-3 Upper layer magnetization angle  $\theta_t$  and bottom layer magnetization  $\theta_b$  during motion for different exchanging coupling constant and current density. The size of the dot is representing the velocity of the domain wall. The color is representing different  $J_{ex}$  from  $J_{ex} = 0.3\text{mJ/m}^2$  to  $J_{ex} = 0\text{mJ/m}^2$  cases with current densities from  $I = 1 \times 10^{11} \text{ A/m}^2$  to  $I = 1 \times 10^{12} \text{ A/m}^2$**

### *6.1.1 Exchanging coupling effect on domain wall motion speed and inner magnetization angle*

To study the exchanging coupling effect, we compare the magnetization change with current for the cases  $J_{ex} = 0.05\text{mJ/m}^2$  and  $J_{ex} = 0.3\text{mJ/m}^2$ . By comparison, we find out that decrease the  $J_{ex}$  rotates the DW inner magnetization towards y-axis for both layers. It also indicates the top layer DW spins align tail to tail with the bottom layer DW spins during motion and rotate together under current.

Figure 6.4 shows the velocities and inner magnetization angle for both layers. It indicates the magnetization of DWs rotate towards y-axis. The red dots are the simulation result of case  $J = 0.05 \text{ mJ/m}^2$ , and the blue dots are the result of  $J = 0.3 \text{ mJ/m}^2$ . The size of the dots represents the speed of domain wall motion. The result indicates that the top layer and bottom layer domain wall are changing towards Bloch wall too when we increase the current. The speed also increases while  $I$  increase. More importantly, all the dots lie in the same line. It means the influence of the change of  $J_{\text{ex}}$  on domain wall magnetization is very small.

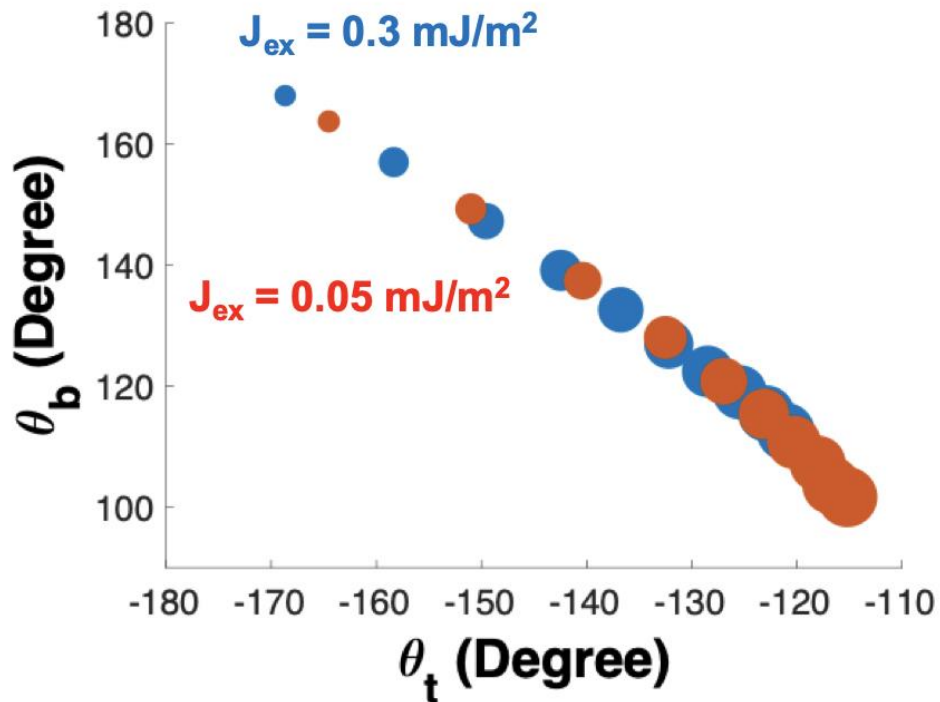
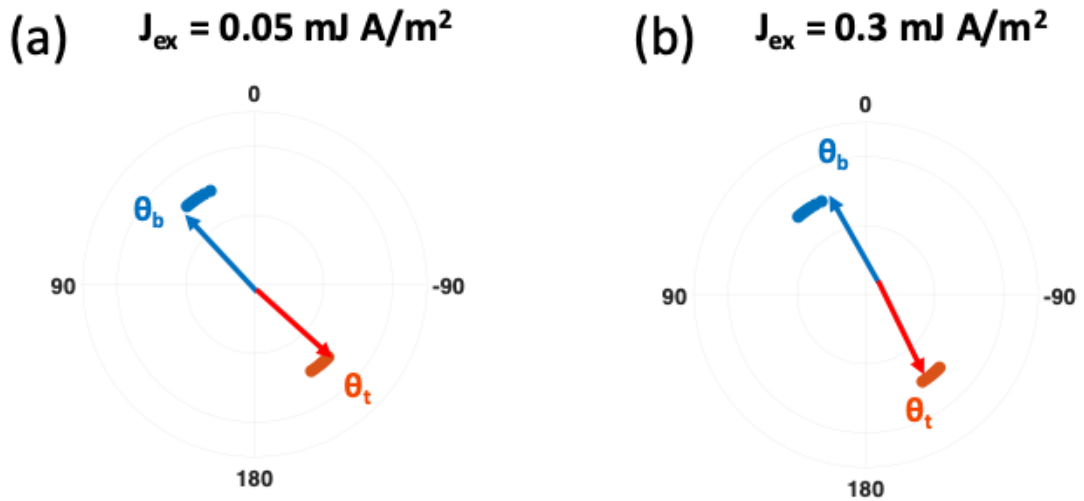


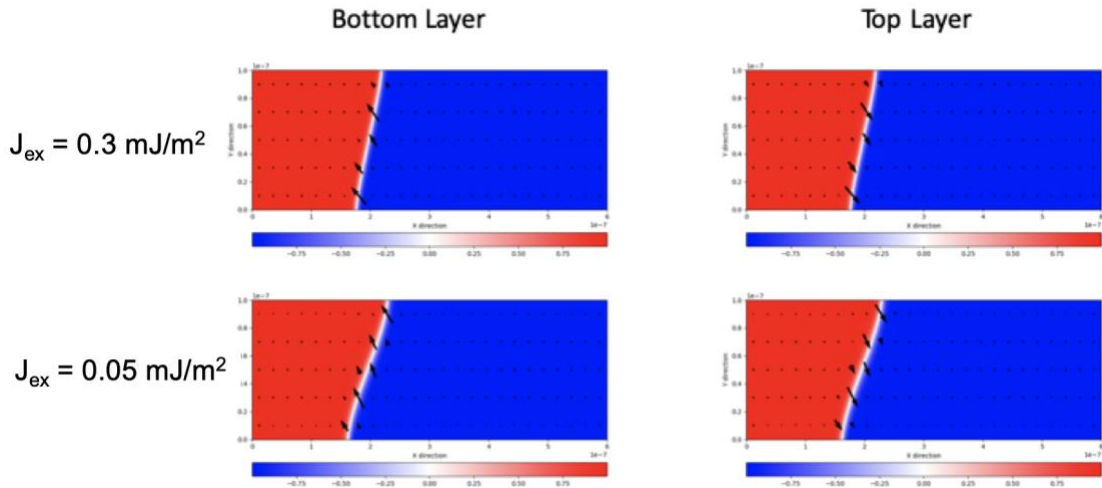
Figure 6-4 Upper layer magnetization angle  $t$  and bot- tom layer magnetization  $b$  during motion at of  $J_{\text{ex}} = 0.3 \text{ mJ/m}^2$  (Blue dots) and of  $J_{\text{ex}} = 0.05 \text{ mJ/m}^2$  (blue dots). The size of the dot is representing the velocity of the domain wall.

Figure 6.5 shows how the domain wall inner magnetization angle changes. We find out that the top layer and bottom layer magnetization angle difference is around 180 degree. When current apply, the magnetization rotates together towards y-axis. Since the different chirality, the domain walls move in the same direction when we apply current to the film. The dipolar interaction and exchanging coupling are keeping the domain walls together. However, the DMI effect force is larger than the RKKY. When current applies, both the top and bottom layer domain walls magnetization changes towards the Bloch wall. The exchanging coupling effect is no longer large enough to keep the two domain walls parallel couples with each other. Hence, the inner magnetization aligns with tail to tail and creates 180 degrees. If we continuously increase the current, both domain walls shift towards Bloch wall. The angle between the two domain wall magnetization is still tail to tail.



**Figure 6-5 Fixed  $I = 5 \times 10^{11} \text{ A/m}^2$  upper layer magnetization angle  $\theta_t$  and bottom layer magnetization  $\theta_b$  at (a)  $J_{ex} = 0.05 \text{ mJ/m}^2$  and  $J_{ex} = 0.3 \text{ mJ/m}^2$**

Figure 6.6 shows the actual domain wall configuration under different  $J_{ex}$ . The lower the  $J_{ex}$ , the larger of DWs tilting angle. Again, the inner magnetization of DWs in the top and bottom layers form a tail to tail configuration. More importantly, DWs start to slant clockwise. When  $J_{ex}$  decreases, the tilting angle increase.



**Figure 6-6 Bottom layer and top layer domain wall shape and magnetization angle during movement of  $J_{ex} = 0.05\text{mJ/m}^2$  and  $J_{ex} = 0.3\text{mJ/m}^2$  at  $I = 1 \times 10^{11} \text{A/m}^2$**

### 6.1.2 Current effect on domain wall motion speed and inner magnetization angle

In this section, we discuss the current density influence on the DWM. The simulation result indicates the increase of the current also rotate the magnetization clockwise towards y-axis. Besides, the current also cause the DWs to tilt.

Here we compared  $I = 1 \times 10^{11} \text{ A/m}_2$  and  $I = 1 \times 10^{12} \text{ A/m}_2$  cases with different  $J_{ex}$ . The simulation result is shown as the dots the blue circle and red circles in Figure 6.7. The bottom layers domain wall shifts from 90 degrees towards 0 degrees, while the top layer shift from -90 degrees to 180 degrees. In other words, all DWs rotate towards y-axis.

For a larger current, the simulation result of domain wall motion under  $I = 1 \times 10^{12} \text{ A/m}_2$  are plotted in the red circle. The result shows the same pattern as the small current case. Both domain walls shift from the Néel wall to the Bloch wall.

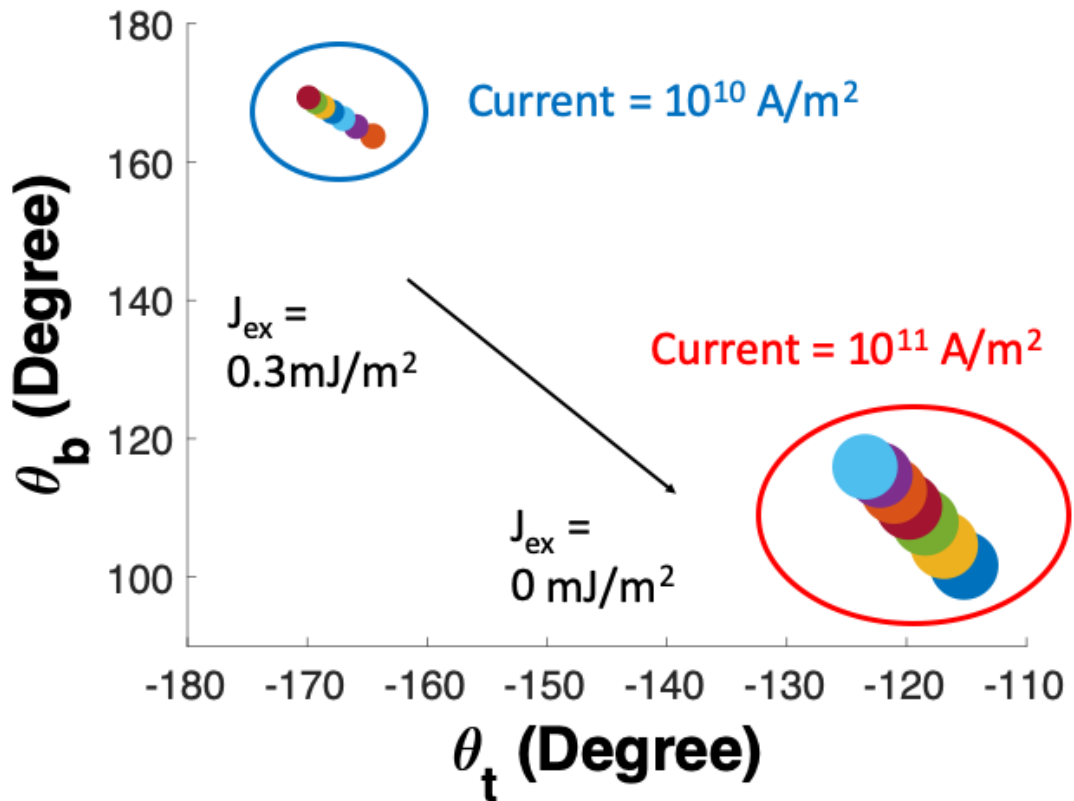


**Figure 6-7 Upper layer magnetization angle  $\theta_t$  and bottom layer magnetization  $\theta_b$  during motion at  $I = 1 \times 10^{11} \text{ A/m}^2$  (blue circle) and  $I = 1 \times 10^{12} \text{ A/m}^2$  (red circle). The size of the dot is representing the velocity of the domain wall. The dots in the circle is reduced from  $J_{ex} = 0.3 \text{ mJ/m}^2$  to  $J_{ex} = 0 \text{ mJ/m}^2$**

Again, all the simulation is in dynamics instead of static. Figure 6.8 shows a closer look for how the domain wall angle changes. Due to the increase of current, the Spin Hall induced field increases. The spin current is trying to align the domain wall inner magnetization to the y-axis and increase the velocities. Hence, the bottom layer and top layer magnetization angle are shifting clockwise. Due to the reduction of exchanging coupling effect, the domain walls are no long FM couples together. The spins a tail to tail align and rotate together.

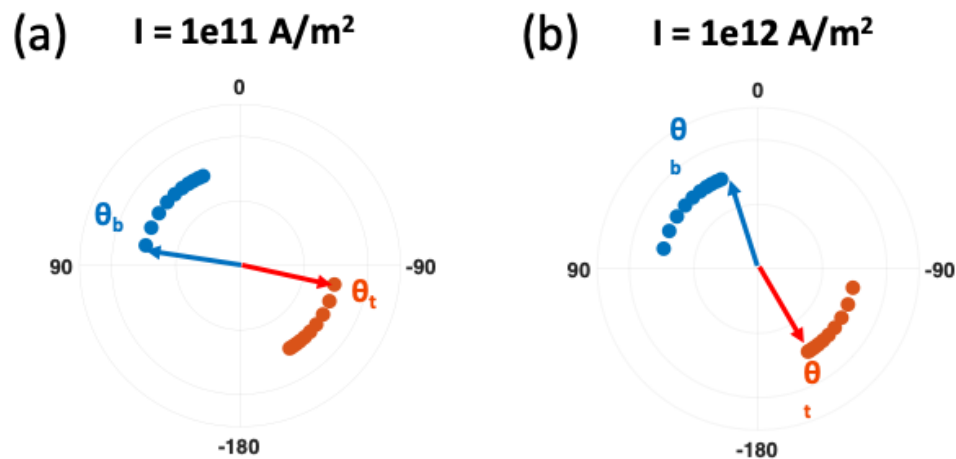


**Figure 6-8 Fixed  $J_{ex} = 0.2 \text{ mJ/m}^2$  upper layer magnetization angle  $\theta_t$  and bottom layer magnetization  $\theta_b$  at (a)  $I = 1 \times 10^{11} \text{ A/m}^2$  and (b)  $I = 1 \times 10^{12} \text{ A/m}^2$ .**

Figure 6.9 shows the DW shape during the motion for  $I = 1 \times 10^{11} \text{ A/m}^2$  and  $I = 1 \times 10^{12} \text{ A/m}^2$  cases. It is clear that higher current density, the DW displacement is larger. It can also be seen from Figure 6.9 that the tilting angle of DW is increase when the current density increase.

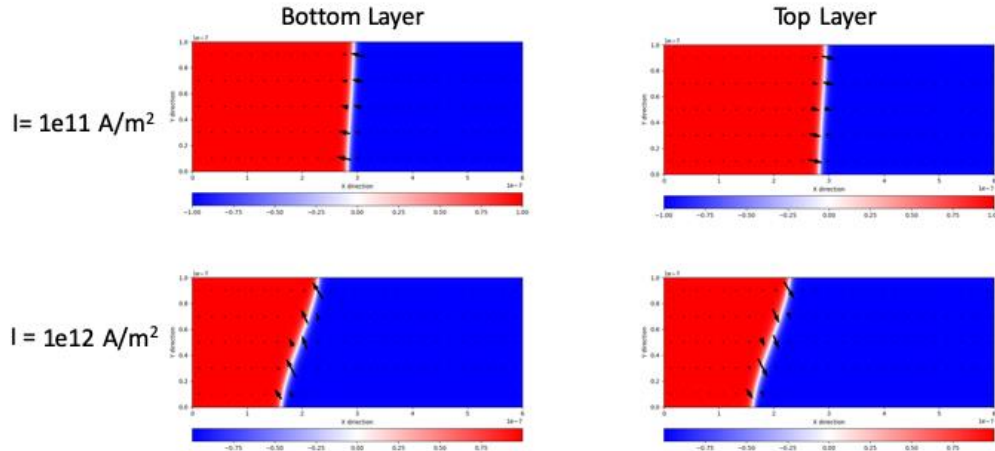


**Figure 6-9 Bottom layer and top layer domain wall shape and magnetization angle during movement at  $I = 1 \times 10^{11} \text{ A/m}^2$  and  $I = 1 \times 10^{12} \text{ A/m}^2$  at  $J_{ex} = 0.1 \text{ mJ/m}^2$**

## 6.2 DWM in dual magnetic structure with AFM interlayer exchanging coupling and DWs antiparallel coupled

As we change the coupling from FM coupling to AFM coupling, the AFM coupling effect force the two domain walls to couple anti-ferromagnetically, partially due to the facilitation of the DMI effect. Hence, there is another exchanging torque accelerates the domain wall motion. In these scenarios, the exchanging coupling constant various from  $J_{ex} = 0 \text{ mJ/m}^2$  to  $J_{ex} = -0.2 \text{ mJ/m}^2$ . The domain wall

configuration is shown in the Figure 6.1(a). The result of the domain wall motion is discussed in the following sections.

The domain wall velocities and current relation for different  $J_{ex}$  are plotted in Figure 6.10. We find out that AFM coupling yields higher DWM speed and then, the velocity would saturate at large current densities.

Like all the other cases, the domain wall motion velocity increases when current density increases. It can also be seen in Figure 6.10 that the domain wall velocity increases when we increase the strength of exchange coupling from  $0\text{mJ/m}^2$  to  $-0.2\text{mJ/m}^2$ . Moreover, the velocity is larger than that for the case of zero exchange coupling. It is because that the additional torque resulted from the exchange coupling effect would effectively assist the domain wall motion.

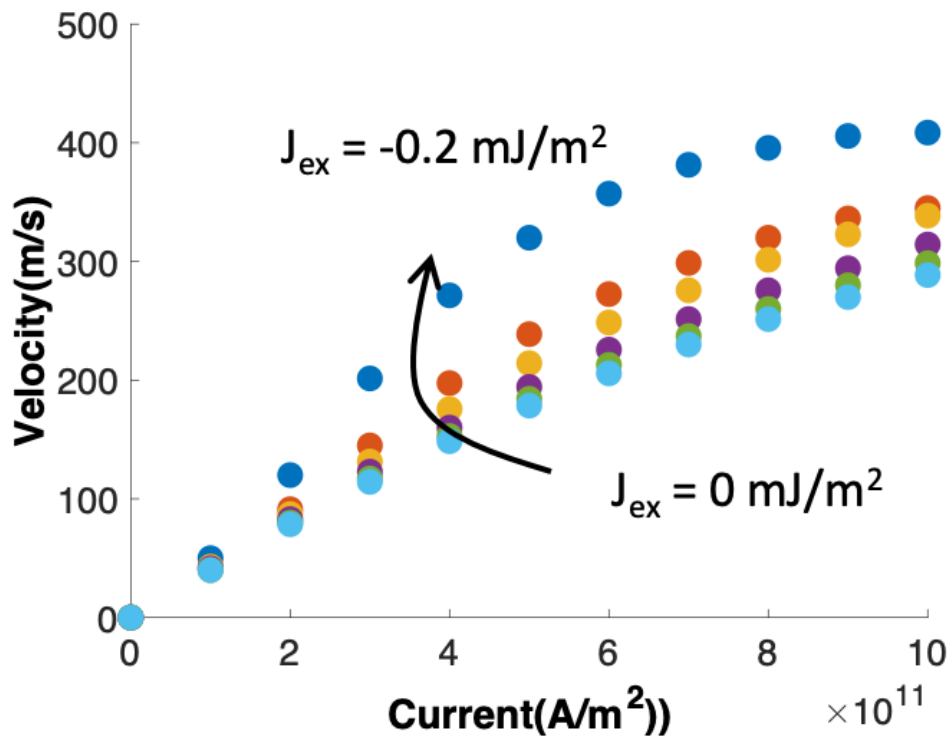


**Figure 6-10 Current and the velocity of domain wall relationship for different exchanging constant. The top line is the  $J_{ex} = -0.2\text{mJ}/\text{m}^2$  case and bottom line is  $J_{ex} = 0\text{mJ}/\text{m}^2$ . The step is  $-0.05\text{mJ}/\text{m}^2$ .**

The magnetization angle at the center of the wall is plotted for both the bottom and top layers in Figure 6.11. The associated wall velocities are shown as size of the symbols as well as color distinctions. It can be concluded from the results shown in the figure that DWs travel in a Bloch type of wall under current, likely due to the spin orbital torque. The domain wall magnetization changes with increase current lie on the same line at first, especially from  $J_{ex} = 0\text{mJ}/\text{m}^2$  to  $J_{ex} = -0.2\text{mJ}/\text{m}^2$ . Just like the cases above, the change of magnetization is smaller. Both DWs' inner magnetization rotates clockwise with current and tend to align with y-axis. The bottom domain wall starts as a left-handed Néel wall while the top layer is right-handed Néel wall. When we increase the current, the bottom layer domain wall starts to shift from the left-handed Néel wall to a Bloch wall. The top layer also shifts from the right-handed Néel wall to a Bloch wall.

The influence of exchanging coupling effect and current density is explained in detail in following section.

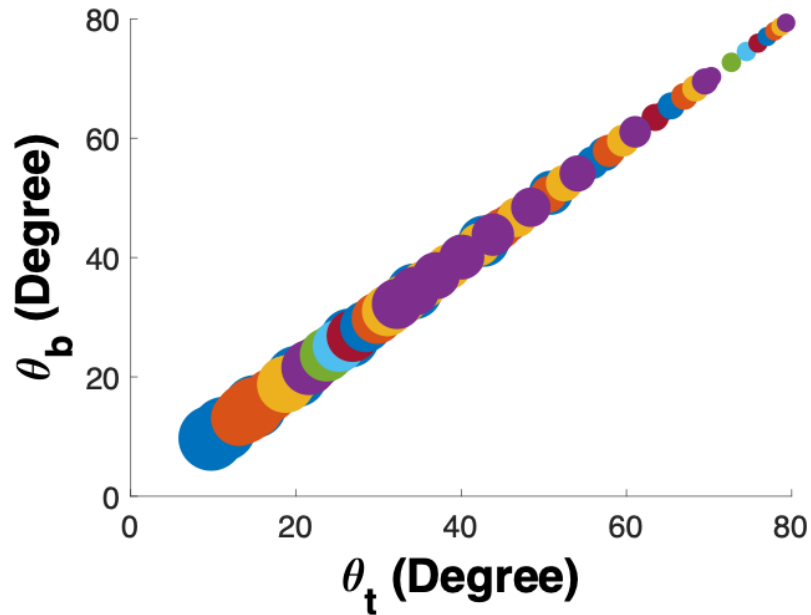


**Figure 6-11 Upper layer magnetization angle  $\theta_t$  and bottom layer magnetization  $\theta_b$  during motion for different exchanging coupling constant and current. The size of the dot is representing the velocity of the domain wall. The color is representing different  $J_{ex}$  from  $J_{ex} = 0\text{mJ/m}^2$  to  $J_{ex} = -0.2\text{mJ/m}^2$  cases with current densities from  $I=1\times 10^6\text{ A/m}^2$  to  $I=1\times 10^7\text{ A/m}^2$ .**

### *6.2.1 Interlayer exchanging coupling effect on domain wall motion speed and inner magnetization angle*

The next section is the detail of comparing the cases of fixing current with different  $J_{ex}$ . Figure 6.12 shows the velocities and inner magnetization angle for both layers under the different  $J_{ex}$  and same current. We find out that increasing the exchanging coupling strength rotates the magnetization towards y-axis.

The size of the dots represents the speed of domain wall motion. The result indicates that the top layer and bottom layer domain wall are changing towards

Bloch wall when we increase the current. The speed also increases while  $I$  increase. More importantly, all the dots lie in the same line. However, we can see with larger  $J_{ex}$ , the velocities are larger, and the domain wall is closer to Bloch wall.

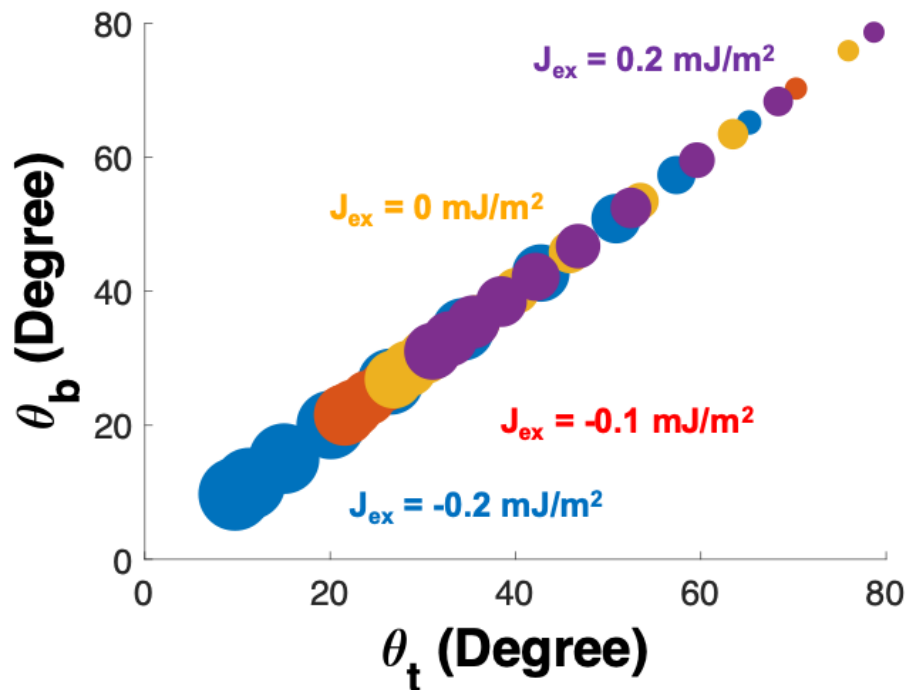
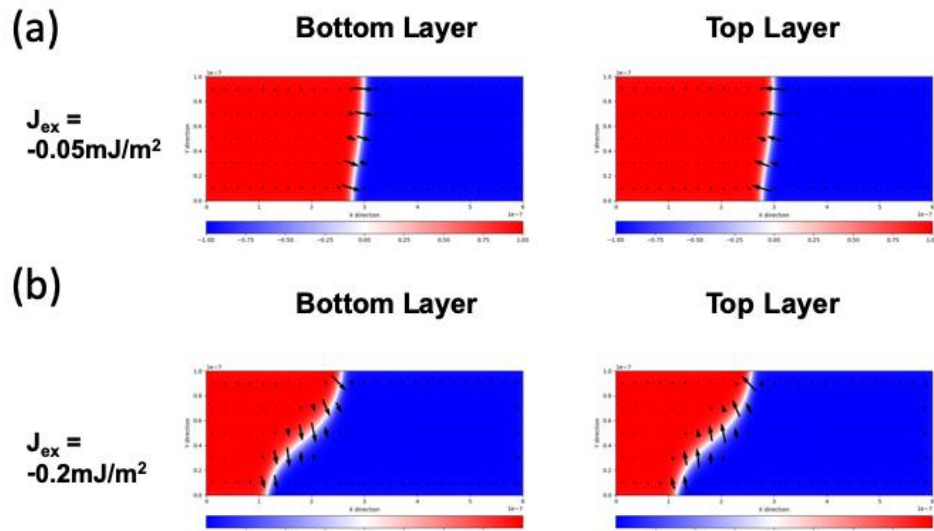


Figure 6-12 Upper layer magnetization angle  $t$  and bottom layer magnetization  $b$  during motion at  $J_{ex} = 0.2$  mJ/m<sup>2</sup>,  $J_{ex} = 0$  mJ/m<sup>2</sup>,  $J_{ex} = -0.1$  mJ/m<sup>2</sup> and  $J_{ex} = -0.2$  mJ/m<sup>2</sup>. The size of the dot is representing the velocity of the domain wall. The different dot is representing current from  $I = 1 \times 10^{11}$  A/m<sup>2</sup> to  $I = 1 \times 10^{12}$  A/m<sup>2</sup>

Figure 6.13 shows two cases with different  $J_{ex}$  which results in variations in DW shape during the motion under the same current. We find out that the DWs elongate and deform into a “S” shape to minimize the domain wall energy. At weaker exchanging coupling,  $J_{ex} = -0.05 \text{ mJ/m}^2$ , the domain wall starts to deform, but the shape is still like a line. However, when increase the  $J_{ex}$  to  $-0.2 \text{ mJ/m}^2$  the domain wall starts to elongate and become closer to a “S” shape. This “S” shape domain wall travels together with current. It might be more and more spin in the DWs align parallel to the y-axis. The formation of the S-shaped domain wall during the current-driven DWM is likely due to the following: As the current-resulted spin orbital torque forces the magnetization at the center of the wall orient towards the y-axis, a segment of the wall parallel to the x-axis would be more energetically preferred under the influence of DMI. The greater the DMI strength, the longer this segment would be, i.e. the longer the middle of the “S” shaped wall. (This insight should be attributed to the discussion with Professor Vincent Sokalski, who is one of the members in this thesis committee.)



**Figure 6-13 Bottom layer and top layer domain wall shape and magnetization angle during movement of  $J_{ex} = -0.05 \text{ mJ/m}^2$  and  $J_{ex} = -0.2 \text{ mJ/m}^2$  at  $I = 1 \times 10^{12} \text{ A/m}^2$ .**

### 6.2.2 Current effect on domain wall motion speed and inner magnetization angle

Figure 6.14 shows the effect of current strength on the domain wall motion. Besides increasing current always enhances the domain wall motion, it also shifts domain walls in both layers towards Bloch wall configuration. If we look at the actual domain wall, the difference is much more obvious.

At  $J_{ex} = -0.2 \text{ mJ/m}^2$ , which is plotted in Figure 6.15, the domain wall forms an "S" shape instead of a "/" shape angle during motion at larger current. It is because an

"S" shape domain wall can reduce the exchanging coupling field by forming tail to tail configuration in the middle of the domain wall.

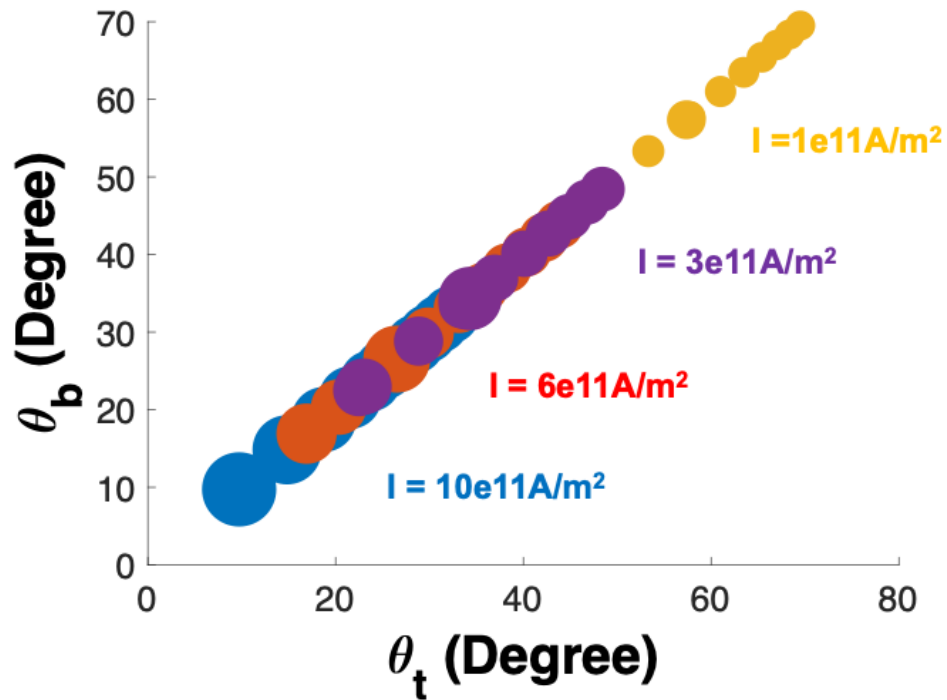
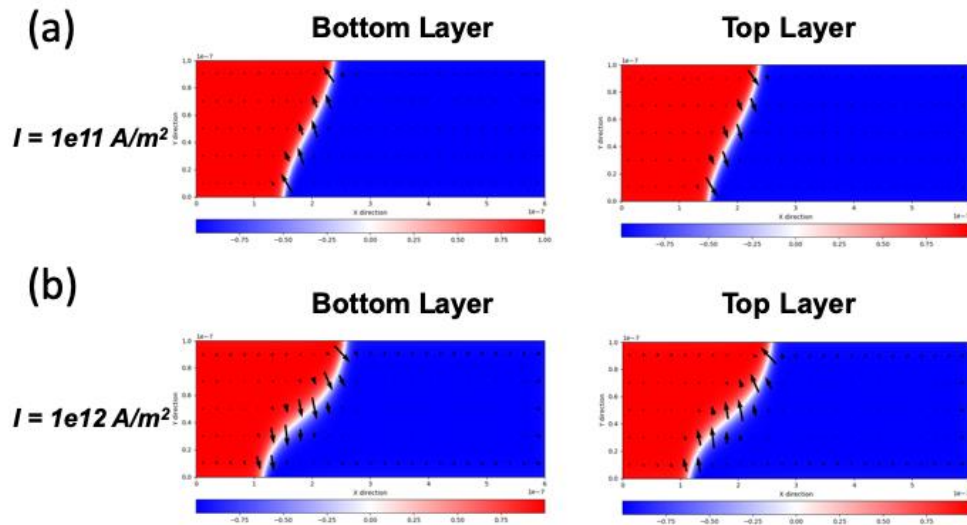


Figure 6-14 Upper layer magnetization angle  $\theta_t$  and bottom layer magnetization  $\theta_b$  during motion at  $I = 1 \times 10^{11} \text{ A/m}^2$ ,  $I = 3 \times 10^{11} \text{ A/m}^2$ ,  $I = 6 \times 10^{11} \text{ A/m}^2$ , and  $I = 10 \times 10^{11} \text{ A/m}^2$ . The size of the dot is representing the velocity of the domain wall. The exchanging stiffness is fixed at  $J_{ex} = -0.2 \text{ mJ/m}^2$ .



**Figure 6-15 Bottom layer and top layer domain wall shape and magnetization angle during movement at  $I = 1 \times 10^{11} \text{ A/m}^2$  and  $I = 1 \times 10^{12} \text{ A/m}^2$  with fixed  $J_{ex} = -0.2 \text{ mJ/m}^2$ .**

### 6.3 Comparison between FM coupling and AFM coupling

Here we compare the difference of the effects due to the FM and AFM coupling in terms of their influence on the DW behavior. First, we would like to point out that in all the cases, the DWs travel as a Bloch wall configuration. The difference between the top and bottom layer magnetization angle is around 180 degrees. However, the AFM type coupling cause the DWs to deform into a tilted “S” shape while the FM type only cause tilting.

Figure 6.16 shows how the domain wall inner magnetization angle changes with different  $J_{ex}$  and current. It is clear to see in the figure for both increase current and decrease the exchanging coupling effect, the magnetization rotates towards y-axis. It is also obvious to see that the angle difference between the top and bottom layer DW magnetization is around 180 degree. The magnetization rotates together under current. Although the coupling type is different, it seems, in the simulation condition, that travel as a Bloch wall increase the velocities of the DWM.

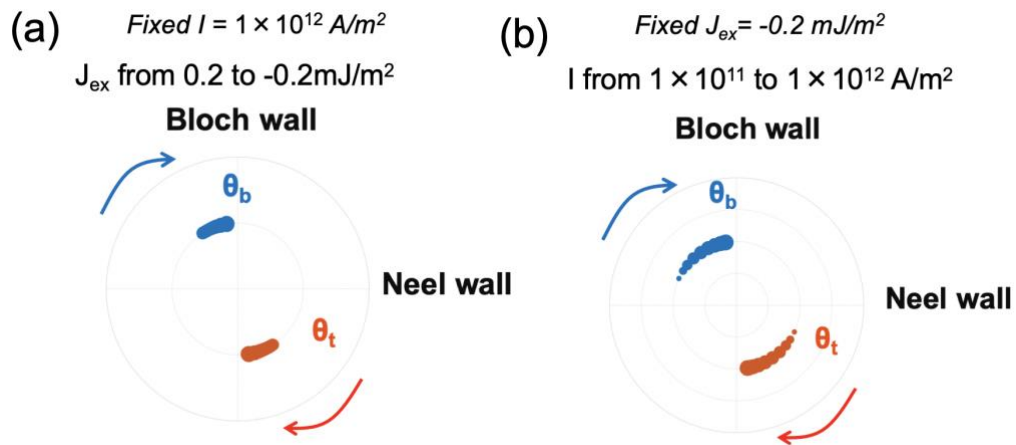


**Figure 6-16 Comparison of from Upper layer magnetization angle  $\theta_t$  and bottom layer magnetization  $\theta_b$  for different  $J_{ex}$  and current, (a) Fixed  $I = 1 \times 10^{11} \text{ A/m}^2$  with  $J_{ex}$  various from 0.2 to  $-0.2 \text{ mJ/m}^2$  (b) fix  $J_{ex} = -0.2 \text{ mJ/m}^2$  and change the current from  $I = 1 \times 10^{11} \text{ A/m}^2$  and  $I = 1 \times 10^{12} \text{ A/m}^2$ .**

Figure 6.17 compared the DW shape during the motion between FM type and AFM type of exchanging coupling. Again, we find out that the DWs deform from “/” to “S” type when we change the type of coupling. In Figure 6.17, from left to right,

different color represents DW shape at different time. Figure 6.17(a) is  $J_{ex} = 0.1 \text{ mJ/m}^2$ . It is obvious that the DWs start to tilt and then displace from left to right. There is not curvature for the DWs. However, for an AFM type in Figure 6.17(b), the  $J_{ex} = -0.2 \text{ mJ/m}^2$ , the DWs not only tilt but also create curvature. After equilibrium, the “S” type domain wall starts to travel under current.

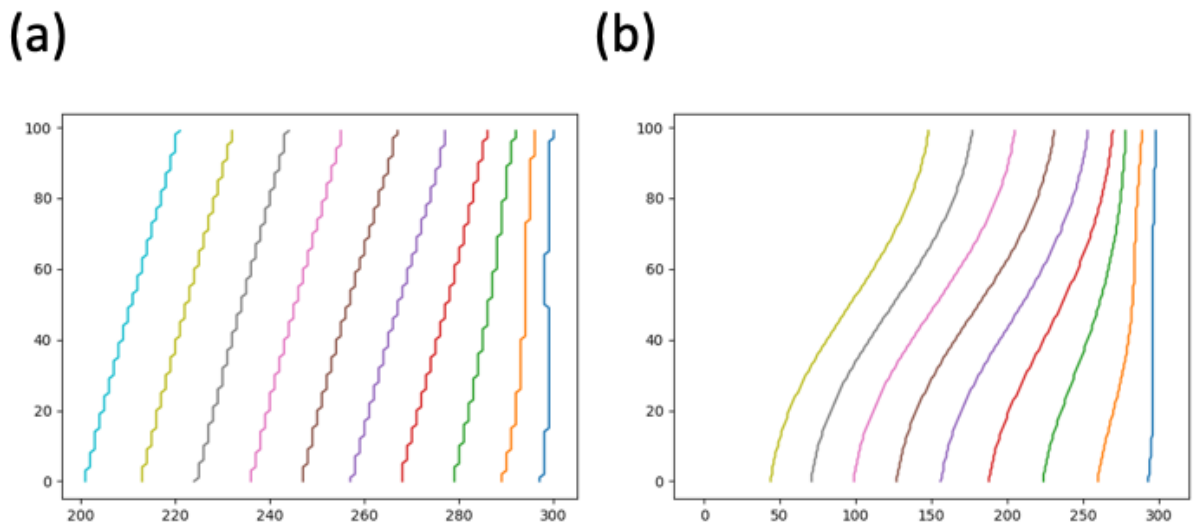


**Figure 6-17 Comparing the domain wall configuration at (a)  $J_{ex} = 0.1 \text{ mJ/m}^2$  and (b)  $J_{ex} = -0.2 \text{ mJ/m}^2$ . The different color representing the same domain wall at different time under  $I = 1 \times 10^{12} \text{ A/m}^2$ .**

## **CHAPTER 7. CONCLUSIONS AND OUTLOOK**

This thesis focuses on the dual magnetic layer current induced domain wall motion. In this system, the domain wall motion is driven by a combination of spin-orbit torque and chiral torque arising from Dzyaloshinsky-Moriya interaction (DMI). Furthermore, the interlayer exchanging coupling has great influence for the domain wall motion. The micromagnetic simulations study about different type and strength of exchanging coupling is performed in the thesis. There are a few possible implementations and applications for this structure, which we discuss in following section.

### **7.1 Summary and comparison**

This thesis has explored domain wall dynamics with magnetic domain walls in nanowires in non-traditional magnetic systems. The magnetic anisotropy in our thin-film system is perpendicular. By engineering the film stacks, the interlayer exchanging coupling effect and DMI effect can determine the chirality of the domain wall. By using the Spin Hall effect induced spin current, the domain wall motion velocities and behaviors are controlled. The micromagnetic simulation gives a platform to study the domain wall behavior under the complex influence. By studying the simulation result, it indicates the domain wall inner magnetization angle of different layers is critical to the domain wall motion.

In the first part of the thesis, we first validate the simulation tool Mumax3. We use the various standard problems posted on the internet and also the real experiment data from some reference papers. Both the standard problems calculations and results compared with published experiment data have demonstrated the Mumax3 is a valid tool for domain wall motion study and validated the use of the software in the context of this thesis

The next part of the thesis is the simulation result of single layer domain wall motion. The model we use is HM/FM/HM film stacks. By control the DMI of the HM, we can control the chirality of the domain wall. Combining the Spin Hall effect, the domain wall motion can be determined dynamically. The simulation result is consistent with the reported domain wall motion result.

By confirming the result of single layer domain walls, we further discuss the multilayer samples. The model we used in the thesis is HM/FM/Spacer/FM/HM film stacks. In this model, there is an interlayer exchanging coupling effect besides the DMI and Spin Hall effect. By changing the exchanging coupling effect strength and sign, the domain walls can be either ferromagnetic or anti-ferromagnetic coupled together. There are three different scenarios by controlling the strength of DMI and exchanging the coupling effect, which is shown in Figure 7.1. Experimentally, the exchange coupling effect can be controlled by spacer materials selection and engineering. In our thesis, we choose Ir as the spacer materials. The RKKY effect can be adjusted by controlling the thickness of Ir. We successfully manipulate the Ir thickness in Pt/Co/Ir/Co/Pt film stack to obtain Co/Co ferromagnetic coupling or anti-ferromagnetic coupling. The simulation result shows that ferromagnetic

coupling state domain wall motion is slower than no coupling sample. However, we find out that by reducing the coupling strength, the velocity is increased by creating a nearly 90-degree angle between the upper and bottom layer magnetization during motion. If we continuously decrease the exchanging coupling strength, the RKKY effect is no longer the predominant effect. In this scenario, the top layer domain wall starts as a right-handed Néel wall and bottom layer left-handed Néel wall. When the current applies, both layer domain walls move in the same direction. The angle difference between different walls is around 180 degrees. However, due to the FM coupling, the domain wall motion velocities are still lower than the no coupling case. If we change the sign of exchange coupling, the domain walls start to AFM couple together. Again, both layers domain walls move in the same direction. The velocities, in this case, are higher than the no coupling case due to the exchanging coupling torque. The domain wall is no longer “/” shape but form an “S” shape to lower the demagnetization energy in y-axis.

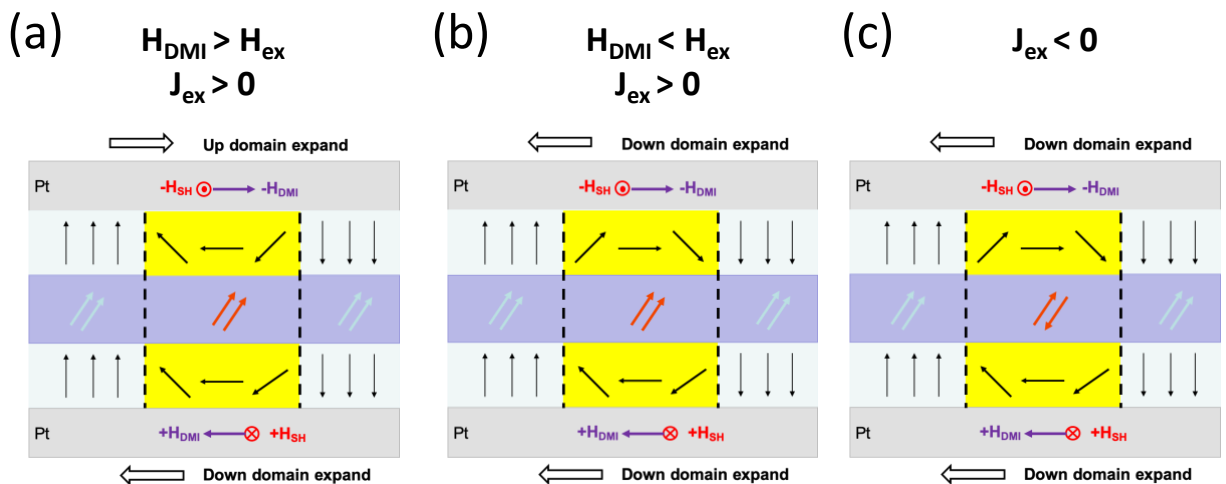
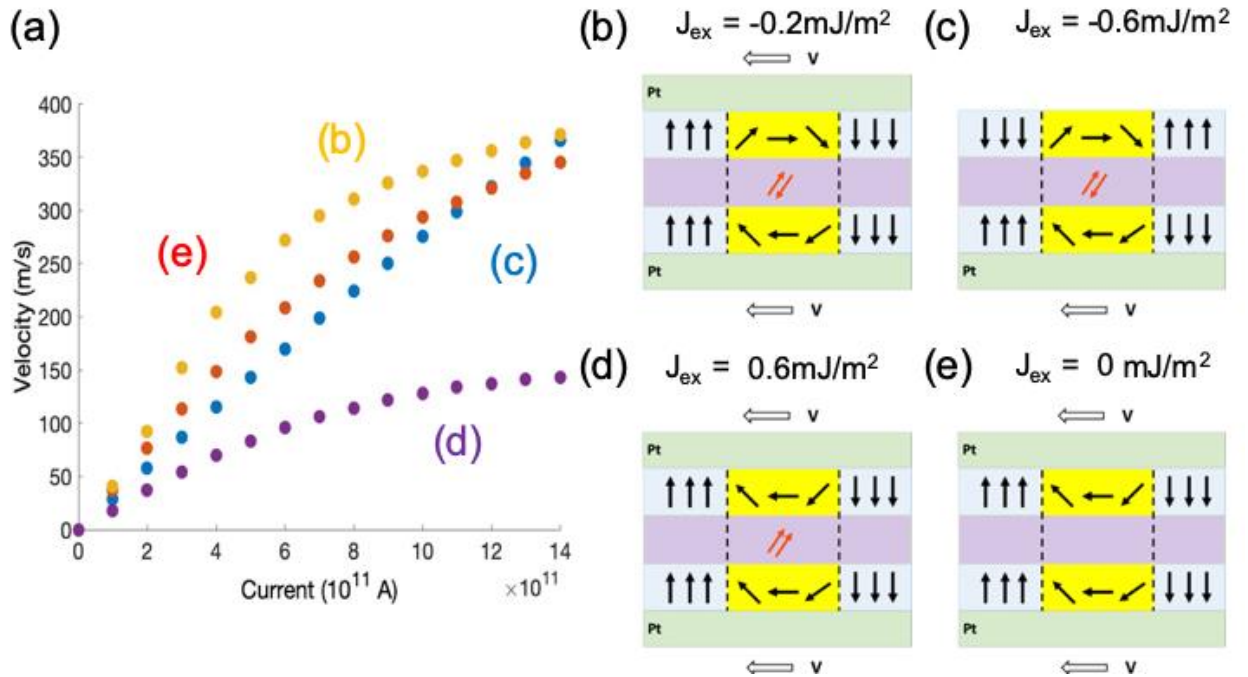


Figure 7-1 Simulation set up for different exchanging coupling cases.

The simulation result shows that ferromagnetic coupling state domain wall motion is slower than no coupling sample. However, we find out that by reducing the coupling strength, the velocity is increased by creating a nearly 90-degree angle between the upper and bottom layer magnetization during motion. Further reduce the exchanging coupling strength increase the domain wall motion. It is because of the exchanging coupling torque acting on the domain walls.

We compare the velocity of domain wall motion for the different scenario in Figure 7.2. The bottom line in purple is the case of  $J_{ex} = 0.6 \text{ mJ/m}^2$ . The next line in blue is the AFM coupling sample ( $J_{ex} = -0.6 \text{ mJ/m}^2$ ) with only one current source. The simulation result shows both cases the domain wall motion is slower than no coupling sample when the current is smaller than  $1.4 \times 10 \text{ A/m}^2$ . The result with no exchanging coupling sample is shown in red. The highest velocity result is the weak AFM coupling sample with  $J_{ex} = -0.2 \text{ mJ/m}^2$ . The saturation for velocity is due to the align of domain wall with y axis. Hence, this configuration is intriguing for the application of domain wall motion related memory, especially under low current.



**Figure 7-2 (a) Current and velocity relation for different ex-coupling state films. Simulation set up for different cases (b)  $J_{ex} = 0.6$  mJ/m<sup>2</sup> (c)  $J_{ex} = -0.6$  mJ/m<sup>2</sup> (d)  $J_{ex} = 0$  mJ/m<sup>2</sup> and (e)  $J_{ex} = -0.2$  mJ/m<sup>2</sup>**

## 7.2 Outlook on future developments

## 7.3 Skyrmion dynamics in synthetic antiferromagnetic structures

Over the past few years, a tremendous effort has been made to investigate the magnetic skyrmion and how the skyrmion appear and displaced in ultrathin ferromagnetic films and nanotracks.[54]–[62] The skyrmion are localized spin texture that spin orientation gradually changes in the opposite direction from the center to the perimeter. Interestingly, the chiral spin texture of skyrmion is protected by topology and provides additional stability against material defects,

field perturbations, and temperature variations. It allows us to develop next generation of spintronics with high speed and low power.[63]–[67]

Recently, the research in broken inversion symmetry has led to significant development in this area. Breaking inversion symmetry allows the spin orbit torques and improve the efficiency of current induced domain wall motion. On the other hand, through DMI, this allows us to engineer DW chirality and lower the DW energy, which stabilizes the skyrmion at room temperature.[68]–[71]

In this thesis, the symmetric dual magnetic layer system with synthetic antiferromagnetic structures has been demonstrated for DW based memory application. This system has large interfacial DMI and strong spin orbit coupling. It meets all the requirements to host skyrmion since the control of DW chirality and energy is assisted by dipolar coupling. It results in two superimposed skyrmion, strongly coupled through their dipolar stray field, which behaves like a single particle called skyrmion hereafter for simplicity. It has been reported in simulation and experiments, shown in Figure 7.3.

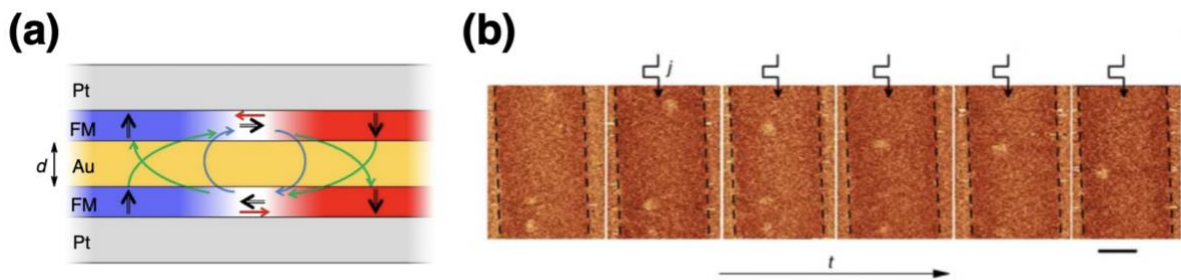


**Figure 7-3 (a) Sketch of the Pt/FM/Au/FM/Pt stack. The black arrows indicate magnetization orientation inside the two layers (b) Series of**

**images showing skyrmion shift along the track between 3 ns,  $j = 3.9 \times 10^{11} \text{A/m}^2$  electric pulses. Scale bar, 500 nm. Reprinted with the permission from A. Hrabec *et al.*, *Nat. Commun.*, vol. 8, Jun. 2017. Ref.[72]**

Theoretically, a pair of antiferromagnetically coupled skyrmion can move in a straight line in nanostrips due to the RKKY interlayer interaction. It is essential to have straight motion particles for ultra-dense and ultrafast storage and/or logic devices. Due to the Magnus force, the skyrmion motion is not parallel to the current direction, shown in Figure 7.4(a). The skyrmion are deflected and destroyed at the edges of the nano-tracks, causing information loss. However, the antiferromagnetic exchanging coupling can surpass the Magnus force and driven the skyrmion to move in a straight line, which is demonstrated in Figure 7.4(b).

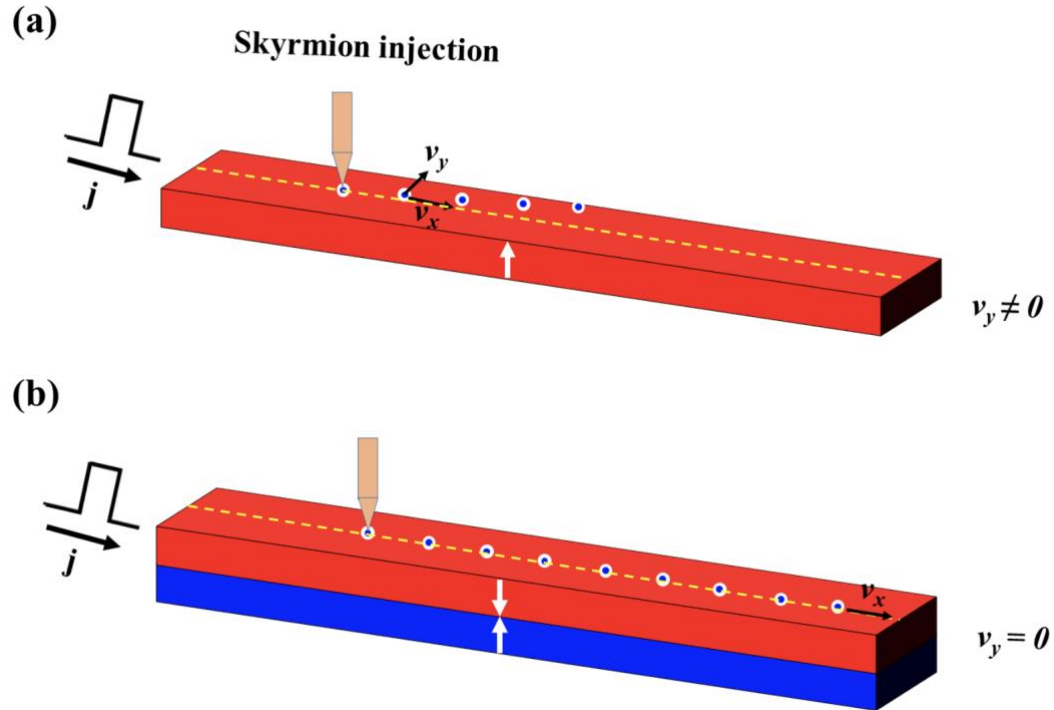


**Figure 7-4 Schematic diagram for skyrmion memory. (a) The skyrmion are annihilated at the edge of PMA wires due to Magnus force. (b) The skyrmion moves in a straight line in SAF wire. Replotted with the permission from R. Tomasello *et al.*, *J. Phys. D: Appl. Phys.*, vol. 50, no. 32, Jul. 2017. Ref.[19]**

Our symmetric dual magnetic system not only provides a way to stabilize the skyrmion and also a way to drive it with reduced power while achieving high motion speed. The skyrmion, coupled via RKKY antiferromagnetic coupling, is similar to the DWs motion in the nanowires. As we showed in this thesis, the DWs in the symmetric dual magnetic layer with antiferromagnetic exchanging coupling can be driven in fast speed with low current density. Hence, it would be interesting to play with the RKKY exchange strengths to investigate the skyrmion dynamics in the SAF structures. In addition, the skyrmion dynamics can also be controlled by engineering the spin current at two interfaces of the SAF stack.[73]–[77]

#### **7.4 Interaction between the domain walls in synthetic antiferromagnetic wires**

Current-driven Domain wall motion memory devices have been a candidate for the next generation of memory devices. It can be non-volatility, ultra-high density storage, and low power consumption [78]–[82]. One major limitation in the application of this kind of memory is the density of packing of the DW memory bits along the magnetic nanowires in racetrack memory. This packing density is limited by magnetic dipole fringing fields and the field rise interaction between DWs. A novel method of DW injection and driving has been investigated in SAF wires, where the stray field from a wire has been reduced. The structure and result are shown in Figure 7.5.

In our thesis, we compared this structure with our symmetric dual magnetic system. The advantages are evident. First, the symmetric structure has two spin current sources. It significantly reduces the critical depinning current density. Second, the interlayer exchanging coupling can be controlled by the interlayer thickness, which increases the DWM velocities. This structure can be further investigated for applications in racetrack memories for achieving high speed and low power performance

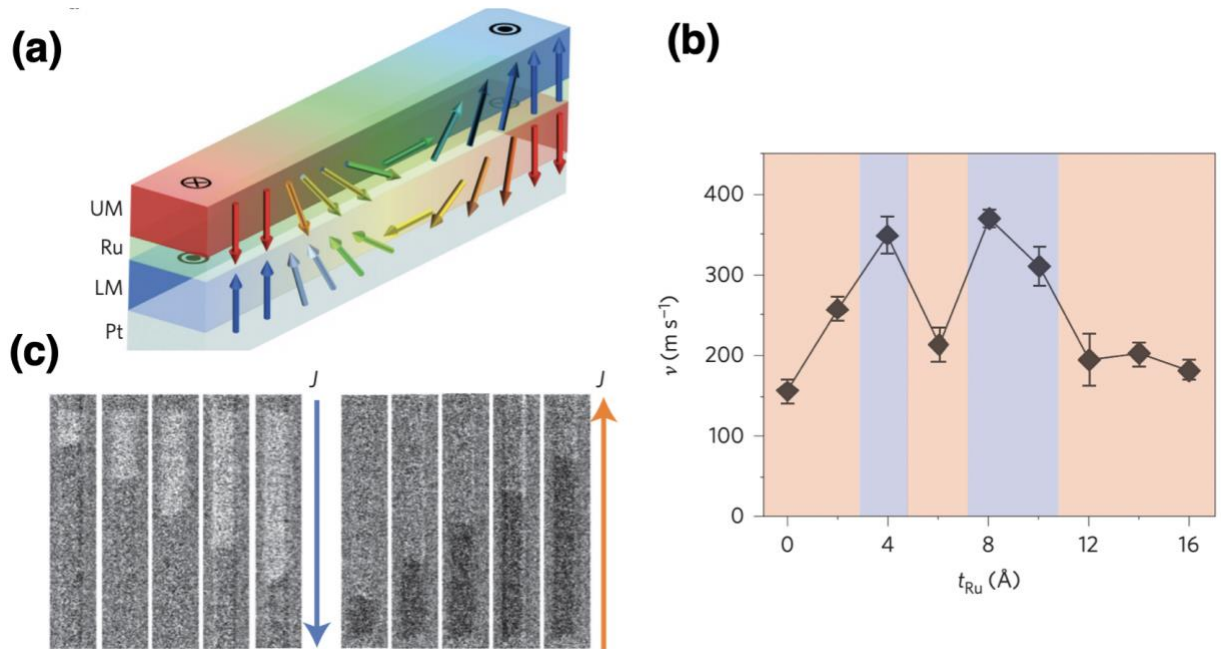


**Figure 7-5** (a) Schematic illustrations of DWs in the upper (UM) and lower (LM) magnetic layers in perpendicularly magnetized with antiferromagnetic coupling (b) as a function of  $t_{\text{Ru}}$  for 20 TaN|15 Pt|3 Co|7 Ni|1.5 Co| $t_{\text{Ru}}$  Ru|1.5 Co|7 Ni|1.5 Co|50 TaN. Orange and blue shaded regions correspond to SF ( $J_{\text{ex}} > 0$ ) and SAF ( $J_{\text{ex}} < 0$ ), respectively (c) Kerr microscope images of a single DW moving along a nanowire formed from 20 TaN|15 Pt|3 Co|7 Ni|1.5 Co| $t_{\text{Ru}}$  Ru|1.5 Co|7 Ni|1.5 Co|50 TaN with and  $t_{\text{Ru}} = 8$  (SAF). Reprinted with the permission from S.-H. Yang, K.-S. Ryu, and S. Parkin, *Nat. Nanotechnol.*, vol. 10, p. 221, Feb. 2015. Ref. [83]

## 7.5 Synthetic antiferromagnets in magnetic tunnel junctions

Semiconductor memories such as SRAM and DRAM need power to maintain their memory states whereas the leakage current has become a major power consumption. An alternating way to improve the situation is the replacement of the DRAM and SRAM cache memories by the non-volatile spintronics memories. Among emerging spintronics memory devices, the spin orbit torque magnetic

random access memory (SOT-MRAM) has been getting significant attention as an important competitive candidate. [45], [84]–[89] In these devices, the SHE has been adopted as the main source for SOT injection. It has been demonstrated that the SHE can trigger magnetization switching of in-plane magnetic tunnel junctions. However, for high density memory, an in-plane magnetic field has to be applied for SHE induced switching.

One way to introduce a local in-plane field is by using exchange bias or interlayer exchange coupling. [90]–[94] Figure 7.6 shows a way of utilizing the Ir as an interlayer to achieve deterministic magnetization switching without an external in-plane field. The Ir provides interlayer exchange coupling when sandwiched by two ferromagnetic layers that facilitate the switching process.

In our thesis, the symmetric structure of Pt/Co/Ir/Co/Pt can also induce an exchanging coupling between the Co layer. It will be interesting to see how it can be used for magnetization switching. Moreover, both our result shows that the DWs were propagating as a Bloch wall to increase the DWM velocities. Our thesis helps in understanding how the exchanging coupling influence the DWs propagation process.

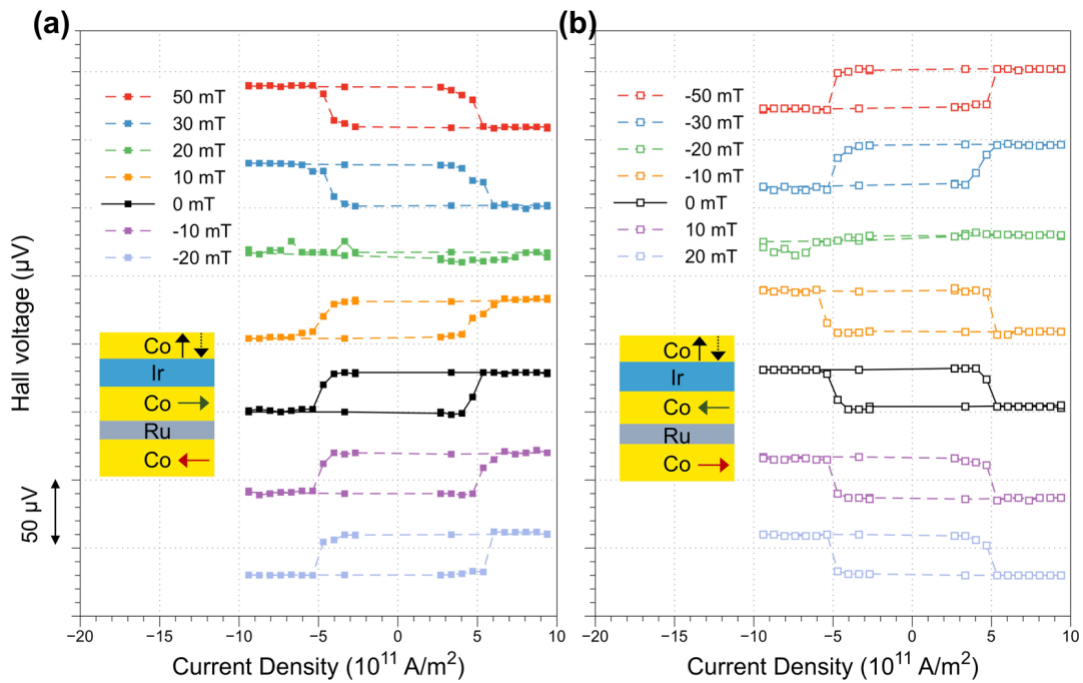


**Figure 7-6 Anomalous Hall voltage as a function of injected current density in the Ir layer with various external magnetic fields  $H_x$  along the current direction. Bottom SAF is set as (a)  $\rightleftharpoons$ , and (b)  $\leftarrow$ . Reprinted with the permission from Y. Liu, B. Zhou, and J.-G. (Jimmy) Zhu, *Sci. Rep.*, vol. 9, p. 325, 2019. Ref.[1]**

## REFERENCES

- [1] Y. Liu, B. Zhou, and J.-G. (Jimmy) Zhu, “Field-free Magnetization Switching by Utilizing the Spin Hall Effect and Interlayer Exchange Coupling of Iridium,” *Sci. Rep.*, vol. 9, p. 325, 2019.
- [2] M. Shen, Y. Zhang, L. You, and X. Yang, “Readable racetrack memory via ferromagnetically coupled chiral domain walls,” *Appl. Phys. Lett.*, vol. 113, no. 15, p. 152401, Oct. 2018.
- [3] J. G. J. Zhu, D. M. Bromberg, M. Moneck, V. Sokalski, and L. Pileggi, “MLogic: All spin logic device and circuits,” in *2015 4th Berkeley Symposium on Energy Efficient Electronic Systems, E3S 2015 - Proceedings*, 2015.
- [4] K.-J. Kim *et al.*, “Fast domain wall motion in the vicinity of the angular momentum compensation temperature of ferrimagnets,” *Nat. Mater.*, vol. 16, p. 1187, 2017.
- [5] H. Shi *et al.*, “Exciton Dynamics in Suspended 2D Crystals,” *ACS Nano*, no. 2, pp. 1072–1080, 2013.
- [6] O. Alejos, V. Raposo, L. Sanchez-Tejerina, R. Tomasello, G. Finocchio, and E. Martinez, “Current-driven domain wall dynamics in ferromagnetic layers synthetically exchange-coupled by a spacer: A micromagnetic study,” *J. Appl. Phys.*, vol. 123, p. 13901, 2018.

- [7] S. Krishnia *et al.*, “Role of RKKY torque on domain wall motion in synthetic antiferromagnetic nanowires with opposite spin Hall angles,” *Sci. Rep.*, vol. 7, p. 11715, 2017.
- [8] A. Vansteenkiste, J. Leliaert, M. Dvornik, M. Helsen, F. Garcia-Sanchez, and B. Van Waeyenberge, “The design and verification of MuMax3,” *AIP Adv.*, vol. 4, p. 107133, 2014.
- [9] C. B. Muratov, V. V Slastikov, A. G. Kolesnikov, and O. A. Tretiakov, “Theory of the Dzyaloshinskii domain-wall tilt in ferromagnetic nanostrips,” *Phys. Rev. B*, vol. 96, p. 134417, 2017.
- [10] L. D. A. Ho, M. T. Tran, X. H. Cao, V. A. Dao, D. T. Ngo, and D. Q. Hoang, “Field-driven single domain wall motion in ferromagnetic nanowires,” *RSC Adv.*, vol. 8, no. 26, pp. 14539–14551, 2018.
- [11] S. Sundara Mahalingam, B. V. Manikandan, and S. Arockiaraj, “Review - Micromagnetic Simulation Using OOMMF and Experimental Investigations on Nano Composite Magnets,” in *Journal of Physics: Conference Series*, 2019, vol. 1172, no. 1.
- [12] D. Bang, P. Van Thach, and H. Awano, “Current-induced domain wall motion in antiferromagnetically coupled structures: Fundamentals and applications,” *J. Sci. Adv. Mater. Devices*, vol. 3, no. 4, pp. 389–398, 2018.
- [13] S. Emori, U. Bauer, S.-M. Ahn, E. Martinez, and G. S. D. Beach, “Current-driven dynamics of chiral ferromagnetic domain walls,” *Nat. Mater.*, vol. 12, p. 611,

2013.

- [14] T. Schulz *et al.*, “Modification of Dzyaloshinskii-Moriya-Interaction-Stabilized Domain Wall Chirality by Driving Currents,” *Phys. Rev. Lett.*, vol. 121, no. 14, p. 147203, 2018.
- [15] Y. Liu, X. Liu, and J.-G. Zhu, “Tailoring the Current-Driven Domain Wall Motion by Varying the Relative Thickness of Two Heavy Metal Underlayers,” *IEEE Trans. Magn.*, vol. 54, pp. 1–5, 2018.
- [16] T. Lin *et al.*, “Observation of room-temperature magnetic skyrmions in Pt/Co/W structures with a large spin-orbit coupling,” *Phys. Rev. B*, vol. 98, p. 174425, 2018.
- [17] Y. Kurokawa and H. Awano, “Multilayered current-induced domain wall motion in Pt/Tb-Co/Ta/Tb-Co/Pt magnetic wire,” *AIP Adv.*, vol. 8, no. 2, 2018.
- [18] K.-S. Ryu, L. Thomas, S.-H. Yang, and S. Parkin, “Chiral spin torque at magnetic domain walls,” *Nat. Nanotechnol.*, vol. 8, pp. 527–533, 2013.
- [19] R. Tomasello *et al.*, “Performance of synthetic antiferromagnetic racetrack memory: Domain wall versus skyrmion,” *J. Phys. D: Appl. Phys.*, vol. 50, no. 32, Jul. 2017.
- [20] W. S. Zhao, T. Devolder, Y. Lakys, J. O. Klein, C. Chappert, and P. Mazoyer, “Design considerations and strategies for high-reliable STT-MRAM,” *Microelectron. Reliab.*, vol. 51, no. 9–11, pp. 1454–1458, 2011.
- [21] Y.-C. Liang, P.-B. He, M.-Q. Cai, and Z.-D. Li, “Motion and stability of chiral

- domain walls driven by non-gradient spin torques: antiferromagnets and ferromagnets compared,” *J. Magn. Magn. Mater.*, 2019.
- [22] P. C. Filippou *et al.*, “Chiral domain wall motion in unit-cell thick perpendicularly magnetized Heusler films prepared by chemical templating,” *Nat. Commun.*, vol. 9, no. 1, p. 4653, 2018.
- [23] D.-Y. Kim *et al.*, “Magnetic domain-wall tilting due to domain-wall speed asymmetry,” *Phys. Rev. B*, vol. 97, p. 134407, 2018.
- [24] I. M. Miron *et al.*, “Fast current-induced domain-wall motion controlled by the Rashba effect,” *Nat. Mater.*, vol. 10, p. 419, May 2011.
- [25] T. Moriya, “Anisotropic superexchange interaction and weak ferromagnetism,” *Phys. Rev.*, vol. 120, no. 1, pp. 91–98, Oct. 1960.
- [26] I. Dzyaloshinsky, “A thermodynamic theory of ‘weak’ ferromagnetism of antiferromagnetics,” *J. Phys. Chem. Solids*, vol. 4, no. 4, pp. 241–255, 1958.
- [27] M. I. D. and V. I. Perel, “Possibility of orientating electron spins with current,” *Sov. Phys. JETP Lett.*, vol. 13, p. 467, 1971.
- [28] M. I. Dyakonov and V. I. Perel, “Current-induced spin orientation of electrons in semiconductors,” *Phys. Lett. A*, vol. 35, no. 6, pp. 459–460, Jul. 1971.
- [29] M. I. Dyakonov, “Spin Hall Effect,” *Futur. Trends Microelectron.*, p. 70360R, 2008.
- [30] A. Manchon, H. C. Koo, J. Nitta, S. M. Frolov, and R. A. Duine, “New

- perspectives for Rashba spin-orbit coupling,” *Nat. Mater.*, vol. 14, no. 9, pp. 871–882, Aug. 2015.
- [31] Y. K. Kato, R. C. Myers, A. C. Gossard, and D. D. Awschalom, “Observation of the spin hall effect in semiconductors,” *Science (80-. )*, vol. 306, no. 5703, pp. 1910–1913, Dec. 2004.
- [32] E. Saitoh, M. Ueda, H. Miyajima, and G. Tatara, “Conversion of spin current into charge current at room temperature: Inverse spin-Hall effect,” *Appl. Phys. Lett.*, vol. 88, no. 18, May 2006.
- [33] T. Kimura, Y. Otani, T. Sato, S. Takahashi, and S. Maekawa, “Room-temperature reversible spin hall effect,” *Phys. Rev. Lett.*, vol. 98, no. 15, Apr. 2007.
- [34] H. Zhao, E. J. Loren, H. M. Van Driel, and A. L. Smirl, “Coherence control of hall charge and spin currents,” *Phys. Rev. Lett.*, vol. 96, no. 24, 2006.
- [35] S.-G. Je, D.-H. Kim, S.-C. Yoo, B.-C. Min, K.-J. Lee, and S.-B. Choe, “Asymmetric magnetic domain-wall motion by the Dzyaloshinskii-Moriya interaction,” *Phys. Rev. B*, vol. 88, no. 21, p. 214401, Dec. 2013.
- [36] A. V. Khvalkovskiy *et al.*, “Matching domain-wall configuration and spin-orbit torques for efficient domain-wall motion,” *Phys. Rev. B - Condens. Matter Mater. Phys.*, vol. 87, no. 2, pp. 2–6, 2013.
- [37] K. Bouzehouane *et al.*, “Hybrid chiral domain walls and skyrmions in magnetic multilayers,” *Sci. Adv.*, vol. 4, no. 7, p. eaat0415, 2018.

- [38] J. Torrejon *et al.*, “Interface control of the magnetic chirality in CoFeB/MgO heterostructures with heavy-metal underlayers,” *Nat. Commun.*, vol. 5, pp. 1–8, 2014.
- [39] S.-H. Yang, K.-S. Ryu, and S. Parkin, “Domain-wall velocities of up to 750 m s<sup>-1</sup> driven by exchange-coupling torque in synthetic antiferromagnets,” *Nat. Nanotechnol.*, vol. 10, no. 3, pp. 221–226, 2015.
- [40] J. Hong *et al.*, “The Physics of Spin-transfer Torque Switching in Magnetic Tunneling Junctions in Sub-10-nm Size Range,” *IEEE Trans. Magn.*, vol. 9464, no. c, pp. 1–1, 2016.
- [41] Z. Yu *et al.*, “Domain-wall motion at an ultrahigh speed driven by spin-orbit torque in synthetic antiferromagnets,” *Nanotechnology*, vol. 29, no. 17, 2018.
- [42] A. Hrabec *et al.*, “Velocity Enhancement by Synchronization of Magnetic Domain Walls,” *Phys. Rev. Lett.*, vol. 120, p. 227204, 2018.
- [43] J. Leliaert, J. Mulkers, J. De Clercq, A. Coene, M. Dvornik, and B. Van Waeyenberge, “Adaptively time stepping the stochastic Landau-Lifshitz-Gilbert equation at nonzero temperature: Implementation and validation in MuMax3,” *AIP Adv.*, vol. 7, no. 12, Dec. 2017.
- [44] K. Everschor-Sitte, J. Masell, R. M. Reeve, and M. Kläui, “Perspective: Magnetic skyrmions - Overview of recent progress in an active research field,” *J. Appl. Phys.*, vol. 124, no. 24, Dec. 2018.

- [45] C. Abert, “Micromagnetics and spintronics: models and numerical methods,” *Eur. Phys. J. B*, vol. 92, no. 6, Jun. 2019.
- [46] C. M. Pfeiler *et al.*, “Computational micromagnetics with Commics,” *Comput. Phys. Commun.*, 2019.
- [47] G. P. Müller *et al.*, “Spirit: Multifunctional framework for atomistic spin simulations,” *Phys. Rev. B*, vol. 99, no. 22, Jun. 2019.
- [48] O. Laslett, J. Waters, H. Fangohr, and O. Hovorka, “Magpy: A C++ accelerated Python package for simulating magnetic nanoparticle stochastic dynamics,” Jan. 2018.
- [49] J. Leliaert and J. Mulkers, “Tomorrow’s micromagnetic simulations,” *J. Appl. Phys.*, vol. 125, no. 18, May 2019.
- [50] M. D. Dejong and K. L. Livesey, “Analytic theory for the switch from Bloch to Néel domain wall in nanowires with perpendicular anisotropy,” *Phys. Rev. B*, vol. 92, p. 214420, 2015.
- [51] S. Emori and G. S. D. Beach, “Roles of the magnetic field and electric current in thermally activated domain wall motion in a submicrometer magnetic strip with perpendicular magnetic anisotropy,” *J. Phys. Condens. Matter*, vol. 24, no. 2, Jan. 2012.
- [52] A. Fert, V. Cros, and J. Sampaio, “Skyrmions on the track,” *Nature Nanotechnology*, vol. 8, no. 3. Nature Publishing Group, pp. 152–156, 2013.

- [53] S. S. P. Parkin and D. Mauri, “Spin engineering: Direct determination of the Ruderman-Kittel-Kasuya-Yosida far-field range function in ruthenium,” *Phys. Rev. B*, vol. 44, no. 13, pp. 7131–7134, Oct. 1991.
- [54] W. Jiang *et al.*, “Blowing magnetic skyrmion bubbles,” *Science* (80-. ), vol. 349, no. 6245, pp. 283–286, Jul. 2015.
- [55] Y. Zhou *et al.*, “Dynamically stabilized magnetic skyrmions,” *Nat. Commun.*, vol. 6, Sep. 2015.
- [56] C. Ma *et al.*, “Electric Field-Induced Creation and Directional Motion of Domain Walls and Skyrmion Bubbles,” *Nano Lett.*, vol. 19, no. 1, pp. 353–361, Jan. 2019.
- [57] T. H. R. Skyrme, “A unified field theory of mesons and baryons,” *Nucl. Phys.*, vol. 31, no. C, pp. 556–569, 1962.
- [58] S. M. H. Wong, “What exactly is a Skyrmion?,” Feb. 2002.
- [59] N. S. Kiselev, A. N. Bogdanov, R. Schäfer, and U. K. Röler, “Chiral skyrmions in thin magnetic films: New objects for magnetic storage technologies?,” *J. Phys. D. Appl. Phys.*, vol. 44, no. 39, Oct. 2011.
- [60] S. Donati *et al.*, “Twist of generalized skyrmions and spin vortices in a polariton superfluid,” *Proc. Natl. Acad. Sci. U. S. A.*, vol. 113, no. 52, pp. 14926–14931, Dec. 2016.
- [61] U. Al Khawaja and H. T. C. Stoof, “Skyrmions in a ferromagnetic Bose-Einstein condensate,” Nov. 2000.

- [62] X. Zhang, M. Ezawa, and Y. Zhou, “Magnetic skyrmion logic gates: Conversion, duplication and merging of skyrmions,” *Sci. Rep.*, vol. 5, 2015.
- [63] P. J. Hsu, A. Kubetzka, A. Finco, N. Romming, K. Von Bergmann, and R. Wiesendanger, “Electric-field-driven switching of individual magnetic skyrmions,” *Nat. Nanotechnol.*, vol. 12, no. 2, pp. 123–126, Feb. 2017.
- [64] A. O. Leonov and M. Mostovoy, “Multiply periodic states and isolated skyrmions in an anisotropic frustrated magnet,” *Nat. Commun.*, vol. 6, Sep. 2015.
- [65] J. I. Fukuda and S. Žumer, “Quasi-two-dimensional Skyrmion lattices in a chiral nematic liquid crystal,” *Nat. Commun.*, vol. 2, no. 1, 2011.
- [66] N. Romming *et al.*, “Writing and deleting single magnetic skyrmions,” *Science* (80-. ), vol. 341, no. 6146, pp. 636–639, 2013.
- [67] D. A. Gilbert *et al.*, “Realization of ground-state artificial skyrmion lattices at room temperature,” *Nat. Commun.*, vol. 6, Oct. 2015.
- [68] S. Das *et al.*, “Observation of room-temperature polar skyrmions,” *Nature*, vol. 568, no. 7752. Nature Publishing Group, pp. 368–372, 18-Apr-2019.
- [69] S. Woo *et al.*, “Spin-orbit torque-driven skyrmion dynamics revealed by time-resolved X-ray microscopy,” *Nat. Commun.*, vol. 8, May 2017.
- [70] W. Jiang, G. Chen, K. Liu, J. Zang, S. G. E. te Velthuis, and A. Hoffmann, “Skyrmions in magnetic multilayers,” *Physics Reports*, vol. 704. Elsevier B.V., pp. 1–49, 23-Aug-2017.

- [71] J. Hong, G. Catalan, D. N. Fang, E. Artacho, and J. F. Scott, “Topology of the polarization field in ferroelectric nanowires from first principles,” *Phys. Rev. B - Condens. Matter Mater. Phys.*, vol. 81, no. 17, May 2010.
- [72] A. Hrabec *et al.*, “Current-induced skyrmion generation and dynamics in symmetric bilayers,” *Nat. Commun.*, vol. 8, Jun. 2017.
- [73] J. Iwasaki, M. Mochizuki, and N. Nagaosa, “Universal current-velocity relation of skyrmion motion in chiral magnets,” *Nat. Commun.*, vol. 4, 2013.
- [74] S. Mühlbauer *et al.*, “Skyrmion lattice in a chiral magnet,” *Science (80-. )*, vol. 323, no. 5916, pp. 915–919, Feb. 2009.
- [75] X. Zhang, M. Ezawa, and Y. Zhou, “Thermally stable magnetic skyrmions in multilayer synthetic antiferromagnetic racetracks,” *Phys. Rev. B*, vol. 94, no. 6, p. 064406, Aug. 2016.
- [76] R. Wiesendanger, “Nanoscale magnetic skyrmions in metallic films and multilayers: A new twist for spintronics,” *Nature Reviews Materials*, vol. 1, no. 7. Nature Publishing Group, 21-Jun-2016.
- [77] Y. H. Liu and Y. Q. Li, “Dynamics of magnetic skyrmions,” *Chinese Physics B*, vol. 24, no. 1. Institute of Physics Publishing, 01-Jan-2015.
- [78] P. Chureemart, R. F. L. Evans, and R. W. Chantrell, “Dynamics of domain wall driven by spin-transfer torque,” *Phys. Rev. B - Condens. Matter Mater. Phys.*, vol. 83, no. 18, pp. 1–8, 2011.

- [79] A. Makarov, V. Sverdlov, and S. Selberherr, “Emerging memory technologies: Trends, challenges, and modeling methods,” *Microelectron. Reliab.*, vol. 52, no. 4, pp. 628–634, 2012.
- [80] M. Cubukcu *et al.*, “Spin-orbit torque magnetization switching of a three-terminal perpendicular magnetic tunnel junction,” *Appl. Phys. Lett.*, vol. 104, no. 4, pp. 1–5, 2014.
- [81] B. G. Simon, “Domain wall motion in Permalloy nanowires,” 2018.
- [82] Z. Yu *et al.*, “Domain-wall motion at an ultrahigh speed driven by spin-orbit torque in synthetic antiferromagnets,” *Nanotechnology*, vol. 29, no. 17, Mar. 2018.
- [83] S.-H. Yang, K.-S. Ryu, and S. Parkin, “Domain-wall velocities of up to 750 m s<sup>-1</sup> driven by exchange-coupling torque in synthetic antiferromagnets,” *Nat. Nanotechnol.*, vol. 10, p. 221, Feb. 2015.
- [84] S. DuttaGupta *et al.*, “Adiabatic spin-transfer-torque-induced domain wall creep in a magnetic metal,” *Nat. Phys.*, vol. 12, no. 4, pp. 333–336, 2015.
- [85] X. Fong *et al.*, “Spin-Transfer Torque Devices for Logic and Memory: Prospects and Perspectives,” *IEEE Trans. Comput. Des. Integr. Circuits Syst.*, vol. 35, no. 1, pp. 1–22, 2016.
- [86] B. Dieny and M. Chshiev, “Perpendicular magnetic anisotropy at transition metal/oxide interfaces and applications,” *Rev. Mod. Phys.*, vol. 89, no. 2, p. 25008, 2017.

- [87] A. Soumyanarayanan, N. Reyren, A. Fert, and C. Panagopoulos, “Emergent Phenomena Induced by Spin-Orbit Coupling at Surfaces and Interfaces,” *Nat. Publ. Gr.*, vol. 539, no. 7630, pp. 509–517, 2016.
- [88] J. S. Institut *et al.*, “Spin Hall effect devices,” *Nat. Mater.*, vol. 11, no. 5, pp. 382–390, 2012.
- [89] J. Zhang *et al.*, “Role of Micromagnetic States on Spin-Orbit Torque-Switching Schemes,” *Nano Lett.*, vol. 18, no. 7, pp. 4074–4080, Jul. 2018.
- [90] I. Žutić, J. Fabian, and S. Das Sarma, “Spintronics: Fundamentals and applications,” *Reviews of Modern Physics*, vol. 76, no. 2, pp. 323–410, Apr-2004.
- [91] A. D. Kent and D. C. Worledge, “A new spin on magnetic memories,” *Nature Nanotechnology*, vol. 10, no. 3, Nature Publishing Group, pp. 187–191, 05-Mar-2015.
- [92] D. M. Bromberg, M. T. Moneck, V. M. Sokalski, J. Zhu, L. Pileggi, and J. G. Zhu, “Experimental demonstration of four-terminal magnetic logic device with separate read- and write-paths,” in *Technical Digest - International Electron Devices Meeting, IEDM*, 2015, vol. 2015-February, no. February, pp. 33.1.1-33.1.4.
- [93] Z. Diao *et al.*, “Spin-transfer torque switching in magnetic tunnel junctions and spin-transfer torque random access memory,” *J. Phys. Condens. Matter*, vol. 19, no. 16, Apr. 2007.
- [94] E. Chen *et al.*, “Advances and future prospects of spin-transfer torque random

access memory,” in *IEEE Transactions on Magnetics*, 2010, vol. 46, no. 6, pp. 1873–1878.